

Cranfield University

**Marta Sujka**

**Alignment and Rectifying Properties of  
Donor–Electron Bridge–Acceptor Molecules**

**School of Engineering  
PhD**

**Cranfield University**

School of Engineering

Department of Nanomaterials

**PhD**

**2007**

**Marta Sujka**

**Alignment and Rectifying Properties of  
Donor–Electron Bridge–Acceptor Molecules**

**Supervisor: Geoffrey J Ashwell**

**June 2007**

## Abstract

Molecular electronics based on the bottom-up approach appears to be a promising alternative to overcome the limitations of the top-down lithographic fabrication of electronic devices. The ability to manipulate single or small groups of molecules provides a great opportunity to build electronic devices at the molecular level. However, before any device can be constructed, it is vital to understand the parameters that control the device properties such as: molecular structure, conformation and arrangement at the surface, the molecule-substrate and molecule-electrode interactions.

This thesis presents an investigation of the alignment of acceptor-electron bridge-donor structures and describes how the molecular structure and arrangement affect rectifying properties of the monolayers. Studies included typical Langmuir-Blodgett (LB), chevron-shaped, and ionically coupled structures that were characterised using various techniques, such as Quartz Crystal Microbalance (QCM), Surface Plasmon Resonance (SPR), Second Harmonic Generation (SHG) and Scanning Tunnelling Spectroscopy (STS).

The results obtained showed that to achieve high rectification the molecules must form ordered and stable monolayers that are able to withstand the electric field applied to the junction. It was also shown that due to the disordered monolayer formation and presence of certain ions, it was extremely difficult to state without doubt whether the rectification was a result of the donor-electron bridge-acceptor structure proposed by Aviram and Ratner<sup>1</sup>.

Studies of chevron-shaped molecules confirmed the possibility of depositing them using the LB technique. However, the reduction of long aliphatic chains was very likely balanced by the formation of less ordered or unstable monolayers. The highest rectification ratio of  $30 \pm 3$  at  $\pm 1$  V was obtained for 1-butyl-2,6-bis-[2-(4-dibutylamino-phenyl)-vinyl]-pyridinium iodide (dye 7) and the origin of the I-V asymmetry was attributed to back electron transfer from iodide to pyridinium ring. Although dye 1-butyl-2,6-bis-(2-{4-[2-(4-dibutylamino-phenyl)-ethyl]-phenyl}-vinyl)-

pyridinium iodide (dye 9) showed electrical asymmetry ( $RR=16$  at  $\pm 1$  V) shortly after deposition onto the gold-coated highly oriented pyrolytic graphite (HOPG), it seemed to form an unstable alignment and as a consequence the rectification decayed over a period of a few hours.

Improved ordering, stability, and rectification were achieved from ionically coupled structures, where the monolayers were formed using chemisorption and ionic assembly instead of physisorption.

## Acknowledgements

I would like to thank my supervisor, Geoff Ashwell, for supervising, and to the EPSRC for my funding. Thanks also to Professor D.J. Sandman at the University of Massachusetts, US; D. Mattern; Professor David Lacy from University of Hull, Danika Locatelli; and all my colleagues at Cranfield University, especially Dr Anne Whittam, Dr Wyane Tyrrell, and Dr Mukhtar Amiri for help and the synthesis of the various samples that I have used. I would also like to thank all my friends, those who are here and far away.

My special thanks go to my family for their love, support, and faith in me. And finally my thanks to Paul for the patience, cheeky smile, and love that helped me go through tough times.

<b>ABSTRACT.....</b>	<b>I</b>
<b>ACKNOWLEDGEMENTS.....</b>	<b>III</b>
<b>LIST OF CHEMICAL NOMENCLATURE OF STUDIED DYES.....</b>	<b>VII</b>
<b>LIST OF FIGURES.....</b>	<b>VIII</b>
<b>LIST OF TABLES.....</b>	<b>XIII</b>
<b>ABBREVIATIONS.....</b>	<b>XIV</b>
<b>1 INTRODUCTION .....</b>	<b>1</b>
1.1 Nanotechnology.....	1
1.2 The bottom-up approach.....	2
1.3 Aims .....	2
1.4 Summary .....	3
<b>2 BACKGROUND AND LITERATURE .....</b>	<b>4</b>
2.1 Molecular rectification .....	4
2.1.1 The Aviram and Ratner model .....	4
2.2 Molecular rectifiers .....	7
2.2.1 Sigma ( $\sigma$ )-bridged molecular structures .....	8
2.2.2 Rectification studies from Z- $\beta$ -(1-hexadecyl-4-quinolinium)- $\alpha$ -cyano-4-styryldicyanomethanide (C <sub>16</sub> H <sub>33</sub> -Q3CNQ) .....	12
2.2.3 Pi ( $\pi$ )-bridged molecular structures .....	16
2.2.4 The alkyl tunnelling barrier effect on molecular rectification .....	20
2.2.5 Different approaches.....	28
2.2.6 Hybrid structures .....	34
2.2.6.1 Donor /Acceptor assemblies .....	34
2.2.6.2 Donor/Aceptor structures based on the ionic assembly approach.....	37
2.2.6.3 Ionically coupled structures on Au-S-CH <sub>2</sub> CH <sub>2</sub> CH <sub>2</sub> -SO <sub>3</sub> <sup>-</sup> .....	39
2.2.6.4 Further studies of mixed bilayer structures based on the ionic assembly approach.....	40
2.3 Possible applications.....	42
2.4 Monolayer deposition .....	43
2.4.1 Langmuir-Blodgett technique .....	43
2.4.1.1 Materials for Langmuir and LB films .....	43
2.4.1.2 Pressure-area isotherm .....	48
2.4.1.3 Experimental considerations for Langmuir and LB films formation .....	51
2.4.1.4 LB film deposition .....	52

2.4.2	Self-assembled monolayers .....	54
2.4.2.1	Materials used in SAMs .....	54
2.4.2.2	Experimental considerations for SAM preparation.....	57
2.4.2.3	SAM deposition .....	58
<b>2.5</b>	<b>Methods for monolayer characterisation .....</b>	<b>60</b>
2.5.1	Quartz crystal microbalance .....	60
2.5.2	Surface plasmon resonance theory .....	61
2.5.3	Scanning tunnelling microscopy.....	63
2.5.4	Second-harmonic generation .....	65
<b>3</b>	<b>EXPERIMENTAL .....</b>	<b>69</b>
<b>3.1</b>	<b>Substrate preparation .....</b>	<b>69</b>
3.1.1	Hydrophilic glass slides .....	69
3.1.2	Hydrophobic glass slides .....	69
3.1.3	Highly Oriented Pyrolytic Graphite.....	70
3.1.4	Gold coating procedure .....	70
<b>3.2</b>	<b>Langmuir film formation and isotherms .....</b>	<b>71</b>
<b>3.3</b>	<b>LB deposition .....</b>	<b>72</b>
<b>3.4</b>	<b>SAM deposition.....</b>	<b>72</b>
<b>3.5</b>	<b>QCM preparation and measurements .....</b>	<b>73</b>
<b>3.6</b>	<b>SPR measurements .....</b>	<b>75</b>
<b>3.7</b>	<b>STS measurements .....</b>	<b>76</b>
<b>3.8</b>	<b>SHG measurements .....</b>	<b>77</b>
<b>3.9</b>	<b>Chemical characterisation techniques .....</b>	<b>78</b>
3.9.1	UV-VIS spectroscopy .....	78
<b>3.10</b>	<b>Synthesis .....</b>	<b>79</b>
3.10.1	1-Hexyl-2,6-dimethyl-pyridinium iodide .....	79
3.10.2	1-hexyl-2,6-bis-[2-(4-dibutylaminophenyl)-vinyl] pyridinium iodide (dye 8).....	79
3.10.3	1-Butyl-2,6-dimethyl-pyridinium iodide .....	80
3.10.4	1-Butyl-2,6-bis-[2-(4-dimethylamino naphthalen)- vinyl] pyridinium iodide (dye 11).....	81
<b>4</b>	<b>RESULTS AND DISCUSSION .....</b>	<b>82</b>
<b>4.1</b>	<b>Acceptor-<math>\sigma</math>-Donor structures.....</b>	<b>82</b>
4.1.1	Dye 1 .....	82
4.1.2	Dye 2 .....	88
<b>4.2</b>	<b>Acceptor-<math>\pi</math> bridge-donor structures.....</b>	<b>91</b>
4.2.1	Dye 3 .....	91
4.2.2	Hybrid structure 1: Au-S-CH <sub>2</sub> CH <sub>2</sub> CH <sub>2</sub> -SO <sub>3</sub> <sup>-</sup> / dye 4.....	95
<b>4.3</b>	<b>Donor-<math>\pi</math>-Acceptor-<math>\pi</math>-Donor structures.....</b>	<b>98</b>
4.3.1	Dye 5 and dye 6.....	98
4.3.2	Hybrid 2: Au-S-CH <sub>2</sub> CH <sub>2</sub> CH <sub>2</sub> -SO <sub>3</sub> <sup>-</sup> /dye 6.....	101

4.3.3	Dye 7 .....	103
4.3.4	Dye 8 .....	107
4.3.5	Hybrid 3: Au-S-CH <sub>2</sub> CH <sub>2</sub> CH <sub>2</sub> -SO <sub>3</sub> <sup>-</sup> / dye 7.....	110
4.3.6	Dye 9 .....	114
4.3.7	Hybrid 4: Au-S-CH <sub>2</sub> CH <sub>2</sub> CH <sub>2</sub> -SO <sub>3</sub> <sup>-</sup> / dye 9.....	120
4.3.8	Dye 10 .....	123
4.3.9	Hybrid structure 5: Au-S-CH <sub>2</sub> CH <sub>2</sub> CH <sub>2</sub> -SO <sub>3</sub> <sup>-</sup> /dye 10.....	126
4.3.10	Dye 11 .....	129
<b>5</b>	<b>CONCLUSIONS .....</b>	<b>133</b>
<b>6</b>	<b>REFERENCES .....</b>	<b>140</b>



## List of chemical nomenclature of studied dyes

- Dye 1            dodecyloxyphenyl carbamate of 2-bromo-5 (2'-hydroxyethoxy) tetracyanoquinodimethane
- Dye 2            3,5-dinitrobenzyl 7-(1-oxododecylamino)-pyren-2-ylcarbamate
- Dye 3            4-[*p*-(*N*-methyl-*N*-hexadecylamino)styryl]-4'-methyl-1,1'-ethylene-2,2'-bipyridinium dibromide
- Dye 4            4-[*p*-(*N,N*-dibutylamino)styryl]-4'-methyl-1,1'-ethylene-2,2'-bipyridinium dibromide
- Dye 5            4,4'-bis[*p*-(*N*-methyl-*N*-hexadecylamino)styryl]-1,1'-ethylene-2,2'-bipyridinium dibromide
- Dye 6            4,4'-bis[*p*-(*N,N*-dibutylamino)styryl]-1,1'-ethylene-2,2'-bipyridinium dibromide
- Dye 7            1-butyl-2,6-bis-[2-(4-dibutylamino-phenyl)-vinyl]-pyridinium iodide
- Dye 8            1-hexyl-2,6-bis-[2-(4-dibutylamino-phenyl)-vinyl]- pyridinium iodide
- Dye 9            1-butyl-2,6-bis-(2-{4-[2-(4-dibutylamino-phenyl)-ethyl]-phenyl}-vinyl)-pyridinium iodide
- Dye 10           1-butyl-2,6-bis-[2-(7-diethylamino-2-oxo-2H-chromen-3-yl)-vinyl]-pyridinium iodide
- Dye 11           1-butyl-2,6-bis-[2-(4-dimethylamino-naphthalen)- vinyl]-pyridinium iodide

# List of Figures

FIGURE 1-1 MOORE'S LAW .....	1
FIGURE 2-1 STRUCTURE OF A HEMIQUINONE .....	5
FIGURE 2-2 THEORETICAL MOLECULAR RECTIFIER .....	5
FIGURE 2-3 DISTRIBUTION OF THE MOLECULAR ORBITALS OF A RECTIFIER IN RELATION TO METAL ELECTRODES WHEN NO BIAS IS APPLIED; WHERE A AND B ARE HOMO AND LUMO OF THE ACCEPTOR, RESPECTIVELY; C AND D ARE HOMO AND LUMO OF THE DONOR, RESPECTIVELY; $\phi$ IS THE WORK FUNCTION OF ELECTRODES, AND $E_1$ AND $E_2$ ARE ELECTRODES. 6	6
FIGURE 2-4 ELECTRON TRANSPORT THROUGH THE AVIRAM AND RATNER RECTIFIER.....	6
FIGURE 2-5 ELECTRON TRANSPORT WHEN REVERSE POLARISATION IS APPLIED TO THE DEVICE .....	7
FIGURE 2-6 HEMIQUINONE STRUCTURE CONSISTED OF CATECHOL (DONOR), AND QUINONE (ACCEPTOR) .....	8
FIGURE 2-7 PT   DOP-C-BHTCNQ   MG, AG STRUCTURE .....	9
FIGURE 2-8 I-V CHARACTERISTICS OF PT   DOP-C-BHTCNQ   MG, AL SYSTEM, (A) JUST AFTER DEPOSITION, (B) AFTER ANNEALING AT 70°C.....	9
FIGURE 2-9 AG,MG   OHAPY-C-DNB   AG STRUCTURE .....	10
FIGURE 2-10 TTF DONOR- $\sigma$ -ACCEPTOR DIADS .....	11
FIGURE 2-11 C <sub>16</sub> H <sub>33</sub> -Q3CNQ STRUCTURE .....	12
FIGURE 2-12 I-V CHARACTERISTICS OF MG C <sub>16</sub> H <sub>33</sub> -Q3CNQ   PT STRUCTURES, (A) ONE, (B) THREE, (C) FOUR LB MONOLAYERS.....	13
FIGURE 2-13 I-V CHARACTERISTIC OF AG, MG C <sub>16</sub> H <sub>33</sub> -Q3CNQ  AG STRUCTURE .....	14
FIGURE 2-14 I-V CHARACTERISTICS OF (A) AG, MG  $\omega$ -TRICOSENOIC ACID  A <sup>+</sup> - $\pi$ -D <sup>-</sup>   $\omega$ -TRICOSENOIC ACID AG, AND (B) AG, MG  $\omega$ -TRICOSENOIC ACID  AG STRUCTURES.....	15
FIGURE 2-15 STRUCTURE OF (C <sub>10</sub> H <sub>21</sub> ) <sub>2</sub> N <sup>+</sup> -3CNQ <sup>-</sup> .....	16
FIGURE 2-16 STRUCTURES OF 5-(4-DIBUTYLAMINO-BENZYLIDENE)-2-OCTADECYL-5,6,7,8-TETRAHYDRO-ISOQUINOLINIUM OCTADECYLSULFATE AND OCTADECANOIC ACID .....	17
FIGURE 2-17 STRUCTURES OF E-4-[(N-ALKYL-5,6,7,8-TETRAHYDROISOQUINOLINIUM-5-YLIDENE)METHYL]-N,N-DIBUTYLANILINE OCTADECYL SULPHATE, (1) OCTADECYL AND (2) DODECYL ANALOGUES .....	18
FIGURE 2-18 STRUCTURE OF N-ALKYL-5-(4-DIALKYLAMINOBENZYLIDENE)-5,6,7,8-TETRAHYDROQUINOLINIUM IODIDE18	18
FIGURE 2-19 I-V CHARACTERISTICS OF STRUCTURE OF N-ALKYL-5-(4-DIALKYLAMINOBENZYLIDENE)-5,6,7,8-TETRAHYDROQUINOLINIUM IODIDE.....	19
FIGURE 2-20 STRUCTURE OF 4{2-[4-(N,N-DIBUTYLAMINOPHENYL)VINYL]-N-OCTADECYLQUINOLINIUM OCTADECYL SULFATE .....	20
FIGURE 2-21 HS-(CH <sub>2</sub> ) <sub>m</sub> -C <sub>6</sub> H <sub>4</sub> -(CH <sub>2</sub> ) <sub>n</sub> -SH SYSTEM .....	21
FIGURE 2-22 CHANG'S MOLECULE.....	21
FIGURE 2-23 I-V CHARACTERISTIC OF CH <sub>3</sub> CO-S-C <sub>N</sub> H <sub>2N</sub> -Q3CNQ STRUCTURE ( N=3, GREEN), (N=12, RED) .....	22
FIGURE 2-24 (A) ZWITTERIONIC AND (B) QUINOID GROUND STATE OF CH <sub>3</sub> CO-S-C <sub>N</sub> H <sub>2N</sub> -Q3CNQ.....	23
FIGURE 2-25 I-V CHARACTERISTIC OF AU-S-C <sub>10</sub> H <sub>20</sub> -Q3CNQ AFTER PROTONATION.....	23
FIGURE 2-26 STRUCTURE OF A POSSIBLE MOLECULAR RECTIFIER.....	24
FIGURE 2-27 STRUCTURE OF 4-[2-(4-DIMETHYLAMINO-PHENYL)-VINYL]-1-(10-MERCAPTO-DECYL)-QUINOLINIUM IODIDE 25	25

FIGURE 2-28 STRUCTURE OF IODIDE SALT OF A STERICALLY HINDERED D- $\pi$ -A .....	25
FIGURE 2-29 I-V CHARACTERISTICS OF TCNQ <sup>-</sup> SALT OF A STERICALLY HINDERED D- $\pi$ -A MEASURED BY (A) STM, AND (B) MERCURY DROP .....	26
FIGURE 2-30 STRUCTURES OF SA ANALOGUES FOR MOLECULAR RECTIFIERS STUDIED BY ASHWELL <i>ET AL.</i> .....	26
FIGURE 2-31 STRUCTURES OF 1-(10-MERCAPTO-DECYL)-4-[2-(4-METHOXY-PHENYL)-VINYL]-PYRIDINIUM IODIDE.....	27
FIGURE 2-32 STRUCTURE OF 1-(10-ACETYSULFANYLDECYL)-4-{2-(4-DIMETHYLAMINONAPHTHALEN-1-YL)-VINYL}-QUINOLINIUM IODIDE .....	27
FIGURE 2-33 I-V CHARACTERISTICS OF (A) 1-(10-ACETYSULFANYLDECYL)-4-{2-(4-DIMETHYLAMINO NAPHTHALEN-1-YL)-VINYL}-QUINOLINIUM IODIDE MEASURED BEFORE, AND (B) AFTER PROTONATION .....	28
FIGURE 2-34 ELLENBOGEN AND LOVE RECTIFIER.....	29
FIGURE 2-35 STRUCTURE OF PHTHALOCYANINE STUDIED BY ZHOU <i>ET AL.</i> .....	29
FIGURE 2-36 STRUCTURE OF DIMETHYLANILINOAZA[C60]FULLERENE .....	30
FIGURE 2-37 STRUCTURE OF THE CHEVRON-SHAPED MOLECULE' .....	31
FIGURE 2-38 SUGGESTED ALIGNMENT OF THE CHEVRON-SHAPED MOLECULE BETWEEN ELECTRODES .....	31
FIGURE 2-39 U-SHAPED RECTIFIER CONTAINING FULLERENE.....	32
FIGURE 2-40 Ag   SAM1    SAM2   Hg JUNCTIONS STUDIED BY WHITESIDES <i>ET AL.</i> .....	33
FIGURE 2-41 PHENYL AND QUINOID FORMS OF NAB.....	33
FIGURE 2-42 STRUCTURES OF (A) PCPD, (B) PTCDI AND (C) LAYER CONFIGURATION OF THE HYBRID .....	34
FIGURE 2-43 SCHEMATIC DIAGRAM OF THE ESTIMATED ENERGY LEVELS OF THE PCPD AND THE PTCDI COMPARED TO THE GOLD FERMI ENERGY LEVEL .....	35
FIGURE 2-44 STRUCTURE OF CUPC (DONOR) AND ROSE BENGAL (ACCEPTOR) .....	35
FIGURE 2-45 STRUCTURE OF A HYBRID STRUCTURE CONTAINING SQUARAINES .....	36
FIGURE 2-46 I-V CHARACTERISTIC OF A HYBRID STRUCTURE CONTAINING SQUARAINES.....	37
FIGURE 2-47 HYBRID STRUCTURE OF 4,4'-BIPYRIDINIUM AND COPPER PHTHALOCYANINE-3,4',4'',4'''-TETRASULFONATE	37
FIGURE 2-48 I-V CHARACTERISTIC OF HYBRID STRUCTURE OF 4,4'-BIPYRIDINIUM AND COPPER PHTHALOCYANINE-3,4',4'',4'''-TETRASULFONATE .....	38
FIGURE 2-49 STRUCTURE OF THE 7 NM WIRE .....	38
FIGURE 2-50 I-V CHARACTERISTICS OF (A) 7 NM WIRE, (B) HYBRID STRUCTURE OF THE 7 NM WIRE AND PC.....	39
FIGURE 2-51 HYBRID STRUCTURES OF Au-S-C <sub>3</sub> H <sub>6</sub> -SO <sub>3</sub> <sup>-</sup>   A+- $\pi$ -D   Au STRUCTURES .....	40
FIGURE 2-52 Au-S-C <sub>10</sub> H <sub>20</sub> -A+- $\pi$ -D   D <sup>-</sup>   Au STRUCTURES .....	41
FIGURE 2-53 I-V CHARACTERISTIC OF Au-S-C <sub>10</sub> H <sub>20</sub> -A+- $\pi$ -D   D <sup>-</sup>   Au STRUCTURE, WHERE THE CATIONIC MOIETY WAS 5-(4-DIMETHYLAMINOBENZYLIDENE)-5,6,7,8-TETRAHYDROISOQUINOLINIUM, AND THE ANIONIC DONOR (FORMING THE SECOND LAYER) WAS COPPER (II) PHTHALOCYANINE-3,4',4'',4'''-TETRASULFONATE .....	42
FIGURE 2-54 MOLECULAR STRUCTURE OF STEARIC ACID, A TYPICAL AMPHIPHILIC MOLECULE .....	44
FIGURE 2-55 STRUCTURES OF ANTHRACENE DERIVATIVES STUDIED BY STEWART.....	44
FIGURE 2-56 (A) STEARIC ACID, (B) OLEIC ACID, CIS FORM, (C) ELAIDIC ACID, TRANS FORM.....	45
FIGURE 2-57 STRUCTURE OF SQUARAINES STUDIED BY ASHWELL <i>ET AL.</i> .....	45
FIGURE 2-58 STRUCTURES OF DIFFERENT CHEVRON-SHAPED LIQUID CRYSTALS.....	46
FIGURE 2-59 STRUCTURE OF A CHEVRON-SHAPED MOLECULE STUDIED BY ASHWELL.....	47

FIGURE 2-60 STRUCTURE OF A CHEVRON-SHAPED MOLECULE STUDIED BY DUFF <i>ET AL.</i> .....	48
FIGURE 2-61 THE ALIGNMENT OF THE AMPHIPHILIC MOLECULES IN A LANGMUIR FILM AT THE AIR-WATER INTERFACE .....	49
FIGURE 2-62 WILHELMY PLATE ARRANGEMENT.....	49
FIGURE 2-63 THE ISOTHERM OF STEARIC ACID; (A) SOLID PHASE, (B) LIQUID PHASE, (C) GAS PHASE .....	50
FIGURE 2-64 MECHANISM OF DEPOSITION OF THE LANGMUIR FILM ONTO A SOLID SUBSTRATE TO FORM AN LB FILM .....	53
FIGURE 2-65 X,Y AND Z-TYPE ALIGNMENT OF MULTILAYER LB FILMS' .....	53
FIGURE 2-66 SAM FORMATION ON A SUBSTRATE .....	54
FIGURE 2-67 STRUCTURE OF SA MOLECULE.....	55
FIGURE 2-68 MONOLAYER FORMATION VIA DIFFERENT 'HEAD GROUPS' .....	55
FIGURE 2-69 ORGANOSULFUR COMPOUNDS'' .....	56
FIGURE 2-70 STRUCTURE OF PYRIDINE DISULFIDE STUDIED BY TANIGUCHI.....	56
FIGURE 2-71 FORMATION OF SAMs FROM SOLUTION .....	59
FIGURE 2-72 QUARTZ CRYSTAL MICROBALANCE STRUCTURE .....	60
FIGURE 2-73 KRETSCHMANN CONFIGURATION' .....	62
FIGURE 2-74 SPECTRUM OF REFLECTIVITY OF LIGHT AS A FUNCTION OF THE INCIDENCE ANGLE .....	63
FIGURE 2-75 STM APPARATUS .....	64
FIGURE 2-76 SECOND-HARMONIC GENERATION .....	66
FIGURE 3-1 BOC EDWARDS 360 AUTOMATIC COATER .....	71
FIGURE 3-2 LB TROUGH (NIMA 621) .....	71
FIGURE 3-3 TWO-COMPARTMENT LB TROUGH (NIMA 622).....	72
FIGURE 3-4 CIRCULAR LB TROUGH, (NIMA 2000) .....	74
FIGURE 3-5 QCM SETUP .....	74
FIGURE 3-6 SPR SETUP .....	75
FIGURE 3-7 DIGITAL INSTRUMENTS MULTIMODE STM.....	76
FIGURE 3-8 SHG SETUP .....	77
FIGURE 3-9 REACTION SCHEME OF 1-HEXYL-2,6-DIMETHYL-PYRIDINIUM IODIDE .....	79
FIGURE 3-10 REACTION SCHEME OF 1-HEXYL-2,6-BIS-[2-(4-DIBUTYLAMINOPHENYL)-VINYL] PYRIDINIUM IODIDE (DYE VI) 80	
FIGURE 3-11 REACTION SCHEME OF 1-BUTYL-2,6-DIMETHYL-PYRIDINIUM IODIDE .....	81
FIGURE 3-12 REACTION SCHEME OF 1-BUTYL-2,6-BIS-[2-(4-DIMETHYLAMINO NAPHTHALEN)-VINYL] PYRIDINIUM IODIDE (DYE VIII).....	81
FIGURE 4-1 STRUCTURE OF DYE 1.....	82
FIGURE 4-2 ISOTHERMS OF DYE 1.....	83
FIGURE 4-3 UV-VIS SPECTRA OF DYE 1; (A) IN CHLOROFORM SOLUTION, (B) AN LB MONOLAYER ON GLASS SLIDE .....	84
FIGURE 4-4 I-V CHARACTERISTICS OF Au  DYE 1  PTIR; DYE1 WAS DEPOSITED AT DIFFERENT PRESSURES; (1) 10 MN/M, (2) 13 MN/M, RR=6 (3) 16 MN/M, RR=20 (4) 17 MN/M, RR=8 (5) 19 MN/M, RR=8 (6) 20 MN/M .....	86
FIGURE 4-5 STRUCTURE OF DYE 2.....	88
FIGURE 4-6 ISOTHERM OF DYE 2 .....	89

FIGURE 4-7 SPECTRUM OF DYE 2 IN CHLOROFORM SOLUTION .....	90
FIGURE 4-8 REPRESENTATIVE I–V CHARACTERISTICS OF Au   DYE 2   PTIR; (1) RR=1.5 AT ± 1 V, (2) RR=6 AT ± 1 V ....	90
FIGURE 4-9 STRUCTURE OF DYE 3.....	92
FIGURE 4-10 ISOTHERMS OF DYE 3.....	92
FIGURE 4-11 UV-VIS SPECTRA OF DYE 3; (A) IN CHLOROFORM SOLUTION, (B) LB FILM ON A GLASS SLIDE .....	93
FIGURE 4-12 REPRESENTATIVE I–V CHARACTERISTICS OF Au   DYE 3   PTIR; (1) RR=3.4 AT ± 1 V, (2) RR=16 AT ± 1 V	94
FIGURE 4-13 HYBRID STRUCTURE 1 .....	95
FIGURE 4-14 STRUCTURE OF SODIUM 3-MERCAPTO-1-PROPANESULFONATE ON THE GOLD SURFACE .....	96
FIGURE 4-15 THIOL DEPOSITION ONTO QCM.....	96
FIGURE 4-16 QCM OF DYE 4 DEPOSITED BY IMMERSION IN ETHANOL SOLUTION ONTO THE THIOL SURFACE .....	97
FIGURE 4-17 REPRESENTATIVE I–V CHARACTERISTICS OF HYBRID STRUCTURE 1: Au-S-CH <sub>2</sub> CH <sub>2</sub> CH <sub>2</sub> -SO <sub>3</sub> <sup>-</sup> / DYE 4, (DYE 4 WAS DEPOSITED AS SA); (1) RR=11 AT ± 1 V, (2) RR=1 AT ± 1 V, (3) RR=4.5 AT ± 1 V.....	98
FIGURE 4-18 STRUCTURE OF DONOR–π –ACCEPTOR–π –DONOR STRUCTURE, DYE 5 (N=16, M=1), DYE 6 (N=4, M=4) ..	99
FIGURE 4-19 ISOTHERM OF DYE 5 .....	99
FIGURE 4-20 UV-VIS SPECTRA OF DYE 5; (A) IN CHLOROFORM SOLUTION, (B) LB FILM ON GLASS SLIDE .....	100
FIGURE 4-21 I–V CHARACTERISTICS OF DYE 5; (1) RR=3.5 AT ± 1 V, (2) RR=15 AT ± 1 V.....	101
FIGURE 4-22 HYBRID STRUCTURE 2 .....	102
FIGURE 4-23 QCM OF DYE 6 DEPOSITED BY IMMERSION IN ETHANOL SOLUTION ONTO Au-S-CH <sub>2</sub> CH <sub>2</sub> CH <sub>2</sub> -SO <sub>3</sub> <sup>-</sup> SURFACE .....	102
FIGURE 4-24 REPRESENTATIVE I–V CHARACTERISTICS OF HYBRID 2: Au-S-CH <sub>2</sub> CH <sub>2</sub> CH <sub>2</sub> -SO <sub>3</sub> <sup>-</sup> /DYE 6, (DYE 6 WAS DEPOSITED AS SAM); (1) RR=6.5 AT ± 1 V, (2) RR=21 AT ± 1 V .....	103
FIGURE 4-25 STRUCTURE OF DYE 7.....	104
FIGURE 4-26 ISOTHERM OF DYE 7.....	105
FIGURE 4-27 UV–VIS SPECTRUM OF DYE 7, (A) IN CHLOROFORM SOLUTION, (B) ON GLASS SLIDE .....	105
FIGURE 4-28 REPRESENTATIVE I–V CHARACTERISTIC OF Au   DYE 7   PTIR .....	107
FIGURE 4-29 STRUCTURE OF DYE 8.....	108
FIGURE 4-30 ISOTHERM OF DYE 8.....	108
FIGURE 4-31 UV-VIS SPECTRUM OF DYE 8 IN CHLOROFORM SOLUTION .....	109
FIGURE 4-32 REPRESENTATIVE I–V CHARACTERISTIC OF Au   DYE 8   PTIR .....	110
FIGURE 4-33 STRUCTURE OF HYBRID 3: Au-S-CH <sub>2</sub> CH <sub>2</sub> CH <sub>2</sub> -SO <sub>3</sub> <sup>-</sup> / DYE 7.....	111
FIGURE 4-34 QCM OF DYE 7 DEPOSITED BY IMMERSION IN SOLUTION ONTO Au-S-CH <sub>2</sub> CH <sub>2</sub> CH <sub>2</sub> -SO <sub>3</sub> <sup>-</sup> SURFACE .....	112
FIGURE 4-35 REPRESENTATIVE I–V CHARACTERISTICS OF HYBRID STRUCTURE 3: Au-S-CH <sub>2</sub> CH <sub>2</sub> CH <sub>2</sub> -SO <sub>3</sub> <sup>-</sup> / DYE 7, (DYE 7 WAS DEPOSITED AS A SAM); (1) RR~5 AT ±1V, (2) RR~23 AT ±1V .....	112
FIGURE 4-36 REPRESENTATIVE I–V CHARACTERISTIC OF A THIOL MONOLAYER.....	113
FIGURE 4-37 REPRESENTATIVE I–V CHARACTERISTICS OF HYBRID STRUCTURE 3: Au-S-CH <sub>2</sub> CH <sub>2</sub> CH <sub>2</sub> -SO <sub>3</sub> <sup>-</sup> / DYE 7, (DYE 7 WAS DEPOSITED AS AN LB FILM).....	114
FIGURE 4-38 STRUCTURE OF DYE 9.....	115
FIGURE 4-39 ISOTHERM OF DYE 9.....	116

FIGURE 4-40 UV-VIS SPECTRUM OF DYE 9 IN CHLOROFORM SOLUTION .....	116
FIGURE 4-41 REPRESENTATIVE I–V CHARACTERISTIC OF Au   DYE 9   PTIR (AFTER DEPOSITION) .....	117
FIGURE 4-42 REPRESENTATIVE I–V CHARACTERISTIC OF Au   DYE 9   PTIR ( 3 HOURS AFTER DEPOSITION).....	118
FIGURE 4-43 TIME DEPENDENCE OF THE SUPPRESSION OF THE SECOND-HARMONIC INTENSITY OF FOUR LB FILMS FOLLOWING DEPOSITION ON GLASS SUBSTRATES. THE DIFFERENT INITIAL INTENSITIES ARE CONSISTENT WITH THE FILM STRUCTURE BEING INHERENTLY UNSTABLE .....	119
FIGURE 4-44 UV–VIS SPECTRA OF A MONOLAYER LB FILM OF DYE 9, (RED CURVE) JUST AFTER DEPOSITION, (GREEN CURVE) 3 HOURS AFTER THE DEPOSITION.....	120
FIGURE 4-45 HYBRID STRUCTURE 4: Au-S-CH <sub>2</sub> CH <sub>2</sub> CH <sub>2</sub> -SO <sub>3</sub> <sup>-</sup> /DYE 9 .....	120
FIGURE 4-46 QCM OF DYE 9 DEPOSITED ON ANIONIC SURFACE BY IMMERSION IN CHLOROFORM SOLUTION .....	121
FIGURE 4-47 REPRESENTATIVE I–V CHARACTERISTIC OF HYBRID STRUCTURE 4: Au-S-CH <sub>2</sub> CH <sub>2</sub> CH <sub>2</sub> -SO <sub>3</sub> <sup>-</sup> /DYE 9, (DYE 9 WAS DEPOSITED AS A SAM).....	122
FIGURE 4-48 REPRESENTATIVE I–V CHARACTERISTIC OF HYBRID STRUCTURE 4: Au-S-CH <sub>2</sub> CH <sub>2</sub> CH <sub>2</sub> -SO <sub>3</sub> <sup>-</sup> /DYE 9, (DYE 9 WAS DEPOSITED AS LB FILM).....	123
FIGURE 4-49 STRUCTURE OF DYE 10 .....	123
FIGURE 4-50 ISOTHERM OF DYE 10 .....	124
FIGURE 4-51 UV–VIS SPECTRUM OF THE LB MONOLAYER OF DYE 10 ON GLASS SLIDE .....	125
FIGURE 4-52 REPRESENTATIVE I–V CHARACTERISTIC OF Au   DYE 10   PTIR .....	125
FIGURE 4-53 HYBRID STRUCTURE 5: Au-S-CH <sub>2</sub> CH <sub>2</sub> CH <sub>2</sub> -SO <sub>3</sub> <sup>-</sup> /DYE 10.....	126
FIGURE 4-54 REPRESENTATIVE I–V CHARACTERISTICS OF HYBRID STRUCTURE 5: Au-S-CH <sub>2</sub> CH <sub>2</sub> CH <sub>2</sub> -SO <sub>3</sub> <sup>-</sup> /DYE 10, (DYE 10 WAS DEPOSITED AS A LB).....	127
FIGURE 4-55 QCM OF DYE 10 DEPOSITED BY IMMERSION IN ACETONE SOLUTION ONTO AN IONIC SURFACE .....	128
FIGURE 4-56 REPRESENTATIVE I–V CHARACTERISTICS OF HYBRID 5: Au-S-CH <sub>2</sub> CH <sub>2</sub> CH <sub>2</sub> -SO <sub>3</sub> <sup>-</sup> /DYE 10, (DYE 10 WAS DEPOSITED AS A SAM).....	128
FIGURE 4-57 STRUCTURE OF DYE 11 .....	129
FIGURE 4-58 ISOTHERM OF DYE 11 .....	130
FIGURE 4-59 UV–VIS SPECTRA OF DYE 11; (A) IN CHLOROFORM SOLUTION, (B) LB MONOLAYER ON GLASS SLIDE .....	131
FIGURE 4-60 REPRESENTATIVE I–V CHARACTERISTIC OF Au   DYE 11   PTIR .....	132

## List of tables

TABLE 4-1 AREA PER MOLECULE OF DYE 1.....	84
TABLE 4-2 AREA PER MOLECULE OF DYE 11.....	132
TABLE 5-1 I–V CHARACTERISTICS OF ALL COMPOUNDS STUDIED .....	133

## Abbreviations

D–electron bridge–A	Donor–electron bridge–Acceptor
D– $\sigma$ –A	Donor– $\sigma$ bridge–Acceptor
D– $\pi$ –A	Donor– $\pi$ bridge–Acceptor
D– $\pi$ –A– $\pi$ –D	Donor– $\pi$ bridge–Acceptor– $\pi$ bridge–Donor
LB	Langmuir–Blodgett
SA	Self–assembly
SAM	Self-assembled monolayer
QCM	Quartz-crystal microbalance
SPR	Surface plasmon resonance
STM	Scanning tunnelling microscope
STS	Scanning tunnelling spectroscopy
I–V	Current–voltage
RR	Rectification ratio
TCNQ	7,7',8,8'-tetracyanoquinodimethane
TTF	Tetrathiafulvalene
HOPG	Highly-oriented pyrolytic graphite
HOMO	Highest occupied molecular orbital
LUMO	Lowest unoccupied molecular orbital
AFM	Atomic force microscope
IR	Infrared
$A_0$	Molecular area measured at 0 mN/m
$A_c$	Molecular area measured at collapse point of the LB monolayer
$A_t$	Molecular area measured at the transfer pressure



Hybrid structure 1:	$\text{Au-S-CH}_2\text{CH}_2\text{CH}_2\text{-SO}_3^-$ / <b>dye 4</b>
Hybrid structure 2:	$\text{Au-S-CH}_2\text{CH}_2\text{CH}_2\text{-SO}_3^-$ / <b>dye 6</b>
Hybrid structure 3:	$\text{Au-S-CH}_2\text{CH}_2\text{CH}_2\text{-SO}_3^-$ / <b>dye 7</b>
Hybrid structure 4:	$\text{Au-S-CH}_2\text{CH}_2\text{CH}_2\text{-SO}_3^-$ / <b>dye 9</b>
Hybrid structure 5:	$\text{Au-S-CH}_2\text{CH}_2\text{CH}_2\text{-SO}_3^-$ / <b>dye 10</b>

# 1 Introduction

## 1.1 Nanotechnology

In the last few decades, the miniaturisation process has been the driving force of major technological innovations, and a number of important scientific discoveries, what we now call nanotechnology<sup>2,3,4,5</sup>. The idea of nanotechnology can be attributed to Richard Feynman, who gave his famous lecture *'there's plenty room at the bottom'* in 1959<sup>6</sup>. In his talk he outlined the benefits that might occur from manufacturing devices on the very small scale. Among others, he forecasted the possibility of making machines that could pick-up and place single atoms. Later, Drexler<sup>7</sup> defined nanotechnology as, *'the principle of atom manipulation, atom-by-atom, through control of the structure of matter at the molecular level. It entails the ability to build molecular systems with atom-by-atom precision, yielding a variety of nanomachines.'*

Currently, some electronic components such as diodes and transistors are based on silicon<sup>8,9</sup>. In 1965 Moore<sup>10</sup> predicted that integrated circuits (IC) would become the future of the electronics. His law established in the 1960's, showing the exponential decrease of electronic device size with time has so far been fulfilled. It has been achieved thanks to the so-called top-down approach driven by progress in lithographic techniques (see **Figure 1-1**).

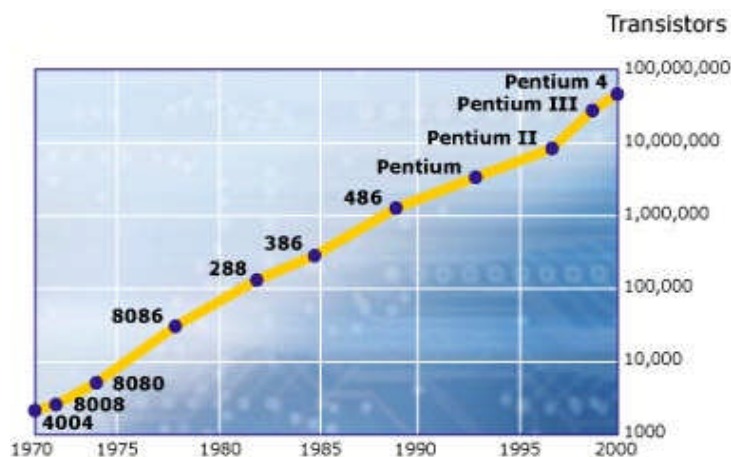


**Figure 1-1 Moore's law<sup>11</sup>**

Moore<sup>10</sup> predicted that the power of silicon-based computer chips would double every 18–24 months. Unfortunately, silicon-based devices are unavoidably approaching their size limits and further miniaturisation soon will not be possible using current technology. Although the industry is continuing to make the existing components smaller and smaller, it has become necessary to find and develop materials<sup>12,13,14,15</sup>, scientific tools<sup>3,16,17</sup> and advanced technologies that overcome the obstacles associated with the miniaturisation process.

## 1.2 The bottom-up approach

A promising alternative to the top-down approach (restricted by physical limitations of lithographic processes) seems to be the bottom-up approach, which gives an opportunity to build nanostructures from atoms, molecules and nanoparticles based on chemical synthesis and/or the highly controlled deposition and growth of materials.

Several new molecular electronic systems have been introduced and explored leading to the development of fully operational devices<sup>2,18,19</sup>. Also the invention of the scanning tunnelling microscope (STM) by Binnig and Rohrer<sup>16</sup> in 1981, and related techniques was a milestone that brought science closer to fulfilling this aim.

## 1.3 Aims

The main objective of the research was to find organic rectifiers with high rectification ratios (RR) for future applications within molecular electronics. The work included the verification of the model proposed by Aviram and Ratner<sup>1</sup>, and attempted to reveal how the molecular structure and alignment affected the rectifying properties of organic molecules. The knowledge of these allowed for a better understanding of the monolayer behaviour and the electron transport through the organic material when deposited between electrodes. In order to fulfil these aims, a number of specific candidates were investigated and they included:

- typical Langmuir-Blodgett (LB) structures,
- chevron-shaped compounds,
- ionically assembled structures, called also hybrid structures.

## 1.4 Summary

A number of organic compounds based on acceptor–electron bridge–donor structure were studied in order to investigate the alignment and rectifying properties when placed between non–oxidisable electrodes. Verification of the Aviram and Ratner concept<sup>1</sup> of a molecular rectifier proved difficult. This was mainly due to the possible presence of  $\Gamma^-$  or  $\text{Br}^-$  ions within the monolayer which could take part in the electron transport through the monolayer. Studies of chevron–shaped molecules showed that molecules without long aliphatic chains can be deposited using the LB technique. However, reduction of the carbohydrate chain resulted in the formation of disordered and unstable monolayers.

This work demonstrated that it is essential to produce stable and ordered monolayer in order to obtain reproducible asymmetric I–V characteristics. Implementation of an ionic assembly as an alternative deposition technique to Langmuir–Blodgett (LB) or self–assembly (SA) seemed to be successful in obtaining this aim. Formation of ionically assembled structures by deposition of chevron–shaped molecules on anionically modified substrates, not only improved the desired ordering and stabilisation, but also improved rectification.

## 2 Background and literature

### 2.1 Molecular rectification

There has been much interest in molecular rectifiers and in molecular electronics<sup>18,20,21</sup>. Years of research which concentrated around organic molecular junctions<sup>22,23,24</sup> showed that the molecular structure defined the conformation, orientation, packing and stabilisation of the molecules within the monolayer and these determined the conductance properties<sup>25,26</sup>. The knowledge allowed for an understanding of the monolayer behaviour, and helped to predict whether the molecule might become a successful material for molecular devices such as diodes.

Early research regarding molecular rectification was reported in 1964 when Meinhard<sup>27</sup> observed the rectification behaviour of an organic junction fabricated from bulk bilayers of n-type and p-type materials. However, as later studies showed<sup>28,29,30</sup>, due to the use of lead electrodes, the rectifying behaviour probably arose from an oxide-induced Schottky barrier<sup>31,32,33</sup>. The Schottky barrier is an intrinsic energy barrier that forms when there is a difference between Fermi energies of the materials generating the junction<sup>31,32</sup>. It arises at the interface of most metal–semiconductor junctions (often between a metal and its oxide) and it can significantly change the I–V characteristics.

Later, in 1974, Aviram and Ratner<sup>1</sup> proposed a breakthrough concept of a molecular rectifier and since then the growth of interest around molecular electronics has been noted.

#### **2.1.1 The Aviram and Ratner model<sup>1</sup>**

The rectifier proposed by Aviram and Ratner<sup>1</sup> comprised of two parts: donor and acceptor subunits, connected by a covalent saturated  $\sigma$ -bridge. The presence of the bridge in the structure was essential, as it provided the necessary isolation between the donor and acceptor sections of the molecule. More recently the model of a molecular rectifier has been modified and a twisted  $\pi$ -bridge<sup>34,35</sup> was used to break the conjugation. The electrical device is formed when the molecular rectifier is aligned

between two metallic electrodes. In order for rectification to occur, it is required for the donor to have a low ionisation potential (IP), while the acceptor has to exhibit a high electron affinity. An organic molecule that could fulfil the requirements of the Aviram and Ratner model<sup>1</sup> was a hemiquinone (see **Figure 2-1**).

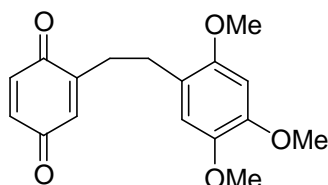


**Figure 2-1 Structure of a hemiquinone<sup>1</sup>**

The oxygen groups (=O) raised the electron affinity of one subunit, whereas the methoxy groups (–OCH<sub>3</sub>) lowered the ionisation potential of the other. Another very well-known simplified schematic of the Aviram and Ratner model<sup>1</sup> is the rectifier depicted in **Figure 2-2**. It is a theoretical molecular rectifier, where the acceptor is 7,7,8,8-tetra-cyanoquinodimethane (TCNQ) and the donor is tetrathiafulvalene (TTF). However, this molecule has never been synthesised.

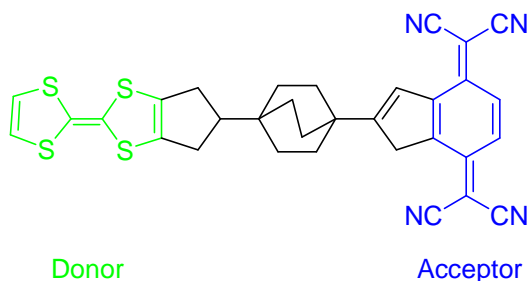


**Figure 2-2 Theoretical molecular rectifier<sup>1</sup>**

According to the Aviram and Ratner theory<sup>1</sup>, when a voltage was not applied to the device, the molecular orbitals of the molecule were distributed in relation to the electrodes as depicted in **Figure 2-3**. It is necessary for orbital B, which represents the lowest unoccupied molecular orbital (LUMO) of the acceptor to be totally or partially empty. It should also be located at, or slightly above the Fermi energy level of the electrode E<sub>1</sub>. Additionally, orbital C, which represents the highest occupied molecular orbital (HOMO) of the donor, should lie below orbital B.

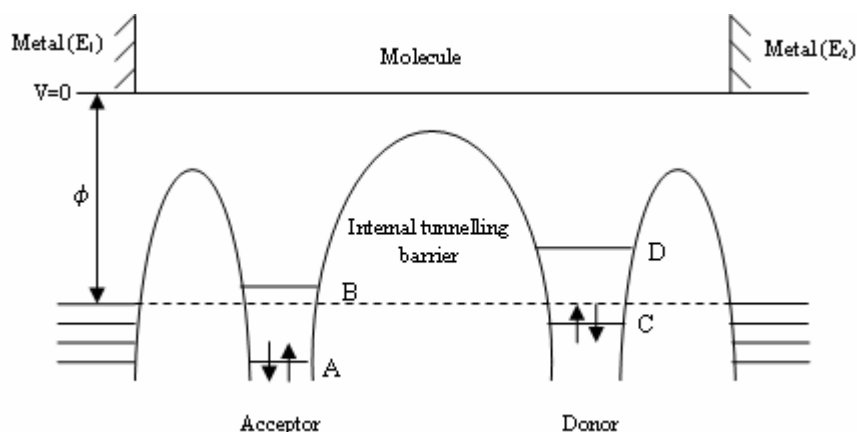


**Figure 2-3** Distribution of the molecular orbitals of a rectifier in relation to metal electrodes when no bias is applied; where A and B are HOMO and LUMO of the acceptor, respectively; C and D are HOMO and LUMO of the donor, respectively;  $\phi$  is the work function of electrodes, and  $E_1$  and  $E_2$  are electrodes<sup>1</sup>.

If these requirements are fulfilled, and an appropriate voltage is applied to the device, then electron transport through the molecule should be observed (see **Figure 2-4**).

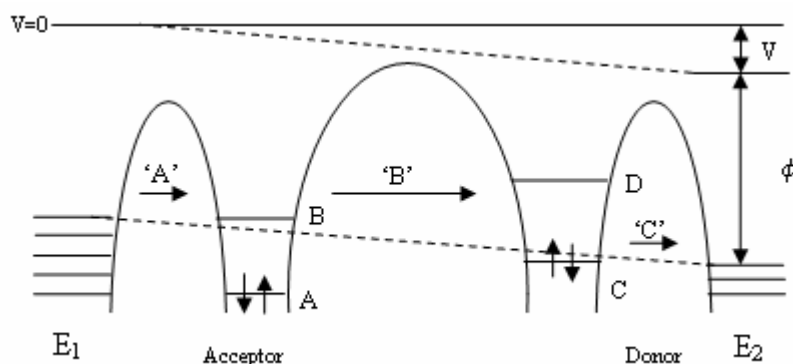


**Figure 2-4** Electron transport through the Aviram and Ratner rectifier<sup>1</sup>

The process of electron transport across a molecule placed between two electrodes can be divided into three steps. During the first step, 'A' (see **Figure 2-4**) an electron tunnels from the cathode to the LUMO of the acceptor subunit. However, this is only possible when the voltage is sufficient to overcome the energy difference between the work function of the cathode and the LUMO of the acceptor. The second step, 'C', occurs simultaneously with the first, with an electron tunnelling to the anode from the HOMO of the donor subunit. This process leads to the excited state of the molecule ( $A^-$ -electron bridge- $D^+$ ). During the final step, 'B', an electron travels from the acceptor to

the donor subunit and as a result, the molecule returns to its ground state (D–electron bridge–A). If the bias is reversed, a larger applied voltage is needed to enable electron tunnelling through the molecule, as there is an energy mismatch between the Fermi energies and the appropriate molecular levels in this direction<sup>1</sup> (see **Figure 2-5**).

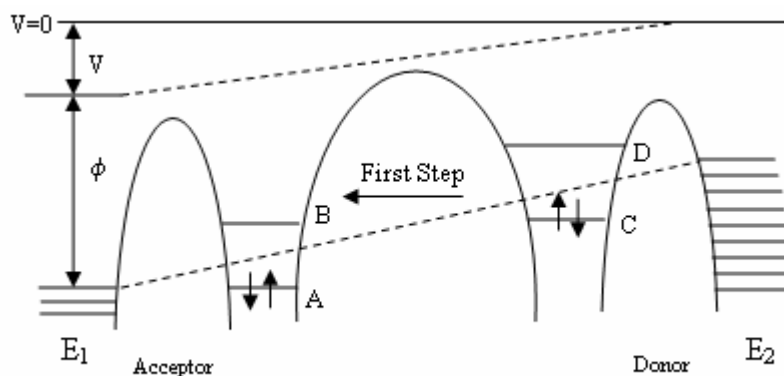


**Figure 2-5** Electron transport when reverse polarisation is applied to the device<sup>1</sup>

## 2.2 Molecular rectifiers

Since the concept of a ‘molecular rectifier’ has been proposed, a considerable amount of effort has been made to understand the mechanism of the electron transport through the molecule. Various molecular structures were assembled using different deposition techniques (LB<sup>36,37,38,39</sup>, SA<sup>40,41</sup>, ionic assembly<sup>42,43</sup>), and different methods used to study the electrical behaviour of organic monolayers (STM<sup>16,44</sup>, atomic force microscopy (AFM)<sup>45</sup>, Hg drop junction<sup>46</sup>, mechanically controlled break junction<sup>47</sup>, nanopore<sup>48</sup>, cross wires<sup>49</sup>, *etc.*). These showed that control over the position of an individual molecule on the surface during I–V measurements could be difficult. Inappropriate metal contacts<sup>50,51</sup> and/or too high voltage bias applied to the studied system<sup>52,53,54</sup> can cause irreversible changes to the monolayer and lead to the misinterpretation of I–V data. In order to avoid this, great care must be taken when the organic junctions are fabricated and when the measurements are performed.



## 2.2.1 Sigma ( $\sigma$ )–bridged molecular structures

The first studies on D– $\sigma$ –A structures were reported in the 1980's. In 1983, Saito *et al.*<sup>55</sup> showed rectification from Langmuir-Blodgett (LB) films based on merocyanine and triphenylmethane dye derivatives. Then in 1985, rectification from films that consisted of mixed monolayers of surfactant derivatives of semiconducting dyes and arachidic acid was reported<sup>56</sup>. However, in both cases, oxidisable aluminium (Al) and silver (Ag) electrodes were used to monitor the diode-like behaviour, and therefore, the rectification was subsequently associated with the formation of a Schottky barrier<sup>33</sup>.

In 1988, the rectifying behaviour of a single molecule (hemiquinone)<sup>57</sup> deposited on a gold surface and contacted via STM tip was reported (see **Figure 2-6**).

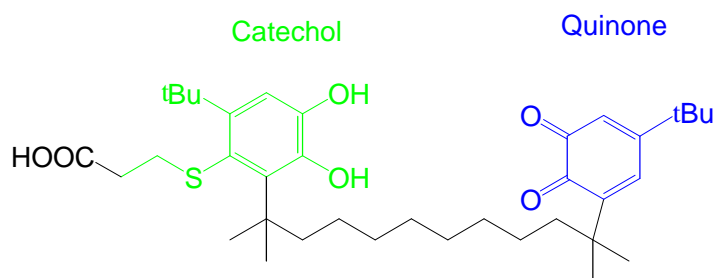


**Figure 2-6** Hemiquinone structure consisted of catechol (donor), and quinone (acceptor)<sup>57</sup>

Rectification (observed at the negative tip bias) was, at the beginning, attributed to the molecular structure. Although hemiquinone represents the A– $\sigma$ –D structure, the electron transport through the junction appeared to have followed a slightly different mechanism to the one proposed by Aviram and Ratner<sup>1</sup>. It was assumed that when the tip was negative and the substrate positive, an electron travelled from the tip to quinone (acceptor) and from catechol (donor) to the substrate. Then the one-proton motion from the positively charged catechol to the negatively charged quinone would produce two neutral semiquinones (free radicals). It was suggested that semiquinones would behave as conductors, which lowered the potential barrier between the tip and the surface and increased current flow through the molecule. This explanation however, was later retracted<sup>58</sup> when similar behaviour was also observed in systems lacking these molecules.

In order to perform an experimental test of the Aviram and Ratner concept<sup>1</sup>, and attempt to fully understand the conduction process through the organic monolayers, Sambles *et al.*<sup>28,59</sup>, studied the systems of Pt | DOP-C-BHTCNQ | Mg, Ag (see Figure 2-7).

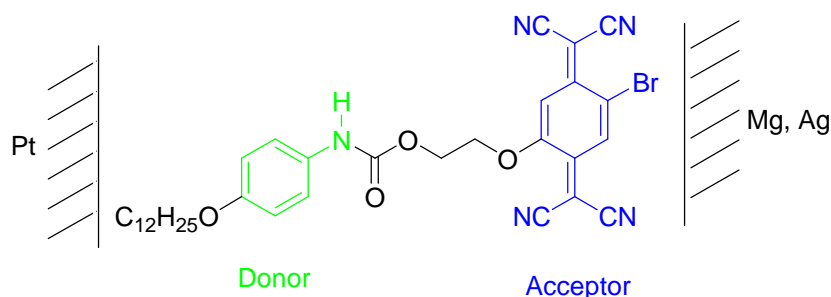


Figure 2-7 Pt | DOP-C-BHTCNQ | Mg, Ag structure<sup>28</sup>

According to the Aviram and Ratner theory<sup>1</sup>, when an organic molecule of the A- $\sigma$ -D structure was sandwiched between two electrodes, the preferable direction of electron flow was from the acceptor to the donor. Sambles *et al.*<sup>28</sup> believed that due to the hydrophobic character of the bottom platinum (Pt) electrode used in the experiment, molecules were aligned in such a way that the acceptor part was located closer to the top electrode, even though the monolayer was deposited on the upstroke. This suggested that when a voltage bias was applied to the system, the higher current should be observed in the positive quadrant of the I-V plot and this agreed with recorded data. However, the measurements showed hysteresis even after annealing the sample at 70°C (see Figure 2-8).

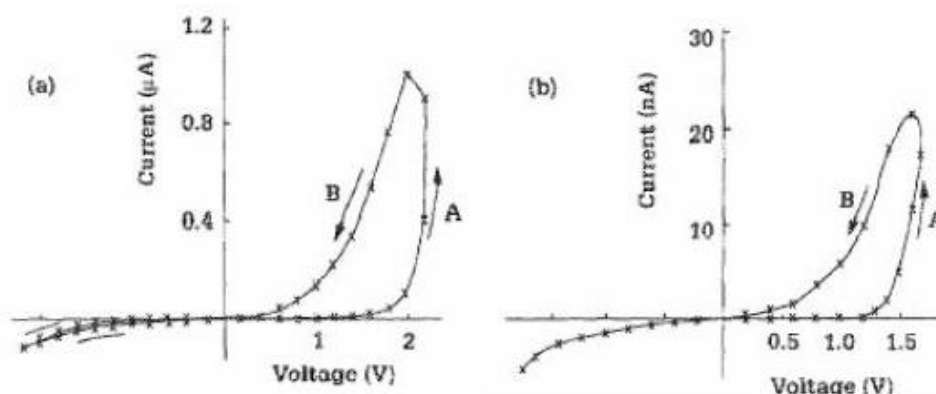
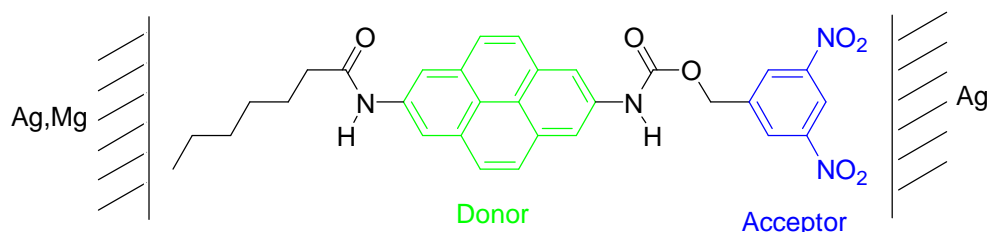


Figure 2-8 I-V characteristics of Pt | DOP-C-BHTCNQ | Mg, Al system, (a) just after deposition, (b) after annealing at 70°C<sup>28</sup>

The presence of a long chain (typical for LB films) that acted as a tunnelling barrier<sup>26,60</sup>, was expected to inhibit the current flow through the junction. Thus, very high values of current and the hysteresis obtained from the measurements had cast doubt as to whether rectification was a result of the proposed by Aviram and Ratner molecular structure<sup>1</sup>. The hysteresis could have been an indication of either contamination in the film<sup>61</sup>, or the flexible  $-\text{NH}-(\text{CO})-\text{O}-\text{CH}_2\text{CH}_2\text{CH}_2-\text{O}-$  bridge<sup>34</sup> within the structure that could have caused changes in the molecular alignment during the deposition and subsequent measurements. Due to the significant difference in work functions of magnesium (Mg) and platinum (Pt) used in the experiments (3.66 and 5.65 eV, respectively)<sup>28</sup>, and the high reactivity of the top magnesium electrode, the observed rectification was more likely attributed to the Schottky effect<sup>31,33</sup>.

Sambles *et al.*<sup>62</sup> later reported asymmetric I–V characteristics for another A– $\sigma$ –D structure (OHAPy-C-DNB). The junction was fabricated by the deposition of OHAPy-C-DNB between a silver-coated glass slide and silver-coated magnesium pads (see Figure 2-9).



**Figure 2-9 Ag,Mg | OHAPy-C-DNB | Ag structure<sup>62</sup>**

The recorded I–V curves showed high RR in excess of 100 before breakdown and no hysteresis was observed<sup>62</sup>. However, the direction of the higher current was in the opposite quadrant to that expected from the Aviram and Ratner theory<sup>1</sup>. Studies of the junction suggested that a predominant process involved in the rectification was probably again the formation of a Schottky barrier<sup>31,32</sup>, which resulted from the use of reactive magnesium as the top electrode. Additionally, it should be noted that the method of evaporating the electrode onto the organic monolayer has been criticised<sup>28,63</sup> due to the high possibility of forming a short circuit.

Twenty years after the Aviram and Ratner breakthrough<sup>1</sup>, studies of tetrathiafulvalene- $\sigma$ -acceptor molecular rectifiers were published<sup>64</sup>. Ho *et al.*<sup>64</sup> investigated TTF D- $\sigma$  bridge-A diads (see **Figure 2-10**). The molecules seemed to be appropriate candidates for molecular electronic devices as they consisted of the strong donor and acceptor separated by a saturated bridge. However, studies of the compound (see **Figure 2-10 (a)**) revealed that the  $\sigma$ -linker was too long and flexible. This introduced an additional tunnelling barrier<sup>26,60</sup>, and also led to an unwanted head-to-tail intramolecular-complex conformation<sup>64</sup>. To eliminate these problems, the next compound had a shorter bridge (see **Figure 2-10 (b)**).

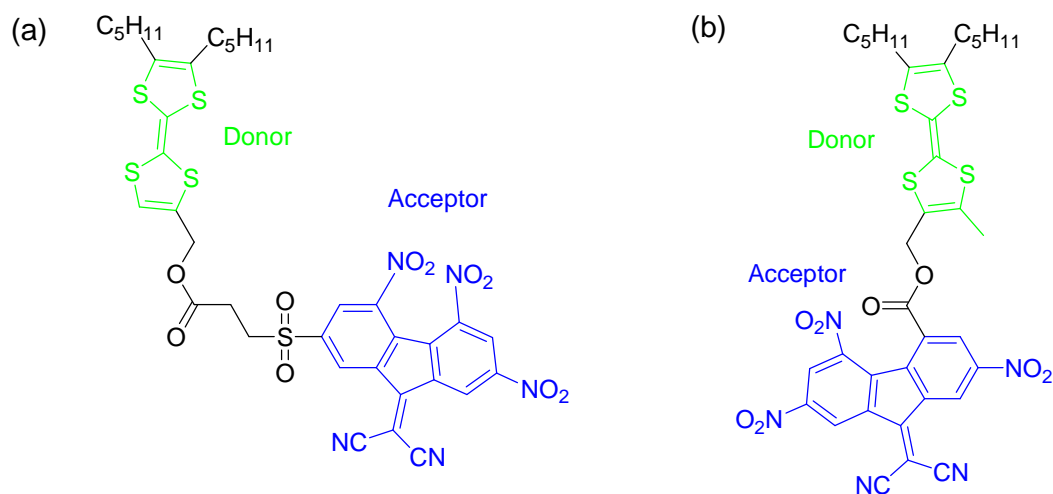


**Figure 2-10** TTF donor- $\sigma$ -acceptor diads<sup>64</sup>

The molecule (see **Figure 2-10 (b)**) was sandwiched between n-Si/SiO<sub>2</sub>/molecule/Ti,Al and I-V measurements were taken which yielded rectification. Although many publications<sup>65,66,67</sup> have criticised the origin of molecular rectification from junctions based on oxidisable electrodes, Ho *et al.*<sup>64</sup> believed that the use of a highly reactive titanium (Ti) electrode instead of a non-oxidisable Au electrode was a better solution. It was assumed that evaporation of Ti would immediately cleave the terminal C-H bonds and form a thin layer of titanium carbide at the studied surface, which would prevent the monolayer from further penetration of Ti atoms. However, it was considered that this explanation was not very strong. Studies of the same molecule<sup>64</sup> sandwiched between Au and Hg electrodes showed rectification in the opposite direction to the one obtained

for n-Si/SiO<sub>2</sub> | molecule | Ti,Al. This confirmed that the rectification originated from electrode effects.

The experimental verification of the Aviram and Ratner concept<sup>1</sup> had proved to be difficult to obtain. Although the presented D-σ-A structures showed rectifying behaviour, the use of reactive electrodes such as Ti<sup>29</sup>, Mg<sup>28</sup> or Al<sup>50</sup> raised some doubt as to whether the true properties of the monolayer were indeed measured. In order to avoid misleading interpretation of I-V characteristics, studies of D-σ-A structures when sandwiched between non-oxidisable electrodes were required<sup>68</sup>.

### 2.2.2 Rectification studies from Z-β-(1-hexadecyl-4-quinolinium)-α-cyano-4-styryldicyanomethanide (C<sub>16</sub>H<sub>33</sub>-Q3CNQ)

Although the original Aviram and Ratner proposal<sup>1</sup> was based on an D-σ-A structure, much research has been devoted to modified molecules, where instead of a σ-bridge, a π-bridge was used<sup>34,67,69</sup>. The reason for this was that sterically hindered π-bridged molecules are more rigid and this allowed a better control of molecular alignment on the substrate, which may result in an improvement of the rectification properties<sup>67</sup>.

Described as a modified Aviram and Ratner model<sup>1</sup>, Z-β-(1-hexadecyl-4-quinolinium)-α-cyano-4-styryldicyanomethanide (C<sub>16</sub>H<sub>33</sub>-Q3CNQ) (see **Figure 2-11**), is the most extensively studied example of an organic rectifier<sup>34,70,71,72,73</sup>. It was also the first molecule, where a sterically hindered π-bridge was utilised to separate the donor from the acceptor part of the molecule.

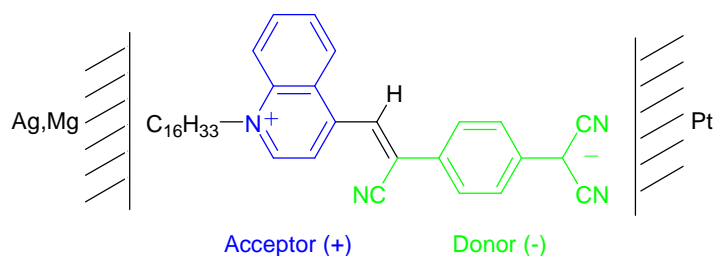


**Figure 2-11** C<sub>16</sub>H<sub>33</sub>-Q3CNQ structure<sup>34</sup>

The earliest studies regarding the rectification process of this molecule were presented by Ashwell *et al.*<sup>34</sup>. The junction was formed by placing the organic films between Ag, Mg | C<sub>16</sub>H<sub>33</sub>-Q3CNQ | Pt. To prevent from oxidation, the Mg electrode was coated with silver prior to breaking the vacuum (see Figure 2-12).

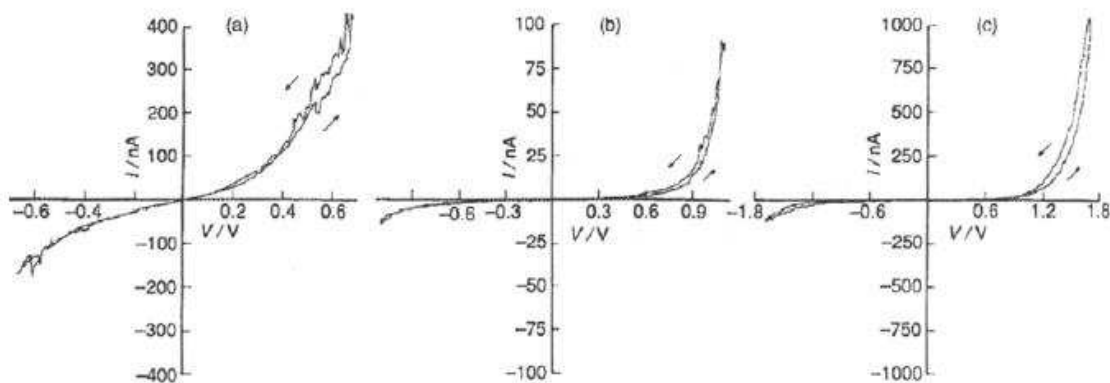
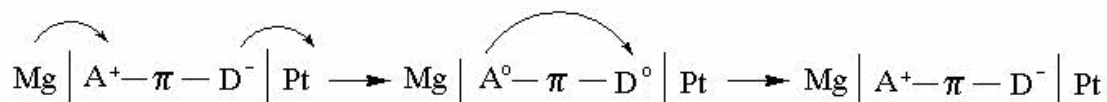


Figure 2-12 I-V characteristics of Mg|C<sub>16</sub>H<sub>33</sub>-Q3CNQ |Pt structures<sup>34</sup>, (a) one, (b) three, (c) four LB monolayers

The process of electron motion through the junction was explained as follows<sup>34</sup>:



Step one: an electron was transferred from the Mg anode to the acceptor (A<sup>+</sup>), which was believed to be a quinolinium cation, and simultaneously, an electron was transferred from the donor (D<sup>-</sup>) to the cathode (Pt). Step two: an electron was transferred from the acceptor (A<sup>0</sup>) to the donor (D<sup>0</sup>). However, the mechanism of rectification was not fully understood and the authors of the publication were aware that this explanation might not be the only interpretation of the observed rectification<sup>34</sup>.

Further investigation of C<sub>16</sub>H<sub>33</sub>-Q3CNQ showed that similar asymmetrical I-V characteristics were obtained when the molecules were sandwiched between Ag, Mg | C<sub>16</sub>H<sub>33</sub>-Q3CNQ | Ag electrodes<sup>65,74</sup>. To prove that the molecular structure was responsible for rectification and not the reactive electrode, the molecules of C<sub>16</sub>H<sub>33</sub>-Q3CNQ were bleached. The bleaching process, which was achieved by the

addition of metallic ions into the water subphase, disrupted the acceptor–donor structure, and therefore rectification was not expected. I–V characteristics obtained from the bleached molecules sandwiched between the same Ag and Mg electrodes confirmed this (see **Figure 2-13**).

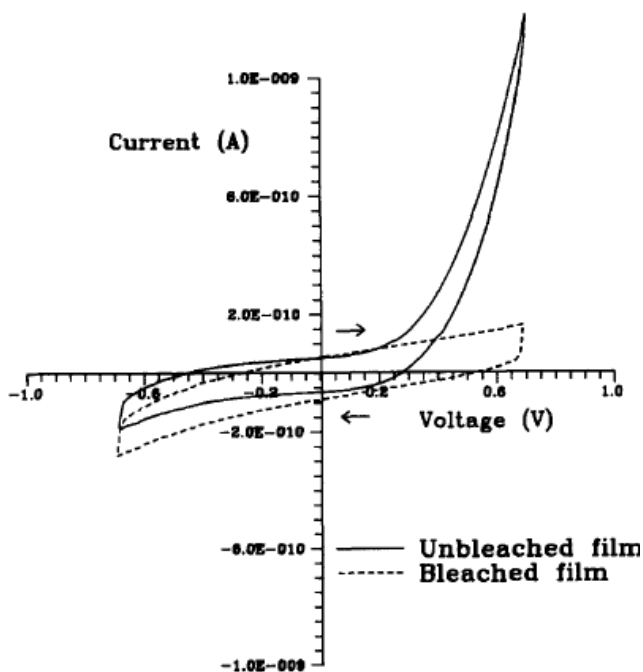


**Figure 2-13** I–V characteristic of Ag, Mg|C<sub>16</sub>H<sub>33</sub>–Q3CNQ|Ag structure<sup>74</sup>

Further evidence was obtained by fabricating a junction, where the same monolayer was separated from both electrodes (Ag/Mg and Ag) using an organic spacer of  $\omega$ -tricosenoic acid<sup>65</sup>. It was believed that this process would successfully eliminate the Schottky barrier<sup>31,32</sup> and provide strong evidence that supported the Aviram and Ratner theory. As expected, Ag, Mg |  $\omega$ -tricosenoic acid | A<sup>+</sup>– $\pi$ –D<sup>–</sup> |  $\omega$ -tricosenoic acid | Ag junction showed asymmetric I–V characteristics (see **Figure 2-14 (a)**)<sup>65,70</sup>.

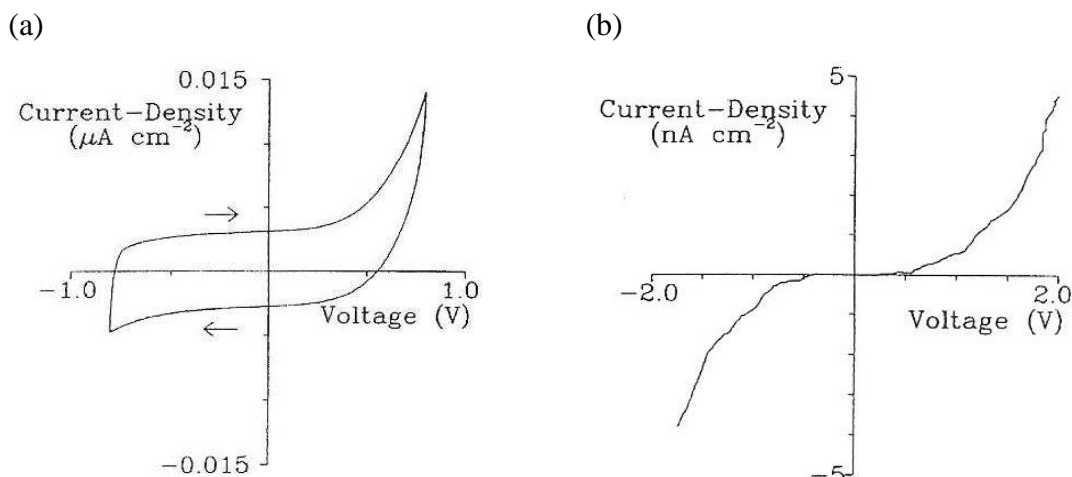


**Figure 2-14** I–V characteristics of (a) Ag, Mg| $\omega$ -tricosenoic acid |A<sup>+</sup>– $\pi$ –D<sup>–</sup>|| $\omega$ -tricosenoic acid|Ag, and (b) Ag, Mg| $\omega$ -tricosenoic acid |Ag structures<sup>65</sup>

Additionally, measurements of the Ag | 8 layers of  $\omega$ -tricosenoic acid | Mg, Ag structure revealed symmetric curves (see Figure 2-14 (b))<sup>65</sup>. This eliminated any doubts that the  $\omega$ -tricosenoic acid layer could contribute to the rectification, and confirmed that the asymmetry obtained was associated with the D– $\pi$ –A structure of the molecule.

Although there has been controversy surrounding oxidisable electrodes<sup>28,29</sup> and their significant influence on rectification, studies of Al | Al<sub>2</sub>O<sub>3</sub> | C<sub>16</sub>H<sub>33</sub>–Q3CNQ | Al<sub>2</sub>O<sub>3</sub> | Al junctions were also reported. Metzger<sup>61</sup> believed that Fermi levels of the metals, such as Mg or Al, were closer to the LUMO of the organic acceptors compared to Au or Pt, and therefore it would not result in the Schottky effect<sup>33</sup>. Two aluminium electrodes were used in order to avoid complicated analysis of I–V plots associated with the usage of electrodes with different work functions<sup>75</sup>. The experimental data showed three types of behaviour for Al | Al<sub>2</sub>O<sub>3</sub> | C<sub>16</sub>H<sub>33</sub>–Q3CNQ | Al<sub>2</sub>O<sub>3</sub> | Al junctions. They included asymmetrical curves with the high current recorded in the positive quadrant of the I–V plot and RR of 20, symmetrical curves, and asymmetrical curves with the high current observed in the negative quadrant of the I–V plot<sup>61</sup>. The variety in the behaviour of the samples studied were attributed to molecular rearrangement within the monolayer that might arise after LB deposition<sup>12,54</sup>, during storage periods<sup>61,76</sup>, metal evaporation process<sup>28</sup> or during STM measurements<sup>52,53,61</sup> (as a consequence of possible interactions between dipole moments and the applied electric field).



The ambiguity associated with using highly reactive materials for electrodes, and/or using electrodes with different work functions was finally eliminated when diode-like behaviour from the same zwitterionic molecule sandwiched between oxide-free gold electrodes was reported<sup>72,70</sup>.

### 2.2.3 $\pi$ -bridged molecular structures

Due to the success of the  $C_{16}H_{33}-Q3CNQ$  as a molecular rectifier, Metzger and Szablewski *et al.*<sup>77</sup> decided to investigate a slightly modified molecule (where  $A^+$  was ammonium, and  $D^-$  was tricyanoquinodimethanide). It was believed that the new structure would also provide the desired asymmetric I-V characteristic with a high rectification (see **Figure 2-15**).

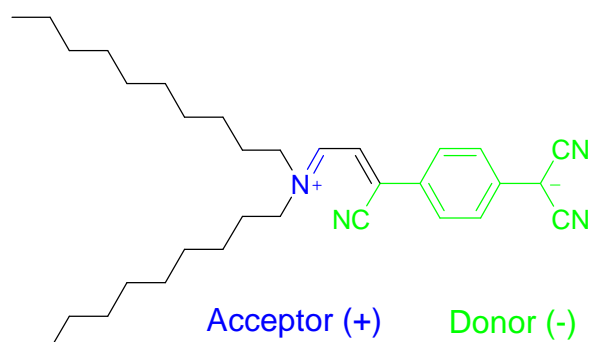


**Figure 2-15** Structure of  $(C_{10}H_{21})_2N^+-3CNQ^-$

The compound was sandwiched between gold electrodes and the measurements revealed a disappointing lack of rectification. The poor result was attributed to a partial or total antiparallel alignment of the molecules in the LB monolayer<sup>77</sup>. It was also believed that the dodecyl chains were not hydrophobic enough to maintain the molecules in a parallel orientation at the air-water interface. However, it is worth considering whether the steric hindrance necessary for D- $\pi$ -A structures was strong enough to effectively separate the donor from the acceptor unit in this case.

Since Aviram and Ratner<sup>1</sup> proposed their concept of the molecular rectifier, a number of experiments have been undertaken to test this hypothesis<sup>35,78,79</sup>. It also involved studies of the dipole reversal effect in cationic D- $\pi$ -A dyes<sup>80</sup>, which were defined as modified versions of the original proposal.

In 2001, rectification was reported from a multilayer containing 100 layers of 5-(4-dibutylaminobenzylidene)-2-octadecyl-5,6,7,8-tetrahydroisoquinolinium octadecylsulfate<sup>66</sup> cationic dye co-deposited with octadecanoic acid and placed between gold electrodes (see **Figure 2-16**).

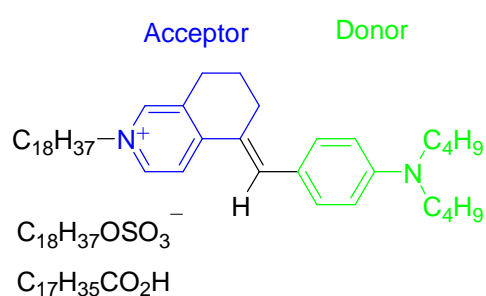


**Figure 2-16** Structures of 5-(4-dibutylamino-benzylidene)-2-octadecyl-5,6,7,8-tetrahydroisoquinolinium octadecylsulfate and octadecanoic acid<sup>66</sup>

Later, studies of the same cationic dye, but with a different aliphatic chain were performed in order to demonstrate that a change of the dipole orientation influenced the rectifying behaviour of the molecule. Each cationic compound was deposited via the LB technique together with the octadecyl sulfate counterion (see **Figure 2-17**), and then sandwiched between two gold electrodes<sup>80</sup>.

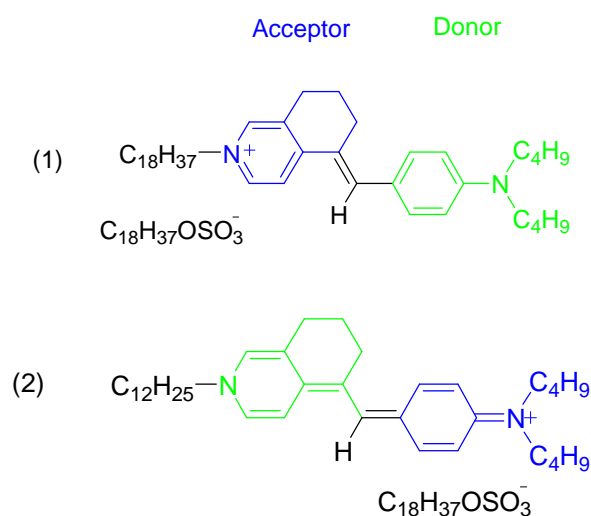


**Figure 2-17** Structures of E-4-[(N-alkyl-5,6,7,8-tetrahydroisoquinolinium-5-ylidene)methyl]-N,N-dibutylaniline octadecyl sulphate, (1) octadecyl and (2) dodecyl analogues<sup>80</sup>

As expected, the results showed that both compounds possessed diode-like characteristics. However, in the case of the octadecyl analogue the higher current was observed in the positive quadrant of the I-V plot, while for the dodecyl analogue, the higher current was observed in the opposite quadrant of the plot. This simple manipulation of the molecular arrangement provided evidence that rectification arose from the molecular structure.

This experiment was further enhanced by studies of LB film-forming isomers of N-alkyl-5-(4-dialkylaminobenzylidene)-5,6,7,8-tetrahydroquinolinium iodide (see **Figure 2-18**), when deposited on a gold-coated substrate and contacted via an Au or PtIr tip<sup>81,82</sup>.

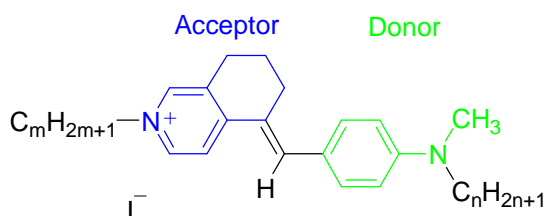


**Figure 2-18** Structure of N-alkyl-5-(4-dialkylaminobenzylidene)-5,6,7,8-tetrahydroquinolinium iodide<sup>81</sup>

Two of the three alkyl substituents were methyl groups and the other was a hexadecyl. The location of the hexadecyl group caused the molecules to be aligned on the substrate in different ways. When the long aliphatic chain was attached to the acceptor, the molecules were deposited with the donor located closer to the substrate, and the acceptor with the alkyl tail was pointing upward. When the hexadecyl chain was attached to the donor, the molecules were aligned in the opposite way. Subsequent I–V measurements demonstrated that the rectification was attributed to the D– $\pi$ –A structure. Both analogues exhibited asymmetric I–V characteristics, however, for the [A– $\pi$ –D–C<sub>n</sub>H<sub>2n+1</sub>] structure the higher current was observed in the negative quadrant of the I–V plot, and for the [D– $\pi$ –A–C<sub>m</sub>H<sub>2m+1</sub>] structure, asymmetry was recorded in the positive quadrant of the I–V plot (see **Figure 2-19**)<sup>81</sup>.

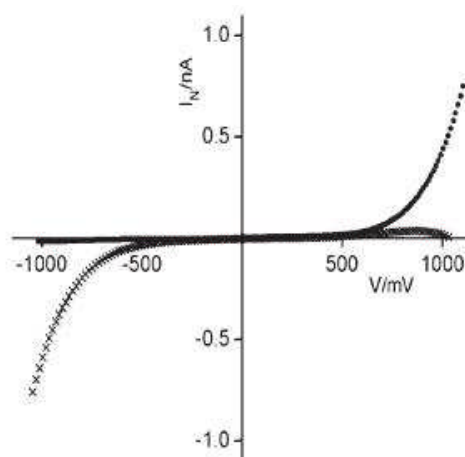


**Figure 2-19** I–V characteristics of structure of N–alkyl–5–(4–dialkylaminobenzylidene)–5,6,7,8–tetrahydroquinolinium iodide<sup>81</sup>

Deposition of the mixture of these two analogues led to symmetrical I–V curves<sup>81</sup>, which were associated with the antiparallel alignment of the active moieties within the monolayer. This showed that rectification, which resulted from the D– $\pi$ –A structure was also dependant upon the arrangement and orientation of the molecules.

Studies of another cationic dye (4{2–[4–(N,N–dibutylaminophenyl)vinyl]–N–octadecyl–quinolinium octadecyl sulphate) sandwiched between gold electrodes also showed rectification<sup>79</sup> (see **Figure 2-20**). However, the electrical asymmetry disappeared

over a period of time, which was attributed to an anion-induced effect. It was assumed that the counterion movement led to the formation of two forms: aromatic and quinonoid with reversed dipoles.

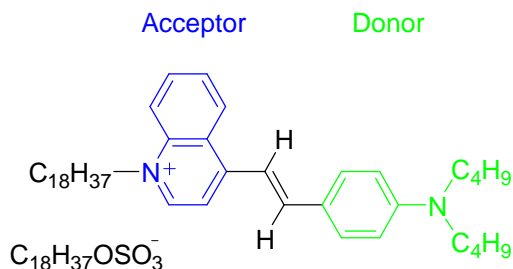
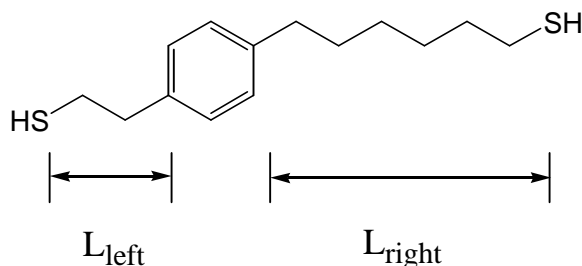


Figure 2-20 Structure of 4{2-[4-(N,N-dibutylaminophenyl)vinyl]-N-octadecylquinolinium octadecyl sulfate<sup>79</sup>

#### 2.2.4 The alkyl tunnelling barrier effect on molecular rectification

Krzeminski *et al.*<sup>83</sup> suggested that the rectification depends not only on the molecule's HOMO and LUMO level positions with relation to the Fermi energy level of the electrodes, as Aviram and Ratner<sup>1</sup> postulated, but also on the position of the electroactive part of the molecule in the monolayer. According to the theoretical studies of C<sub>16</sub>H<sub>33</sub>-Q3CNQ placed between Al and Au electrodes<sup>83</sup>, the  $\pi$ -bridge used to isolate the acceptor from the donor of the molecule did not sufficiently separate the molecular orbitals (localised on either donor or acceptor). Therefore, the molecular orbitals were delocalised over the entire molecule. Krzeminski<sup>83</sup> believed that the extended aliphatic chain, which led to the asymmetric position of the donor-acceptor moiety in relation to the electrodes played a significant role in the rectification process.

Later, Kornilovitch *et al.*<sup>84</sup> inspired by Krzeminski's work<sup>83</sup>, proposed a molecular rectifier based on a conjugated system HS-(CH<sub>2</sub>)<sub>m</sub>-C<sub>6</sub>H<sub>4</sub>-(CH<sub>2</sub>)<sub>n</sub>-SH (see Figure 2-21).



**Figure 2-21**  $\text{HS}-(\text{CH}_2)_m-\text{C}_6\text{H}_4-(\text{CH}_2)_n-\text{SH}$  system<sup>84</sup>

It was thought that the rectification of metal | organic molecule | metal systems could be produced by the asymmetrical positioning of the molecule with respect to the electrodes without needing the D–electron bridge–A structure that Aviram and Ratner postulated<sup>1</sup>. It was estimated that for this system, the highest rectification ratio (RR) possible was 500 for  $m=2$  and  $n=10$ . This work<sup>84</sup> stated that rectification could be obtained from one conducting molecular unit placed closer to one of the electrodes, and that by changing the length of the insulating barriers, the rectification could be symmetrically changed. However, these values are theoretical and have not been confirmed by experiment.

In 2003, Chang *et al.*<sup>29</sup> reported very high rectification of  $5 \times 10^5$  at  $\pm 2.3$  V from a Kornilovitch<sup>84</sup> type rectifier. A SAM of alkoxy-naphthalene thiol was deposited onto the Pt electrode and then overcoated by the Ti electrode (see **Figure 2-22**).

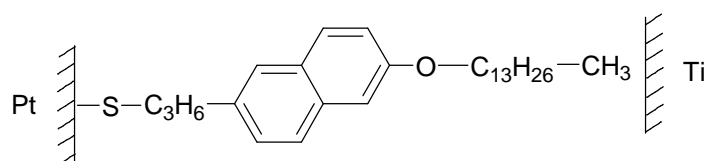


**Figure 2-22** Chang's molecule<sup>29</sup>

According to the results obtained by Chang *et al.*<sup>29</sup>, the monolayer deposited on the Pt electrode was highly ordered. The deposition of the Ti electrode revealed some disruption within the monolayer structure that arose as a result of a reaction with the alkyl chains, but the naphthalenes remained intact. Although Chang *et al.*<sup>29</sup> attributed rectification partly to the contact potential generated by the different work functions of Pt and Ti, and partly to the asymmetric tunnelling barrier of the compound<sup>83,84</sup>. It was

very likely caused by an oxide-induced Schottky barrier formation<sup>31,32</sup>, rather than the molecular structure itself. This statement has been confirmed by others<sup>30</sup> and thus, claims of molecular rectification obtained from studies using oxidisable electrodes should be excluded.

Krzeminski<sup>83</sup> and Kornilovitch's<sup>84</sup> work was questioned when no rectification was reported from the Au-S-C<sub>10</sub>H<sub>20</sub>-squaraine | PtIr tip structure<sup>85</sup>, where the chromophore was asymmetrically positioned between non-oxidisable electrodes.

Attempts to manipulate the position of the chromophore between electrodes were also performed for the CH<sub>3</sub>CO-S-C<sub>n</sub>H<sub>2n</sub>-Q3CNQ structure<sup>70</sup>, where the chain length C<sub>n</sub>H<sub>2n</sub> was changed within the range: 3 ≤ n ≤ 12. All of the samples studied were contacted via Au and PtIr tips, and the results obtained were similar for both tips. All of the samples showed rectification. Ashwell *et al.*<sup>70</sup> believed that the chromophore of the Au-S-C<sub>3</sub>H<sub>6</sub>-Q3CNQ | PtIr system was located approximately midway between the electrodes, as the van der Waals contact between the tip and the molecule were similar to the length of the chain (Au-S-C<sub>3</sub>H<sub>6</sub>-). The almost identical I-V plots for analogues Au-S-C<sub>12</sub>H<sub>24</sub>-Q3CNQ//PtIr and Au-S-C<sub>3</sub>H<sub>6</sub>-Q3CNQ//PtIr (see Figure 2-23), and similar behaviour observed for the rest of the analogues suggested that the position of the chromophore in relation to the electrodes did not influence the rectification behaviour of the device<sup>70</sup>.

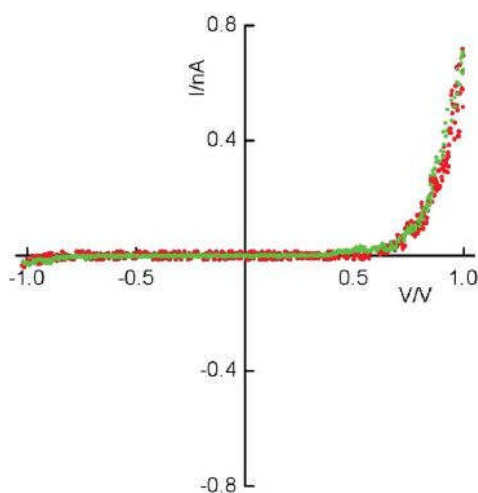
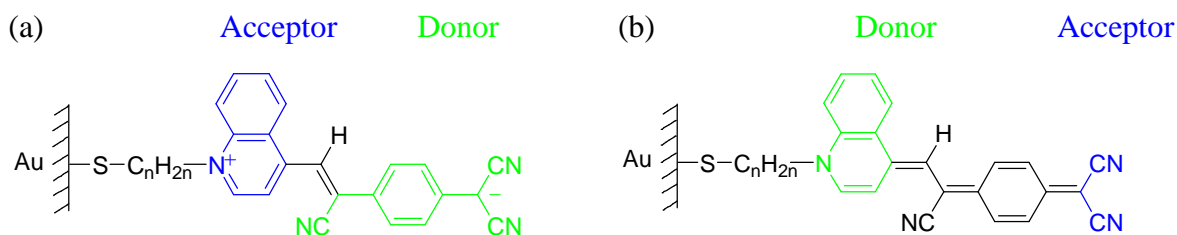


Figure 2-23 I-V characteristic of CH<sub>3</sub>CO-S-C<sub>n</sub>H<sub>2n</sub>-Q3CNQ structure ( n=3, green), (n=12, red)<sup>70</sup>

A high current was observed in the positive quadrant of the I–V plot, which implied that electron flow was from the top electrode and passed through the monolayer to the bottom electrode. Thus the heterocycle acted as a donor, whereas the C(CN)<sub>2</sub> was an acceptor, and this is consistent with a quinoid ground state, rather than the zwitterionic state of the molecule (see **Figure 2-24**)<sup>70</sup>.



**Figure 2-24** (a) Zwitterionic and (b) Quinoid ground state of CH<sub>3</sub>CO–S–C<sub>n</sub>H<sub>2n</sub>–Q3CNQ<sup>70</sup>

The protonation process<sup>70</sup>, which switched off rectification of the Au–S–C<sub>10</sub>H<sub>20</sub>–Q3CNQ structure, provided unambiguous evidence that the effect of geometrical asymmetry was insignificant relative to the rectification produced by the Aviram and Ratner structure<sup>1</sup> (see **Figure 2-25**).

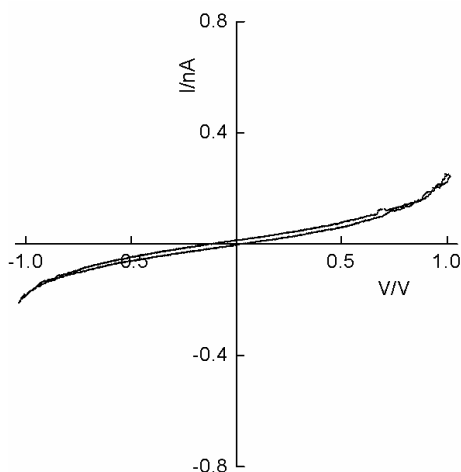


**Figure 2-25** I–V characteristic of Au–S–C<sub>10</sub>H<sub>20</sub>–Q3CNQ after protonation<sup>70</sup>

Continuing the dispute around the asymmetrical geometry, the rectifying behaviour of Au–S–C<sub>3</sub>H<sub>6</sub>–A– $\pi$ –D structure<sup>86</sup> and its C<sub>10</sub>H<sub>20</sub>– analogue<sup>35</sup> were studied. To avoid any



ambiguity associated with the alignment of molecules on the substrate when deposited via the LB technique, and to eliminate the long aliphatic chain that was believed to introduce an additional tunnelling barrier<sup>26,60</sup>, dyes were attached to a gold electrode using a chemisorption process (see **Figure 2-26**).

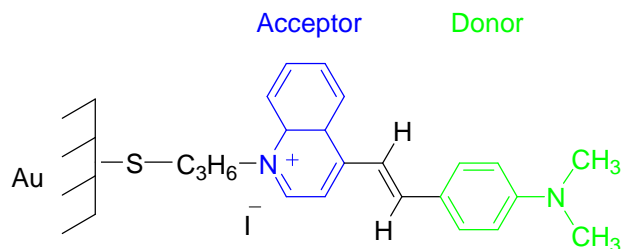


**Figure 2-26** Structure of a possible molecular rectifier<sup>86</sup>

STS measurements revealed rectification of 12 at  $\pm 1$  V from Au-S-C<sub>3</sub>H<sub>6</sub>-A- $\pi$ -D structure<sup>86</sup>. The monolayer was then subjected to a protonation process to verify the origin of the rectification. Upon exposure to HCl vapour, the charge-transfer axis of the structure was disrupted (protonation of the donor group). As a consequence, the rectification decayed and symmetrical I-V characteristics were observed. Exposure to NH<sub>3</sub> vapour removed the proton and consequently restored rectification, although with a reduced RR. This reversibility provided unambiguous evidence that rectification was caused by the D- $\pi$ -A structure.

To manipulate the position of the chromophore between the electrodes, the C<sub>10</sub>H<sub>20</sub>-analogue (see **Figure 2-27**) was contacted by three different tips<sup>35</sup> (an uncoated Au tip, a tip coated by pentanethiolate Au-S-C<sub>5</sub>H<sub>11</sub>, and a tip coated by decanethiolate, Au-S-C<sub>10</sub>H<sub>21</sub>). Although it had been shown that the D- $\pi$ -A structure was the major factor causing rectification, these studies may suggest that rectification could be partly affected by the tunnelling barrier generated by the aliphatic chains because RR values of 18, 11 and 5 at  $\pm 1$  V were observed when an uncoated Au tip, a tip coated by pentanethiolate (Au-S-C<sub>5</sub>H<sub>11</sub>), and a tip coated by decanethiolate (Au-S-C<sub>10</sub>H<sub>21</sub>) were used, respectively<sup>35</sup>.

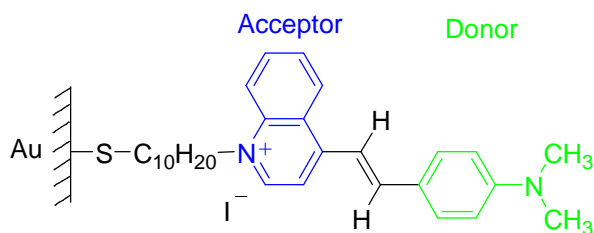


**Figure 2-27 Structure of 4-[2-(4-dimethylamino-phenyl)-vinyl]-1-(10-mercapto-decyl)-quinolinium iodide<sup>35</sup>**

Similar conclusions were made from the results obtained for the molecule<sup>87</sup> with the same acceptor but different donor (see **Figure 2-28**).

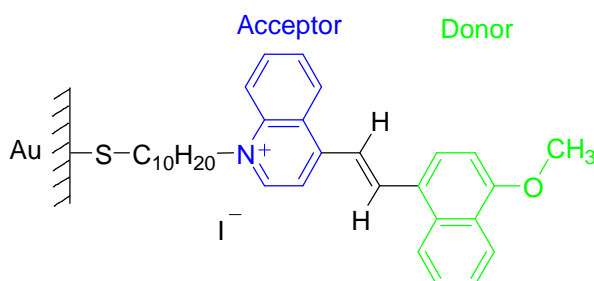


**Figure 2-28 Structure of iodide salt of a sterically hindered D- $\pi$ -A<sup>87</sup>**

Studies showed that when the monolayer was contacted by an uncoated gold tip (see **Figure 2-29(A)**) the RR of 30 at  $\pm 1$  V was obtained, but when the tip was coated with pentanethiolate that positioned the chromophore approximately midway between the electrodes, the RR of 10 at  $\pm 1$  V was obtained. The important fact is that the results obtained via STS were confirmed by using mercury droplet electrodes<sup>87</sup> (see **Figure 2-29 (B)**).

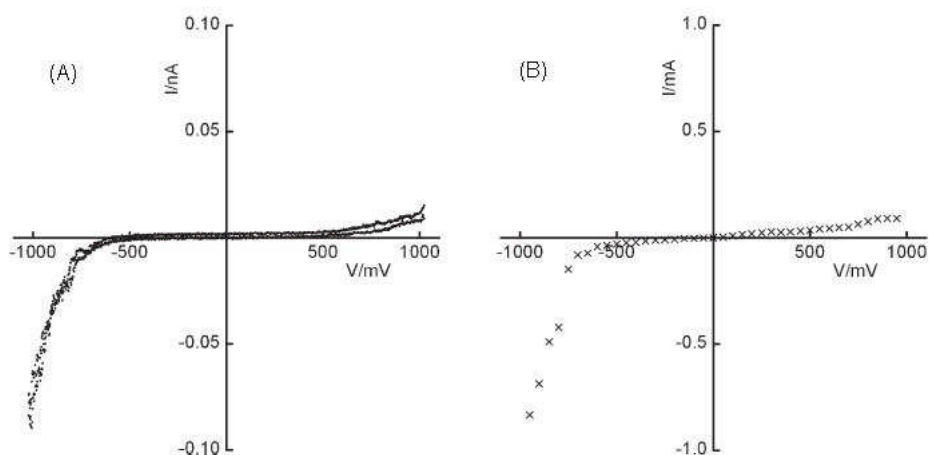


Figure 2-29 I–V characteristics of TCNQ<sup>-</sup> salt of a sterically hindered D– $\pi$ –A measured by (A) STM, and (B) mercury drop<sup>87</sup>

Studies of Au–S–C<sub>10</sub>H<sub>20</sub>–A– $\pi$ –D structures were continued but with different acceptors and donors<sup>35</sup> (see Figure 2-30). If the assumption that the asymmetrical position of the chromophore between electrodes played a key role in rectification<sup>84</sup>, then each molecule should have exhibited rectification.

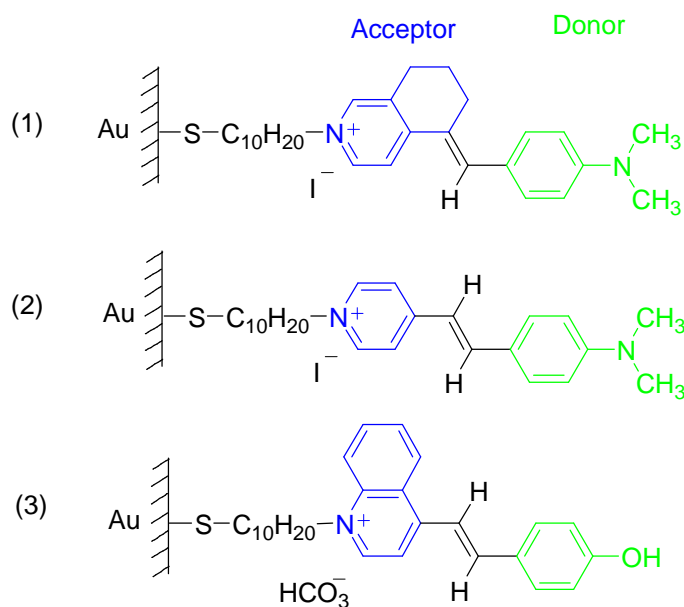
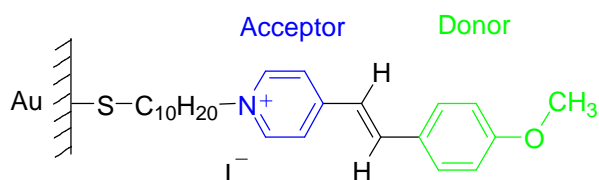


Figure 2-30 Structures of SA analogues for molecular rectifiers studied by Ashwell *et al.*<sup>35</sup>

However, as studies showed<sup>35</sup>, rectification was observed only for the compound (1) (see Figure 2-30 (1)). The two other examples (see Figure 2-30 (2 and 3)) did not yield

asymmetrical I–V characteristics. This was due to a planar structure in the case of compound (2) (see **Figure 2-30 (2)**), and an unstable form of compound (3) (see **Figure 2-30 (2 and 3)**), which very likely reacted with atmospheric  $\text{H}_2\text{CO}_3$ . This investigation revealed that in order to obtain rectification from D– $\pi$ –A molecules, it is vitally important to provide steric hindrance within the structure to enforce a non–planar arrangement to effectively separate the donor from the acceptor<sup>35</sup>. This also confirmed that the aliphatic chain did not have significant influence on rectification and it is extremely important that the molecules form stable monolayers.

Studies of other examples confirmed this statement. The almost planar compound<sup>87</sup> with a pyridinium ring acting as an acceptor (see **Figure 2-31**) did not yield any rectification.



**Figure 2-31** Structures of 1-(10-mercapto-decyl)-4-[2-(4-methoxy-phenyl)-vinyl]-pyridinium iodide<sup>87</sup>.

The sterically hindered dye with a quinolinium acceptor (see **Figure 2-32**) showed rectification between 50–150 at  $\pm 1$  V when placed between two non–oxidised electrodes<sup>67</sup> (see **Figure 2-33 (a)**).

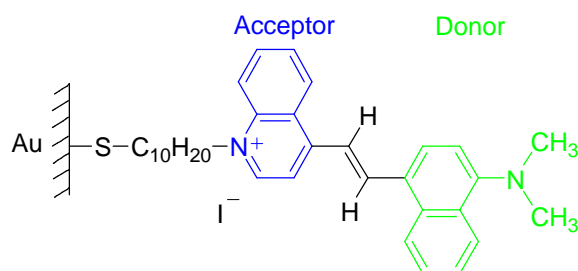


**Figure 2-32** Structure of 1-(10–acetylsulfanyldecyl)–4–[2–(4–dimethylaminonaphthalen–1–yl)–vinyl]–quinolinium iodide<sup>67</sup>

The rectification was partly attributed to the controlled alignment of the D- $\pi$ -A structure, and partly to the steric hindrance that created a non-planar structure and consequently effectively isolated the molecular orbitals of the donor and acceptor subunits from each other<sup>67</sup>. To confirm that the rectification was induced by the molecular structure, the investigated monolayer was briefly exposed to HCl vapour, which suppressed the electron-donating properties of the molecule due to the protonation of the dimethylamino group. The rectifying behaviour was then restored upon exposure to NH<sub>3</sub> (see **Figure 2-33 (b)**)<sup>67</sup>.

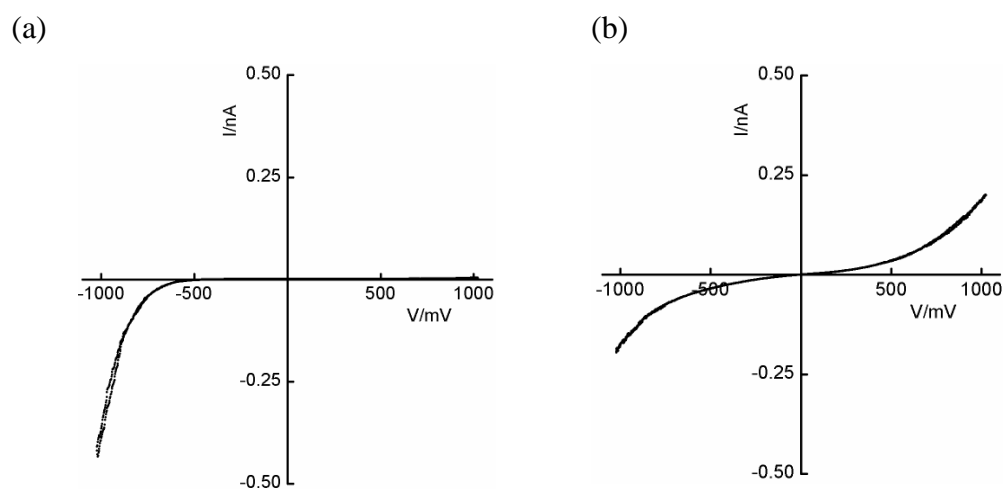


**Figure 2-33** I-V characteristics of (a) 1-(10-acetylsulfanyldodecyl)-4-{2-(4-dimethylamino naphthalen-1-yl)-vinyl}-quinolinium iodide measured before, and (b) after protonation<sup>67</sup>

### 2.2.5 Different approaches

Other approaches arose as a result of research aimed at finding materials that performed with the desired diode-like behaviour.

Ellenbogen and Love proposed a molecular diode<sup>88</sup> based on the Aviram and Ratner concept<sup>1</sup>. The molecule presented (see **Figure 2-34**) was a chemically doped polyphenylene-based molecular wire where X-group provided donor character, Y-group provided acceptor character to the molecule, and the R-group acted as a bridge. However, the model was not supported by experiment.

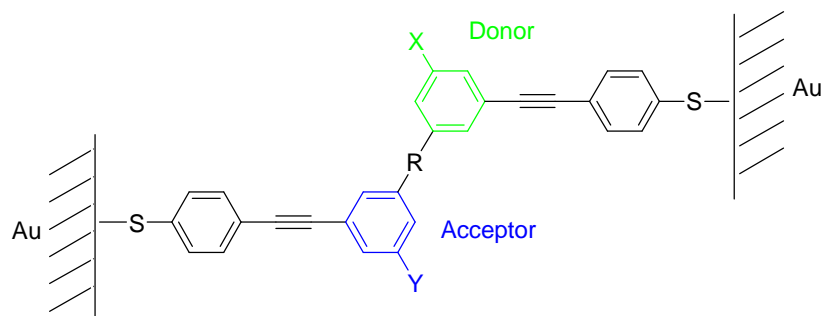


**Figure 2-34 Ellenbogen and Love rectifier<sup>88</sup>**

The research regarding molecular rectification also included the investigation of LB films of phthalocyanines<sup>89,90</sup>, even though they did not possess a typical A- $\sigma$ -D structure<sup>1</sup>. Due to a substitution process, it could be possible to form a donor-phthalocyanine-acceptor type molecule (D-Pc-A). Zhou *et al.*<sup>89,90</sup> published results of asymmetrically substituted phthalocyanines, and the structure of one is depicted in **Figure 2-35**

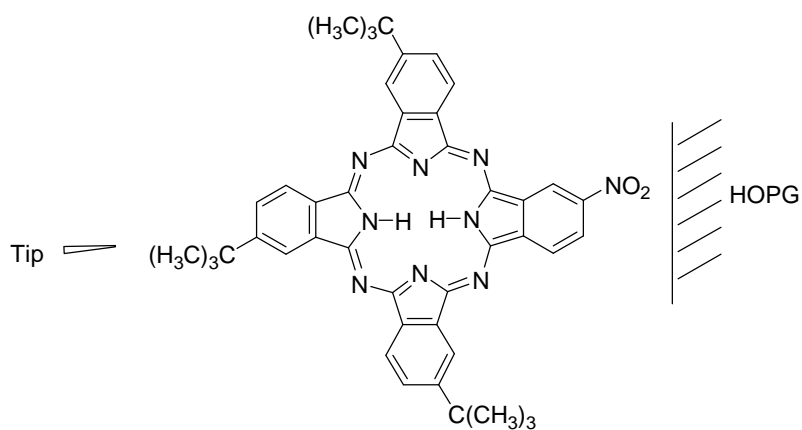


**Figure 2-35 Structure of phthalocyanine studied by Zhou *et al.*<sup>89</sup>**

These molecules were deposited directly onto an HOPG surface that acted as one of the electrodes and contacted via an STM tip (PtIr or tungsten). The use of the STM eliminated a common problem associated with an evaporated top electrode, which could easily lead to a short circuit of the thin films<sup>28,61</sup>. Although it was stated that the rectifying behaviour was partly attributed to the material and geometrical asymmetry<sup>89</sup>,

(i.e. the molecules were located closer to the HOPG surface than the STM tip), it seemed to be unlikely attributed to the Aviram and Ratner mechanism<sup>1</sup>, as the butyl groups did not act as donor groups.

Metzger *et al.*<sup>91</sup> reported asymmetric I–V curves with an incredibly high rectification of  $12000 \pm 2000$  at  $\pm 1.5$  V from a LB film of dimethylanilinoaza [C<sub>60</sub>] fullerene sandwiched between two gold electrodes (see **Figure 2-36**).

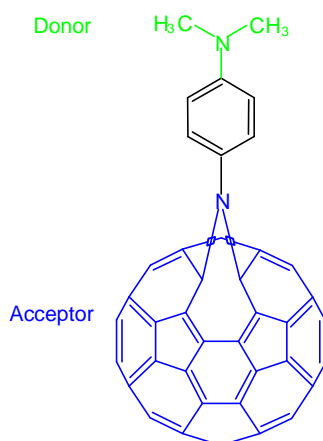


**Figure 2-36** Structure of dimethylanilinoaza[C<sub>60</sub>]fullerene<sup>91</sup>

However, it was considered doubtful whether such a high value of rectification was a consequence of the monolayer itself, and it was suspected that other factors had a significant role in the rectification process. Indeed, extensive studies showed that the high current and RR recorded for this molecule were most likely caused by a formation of gold stalagmites through the gold. After much cycling of the bias, the current had a much lower value and rectification dropped to 2, which was attributed to the destruction of the gold stalagmites<sup>91</sup>.

The controversy associated with the insulation barrier created by a long aliphatic chain and its influence on rectification led to studies of a chevron-shaped compound<sup>69,92,93</sup> (see **Figure 2-37**).

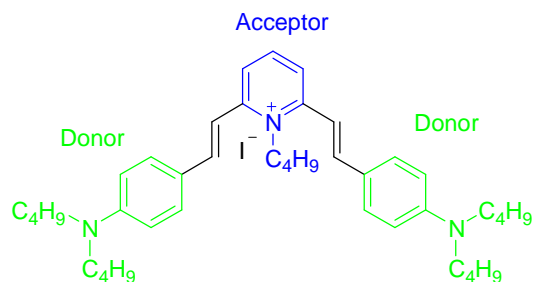


**Figure 2-37 Structure of the chevron-shaped molecule<sup>69,92</sup>**

This molecule represents a novel class of compounds with short aliphatic chains that have been successfully aligned using the LB method. The molecules are comprised of an acceptor located in the middle of two donor limbs (D- $\pi$ -A- $\pi$ -D). Studies of several samples yielded rectification when a monolayer was placed between gold electrodes. The average rectification was 8.4 at  $\pm 1.5$  V with a higher current observed in the positive quadrant of the I-V plot (the top electrode was positive)<sup>69</sup>. This corresponded to electron flow from the bottom electrode to the top. Detailed studies of the molecules implied that the iodide remained in the monolayer and therefore rectification was assigned to back electron transfer from iodide to pyridinium ring. The presence of the iodide could result in two possible alignments of the molecules on the substrate (see Figure 2-38).

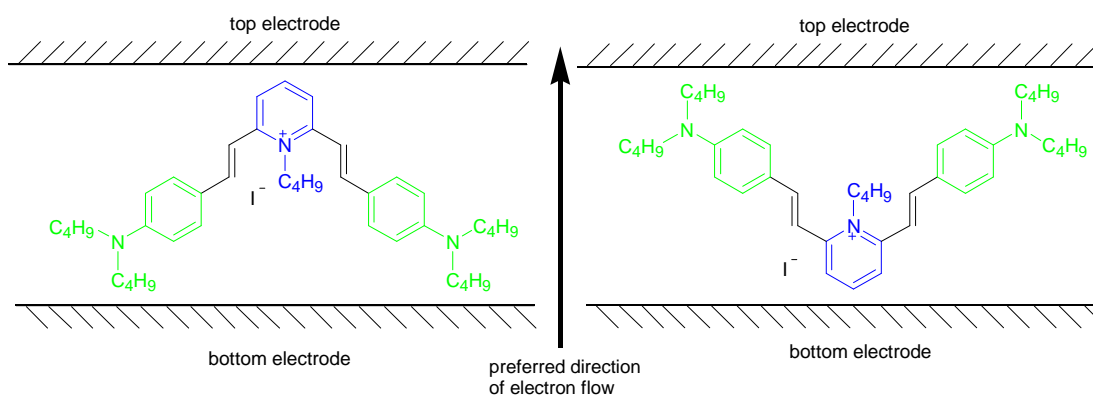


**Figure 2-38 Suggested alignment of the chevron-shaped molecule between electrodes<sup>69</sup>**

Repeated measurements led to a decrease of the asymmetry, and following 5–10 cycles the asymmetry disappeared. This suggested that the molecules rearranged whilst a voltage bias was applied to the junction<sup>52,53</sup>. Therefore, it was impossible to identify the



correct alignment of the molecules on the surface. Further discussion regarding this example and a presentation of other examples of chevron-shaped molecules will be provided in the results section.

Metzger<sup>94</sup> studied a U-shaped organic rectifier containing a fullerene attached to two triphenylamine groups *via* a  $\pi$ -bridge (see **Figure 2-39**).

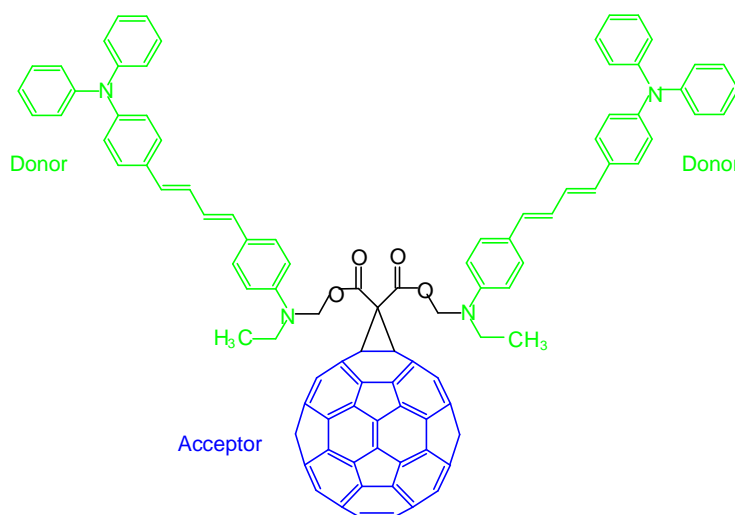


**Figure 2-39** U-shaped rectifier containing fullerene<sup>94</sup>

The molecule was deposited onto a gold-coated substrate and the second gold electrode was deposited on top of the organic monolayer using an evaporation process. Measurements taken from this system revealed that in the low bias range ( $\pm 3$  V) no rectification was observed. However, when the bias was increased to 5.4 V, asymmetric I-V characteristics with a RR up to 16.4 were achieved. According to the authors<sup>94</sup>, the rectification arose as a result of the asymmetric placement of the molecular orbitals of the acceptor and donor subunits with regards to the electrodes. It is worth noting that after much cycling of the bias, the current did not drop, and this was due to its tendency to form rigid and stable LB monolayers.

Whitesides *et al.*<sup>46,95</sup>, demonstrated that Ag | SAM1 || SAM2 | Hg junctions also rectified current, although the molecular system did not possess the typical structure of the Aviram and Ratner model<sup>1</sup>. With SAM1 being a self-assembled monolayer formed

from a derivative of TCNQ, and SAM2 being a self-assembled monolayer formed from alkanethiol ( $\text{HS}(\text{CH}_2)_{n-1}\text{CH}_3$ ,  $n=14,16,18$ ) (see **Figure 2-40**). It was believed that rectification could be achieved in a metal | insulator | metal junction, if an electron acceptor was placed in the insulating layer<sup>46</sup>. Studies showed that each additional  $\text{CH}_2$  group in ( $\text{HS}(\text{CH}_2)_{n-1}\text{CH}_3$ ,  $n=14,16,18$ ) decreased rectification, which suggested that both conductivity and ability of the junction to rectify was dependent on the chain length of the SAM2. However, the obtained data also indicated disorder within SAM1, which could influence the electrical properties of the monolayer.

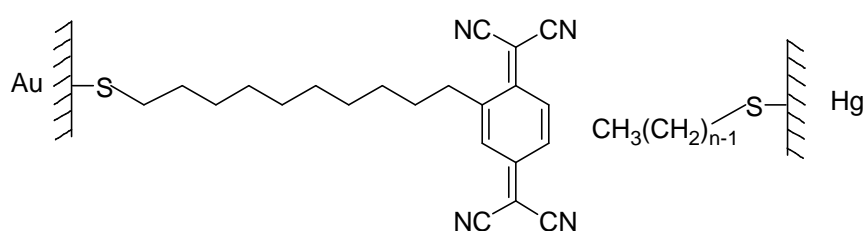


**Figure 2-40** Ag | SAM1 || SAM2 | Hg junctions studied by Whitesides *et al.*<sup>46</sup>

McCreery<sup>96</sup> reported strong rectification of up to 600 at  $\pm 2$  V from a 3.7 nm thick layer of nitrobenzene (NAB). It was claimed that rectification was caused by the molecule, and in particular to ‘switching’ between phenyl and quinoid forms when the bias was applied (see **Figure 2-41**).

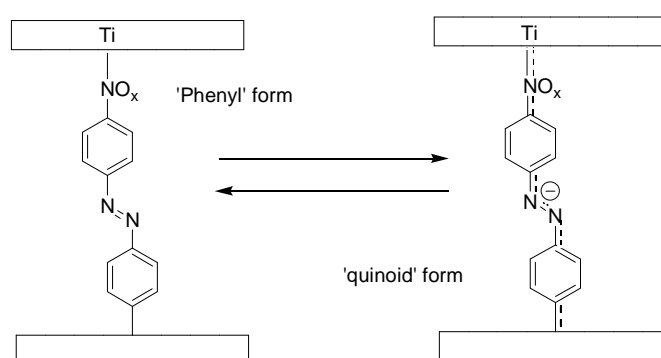


**Figure 2-41** Phenyl and quinoid forms of NAB<sup>96</sup>

However, some researchers argued that the rectification originated from the Schottky effect<sup>31,32</sup> due to the use of oxidisable titanium as a top electrode. Indeed, the results

were retracted, when studies of the same molecule in an oxygen-free environment showed a lack of asymmetry in the I–V characteristics<sup>97</sup>.

## 2.2.6 Hybrid structures

There has been much interest concentrated around hybrid donor/acceptor (D/A) structures<sup>98,99</sup>, which may be described as a modified model of the organic rectifier proposed by Aviram and Ratner<sup>1</sup>. These structures were formed as a result of a layer-by-layer deposition<sup>100</sup>, which allowed the elimination of usually complicated synthetic routes. This very simple technique offered the possibility of selecting donors and acceptors to build a variety of D/A or A/D assemblies with desirable electrical properties.

### 2.2.6.1 Donor /Acceptor assemblies

In 1995 Fisher<sup>99</sup> reported molecular rectification from a hybrid structure: Au | 6 monolayers of PcPd | 6 monolayers of PTCDI | Au (see **Figure 2-42**).

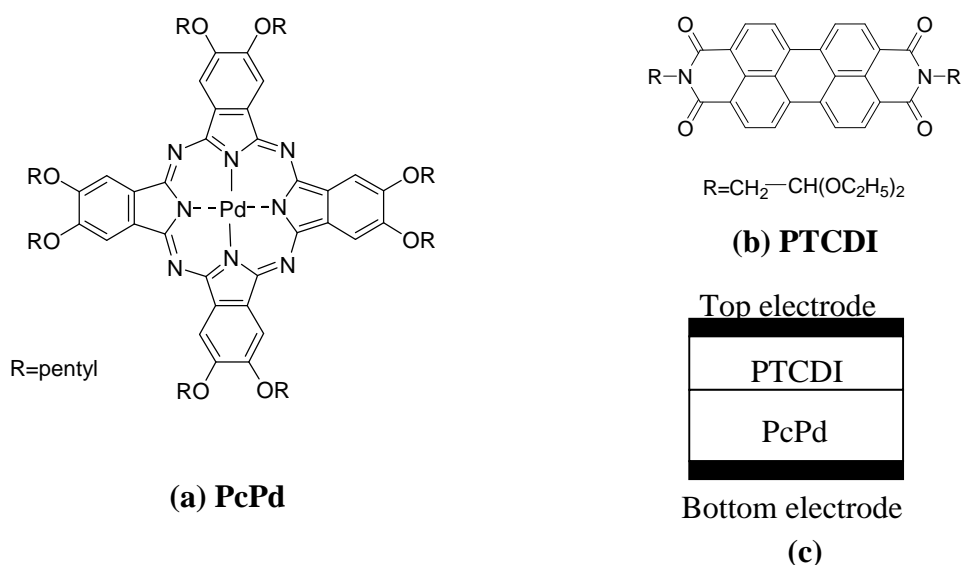


**Figure 2-42** Structures of (a) PcPd, (b) PTCDI and (c) layer configuration of the hybrid<sup>99</sup>

I–V characteristics were obtained at a temperature of 4.2 K. Fisher<sup>99</sup>, as well as Okazaki<sup>60</sup> and Yamada<sup>101</sup> believed that the temperature may have affected the electrical properties of the monolayers. Rectification behaviour from the hybrid structure was observed for both negative and positive bias. However, thresholds for positive and

negative bias occurred at 0.91 V and  $-0.40$  V, respectively. It was believed that rectification arose as a result of the D/A structure, and in particular to the different positions of the energy levels of PcPd and PTCDI with regards to the Fermi energy levels of the electrodes<sup>99</sup> (see **Figure 2-43**).

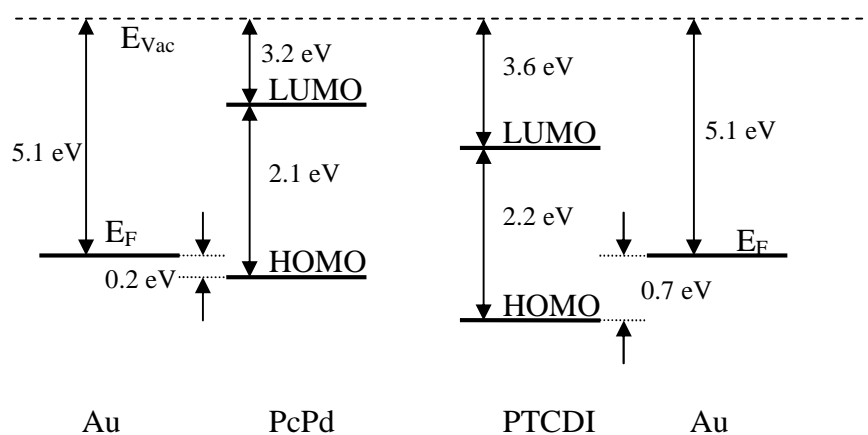


**Figure 2-43** Schematic diagram of the estimated energy levels of the PcPd and the PTCDI compared to the gold Fermi energy level<sup>99</sup>

This conclusion was confirmed by I–V measurements of Au | layers of PcPd | Au and Au | layers of PTCDI | Au structures, which yielded no rectification for either junction.

In 2005, rectification from a D/A structure was also reported by Mukherjee and Pal<sup>102</sup>. The system investigated, consisted of monolayers of the donor (copper phthalocyanine (CuPc)) and the acceptor (rose bengal) that were fabricated using electrostatic bonding (see **Figure 2-44**).

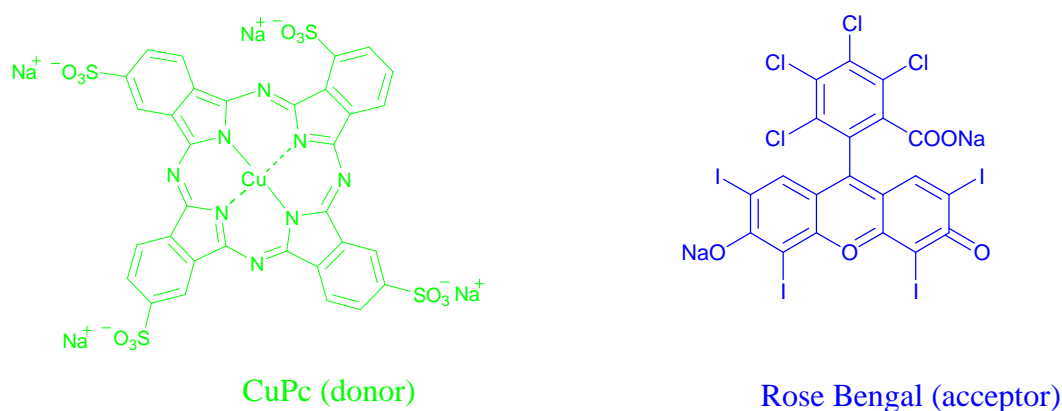


**Figure 2-44** Structure of CuPc (donor) and Rose Bengal (acceptor)<sup>102</sup>

The I–V measurements of the D/A assembly sandwiched between Si and Hg exhibited asymmetric curves with RR of 30 at  $\pm 1.9$  V. Unfortunately, the higher current was recorded in the negative quadrant of the I–V plot, which suggested that the electrons flowed from the donor to the acceptor, (the opposite direction to that expected from the Aviram and Ratner theory<sup>1</sup>). However, Mukherjee and Pal<sup>102</sup> believed that rectification resulted from the D/A structure because when the monolayers were investigated separately via STS, neither the donor nor acceptor showed any rectifying features.

In the same year, the layer–by–layer deposition of squaraines<sup>103</sup> led to orientation–induced rectification. The first layer of the self–assembled D– $\pi$ –A– $\pi$ –D structure was deposited using a chemisorption process. As a result, the molecules were packed vertically with respect to the substrate. The second layer was deposited using the LB technique, but this time the molecules were aligned horizontally on the surface, forming the bilayer structure as depicted in **Figure 2-45**.

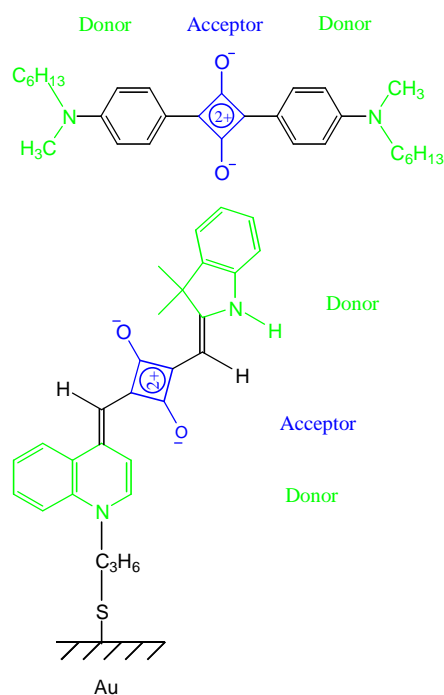


**Figure 2-45** Structure of a hybrid structure containing squaraines<sup>103</sup>

Each monolayer was investigated individually using STS and neither revealed asymmetric I–V characteristics. However, when deposited together as a hybrid

structure<sup>103</sup>, the I–V measurements showed asymmetry with a RR of 12 at  $\pm 1$  V, which was attributed to the Aviram and Ratner mechanism<sup>1</sup> (see **Figure 2-46**).

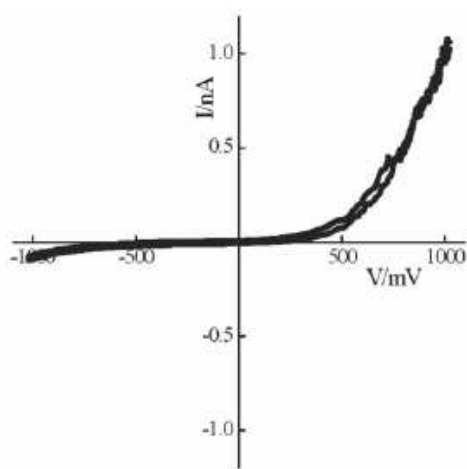


**Figure 2-46** I-V characteristic of a hybrid structure containing squaraines<sup>103</sup>

### 2.2.6.2 Donor/Acceptor structures based on the ionic assembly approach

Recently, Ashwell *et al.*<sup>104</sup>, presented promising results from organic rectifying junctions that were fabricated based on ionic coupling attraction between opposite charges of the molecules. This appeared to be an ideal deposition method for structures without long hydrocarbon chains (required for the LB technique). The structures were formed in two steps. The first layer was formed via chemical bond: Au–S. Then, the second layer was deposited via metathesis (see **Figure 2-47**).

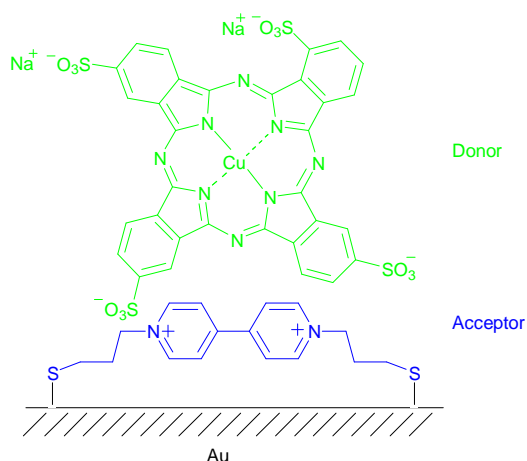


**Figure 2-47** Hybrid structure of 4,4'-bipyridinium and copper phthalocyanine-3,4',4'',4'''-tetrasulfonate<sup>104</sup>

The electrical properties of the structure were investigated using STS and the results showed asymmetric curves with a high rectification between 60–100 at  $\pm 1 \text{ V}^{104}$  (see **Figure 2-48**).

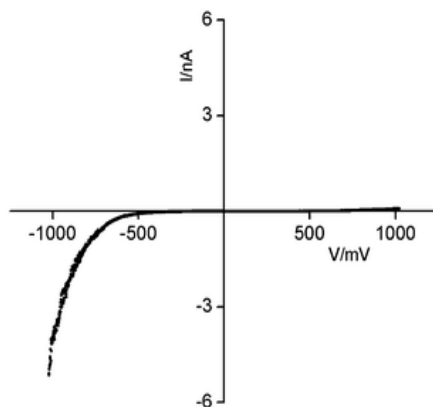


**Figure 2-48** I-V characteristic of hybrid structure of 4,4'-bipyridinium and copper phthalocyanin-3,4',4'',4'''-tetrasulfonate<sup>104</sup>

The high RR was attributed to the D/A structure; in particular to the mechanism proposed by Aviram and Ratner<sup>1</sup>. To provide additional evidence to support this statement, subsequent experiments were undertaken. On top of the phthalocyanine layer a cationic acceptor monolayer (4,4'-bipyridinium) was deposited to obtain an Au | acceptor | donor | acceptor | Au structure. Also, the Au | 4,4'-bipyridinium | Au junction was investigated<sup>104</sup>. The results matched expectations, as both systems showed symmetric I–V characteristics.

To support these results, another D/A structure formed using the ionically assembly method was studied<sup>105</sup>. In this case, a bipyridinium layer acting as an acceptor was replaced by a protonated 7 nm long wire (see **Figure 2-49**). The wire was investigated using STS and showed no rectification when deposited alone on a gold-coated substrate (see **Figure 2-50 (a)**).

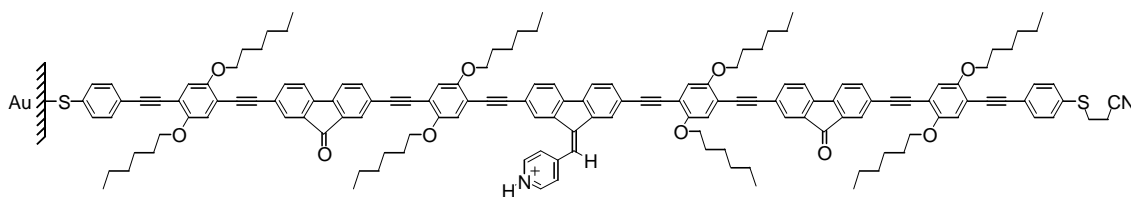


**Figure 2-49** Structure of the 7 nm wire<sup>105</sup>

However, when molecules of an electron-donating phthalocyanine (Figure 2-47) were deposited on top of the wire monolayer, asymmetrical I–V characteristics were observed and the RR ranged between 20 and 80 at  $\pm 1\text{ V}^{105}$  (see Figure 2-50 (b)). The large variation of the RR value might be a consequence of the non-uniform alignment across the whole sample, where some regions may have been better aligned.

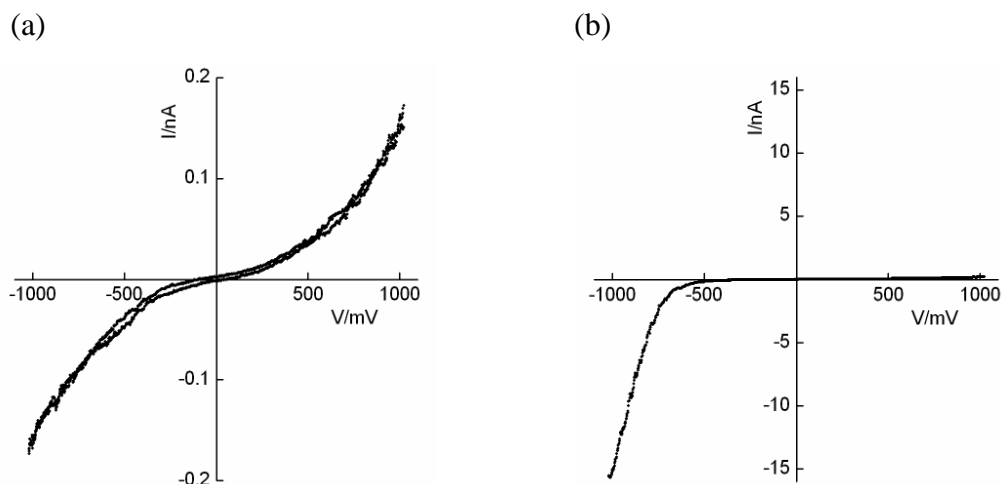


Figure 2-50 I-V characteristics of (a) 7 nm wire, (b) hybrid structure of the 7 nm wire and Pc<sup>105</sup>

This hybrid structure<sup>105</sup> proved that it was possible to assemble electron donating and electron accepting groups into a hybrid structure in order to induce or improve rectification. Due to the promising results obtained, other hybrid structures comprising of molecular wires with different lengths are currently under investigation.

### 2.2.6.3 Ionically coupled structures on Au-S-CH<sub>2</sub>CH<sub>2</sub>CH<sub>2</sub>-SO<sub>3</sub><sup>-</sup>.

The promising results obtained from ionically assembled D/A structures led to studies of cationic D- $\pi$ -A molecules aligned on a self-assembled anionic thiol (sodium 3-mercaptopropylsulfonate)<sup>42</sup>. Ashwell *et.al.*<sup>43</sup> investigated four hybrid structures. Two of the cationic D- $\pi$ -A molecules showed similar results to those obtained from the ionically coupled structure on Au-S-CH<sub>2</sub>CH<sub>2</sub>CH<sub>2</sub>-SO<sub>3</sub><sup>-</sup>. Two other examples (see Figure 2-51) revealed an improvement of rectification. The first hybrid structure<sup>43</sup> (see Figure 2-51 (1)) provided a very high RR of 450 at  $\pm 1\text{ V}$  compared to only 14 at  $\pm 1\text{ V}$  for the analogue that was deposited using the SA technique<sup>35</sup>. In the case of the second



cationic D- $\pi$ -A dye (see **Figure 2-51 (2)**) the rectification obtained was in the range of 50–150 at  $\pm 1$  V when self assembled via chemisorption<sup>67</sup>. Whereas, the same dye was ionically assembled the initial RR of 30–60 at  $\pm 1$  V was obtained shortly after deposition, and this increased to 100–200 at  $\pm 1$  V after a few hours<sup>43</sup>. This phenomenon was explained by self-organisation of the structure<sup>76,106</sup>.

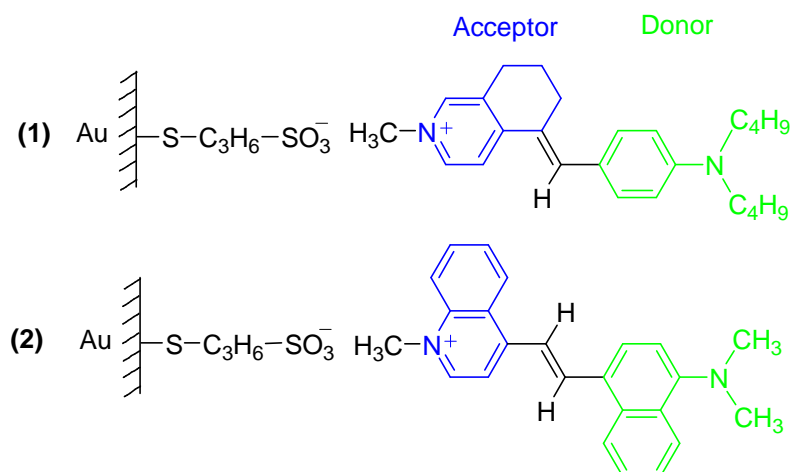


**Figure 2-51** Hybrid structures of Au-S-C<sub>3</sub>H<sub>6</sub>-SO<sub>3</sub><sup>-</sup> | A<sup>+</sup>- $\pi$ -D | Au structures<sup>43</sup>

According to the Aviram and Ratner theory<sup>1</sup> of rectification, these structures should exhibit an asymmetric I-V characteristic with the higher current in the negative quadrant of the plot, and as expected the STS studies confirmed this. These results<sup>43</sup> also demonstrated that the formation of a well-packed and ordered monolayer is extremely important in order to obtain high rectification, and that it can be achieved by the simple modification of the substrate's surface.

#### 2.2.6.4 Further studies of mixed bilayer structures based on the ionic assembly approach

The ionic assembly approach was also used to demonstrate the significant improvement in the rectifying behavior of molecular rectifiers based on the D-electron bridge-A structure<sup>1</sup>. Three separate systems based on the Au-S-C<sub>10</sub>H<sub>20</sub>-A<sup>+</sup>- $\pi$ -D | D<sup>-</sup> | Au structure<sup>107</sup> were studied (see **Figure 2-52**)

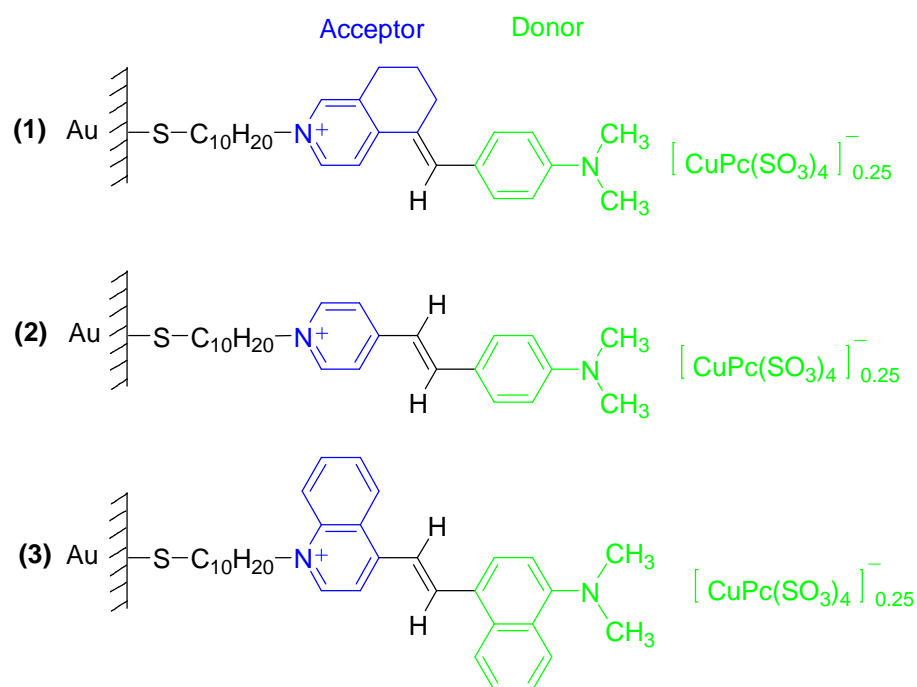


**Figure 2-52** Au-S-C<sub>10</sub>H<sub>20</sub>-A<sup>+</sup>-π-D | D<sup>-</sup> | Au structures<sup>107</sup>

In all cases, a cationic D-electron bridge-A dye was deposited on a gold-coated substrate using the self-assembly technique, and then an anionic donor was placed on the top via ionic assembly. The verification of the methathesis was provided by the UV-VIS spectrum on a glass slide coated with a 10 nm thick platinum film. The STS data yielded rectifying behaviour<sup>107</sup> with an RR of 3000 at  $\pm 1$  V (see **Figure 2-53**), the highest RR observed to date from an experiment that adhered to the Aviram and Ratner model<sup>1</sup>. This high value of RR was obtained from the Au-S-C<sub>10</sub>H<sub>20</sub>-A<sup>+</sup>-π-D | D<sup>-</sup> | Au system, where 5-(4-dimethylaminobenzylidene)-5,6,7,8-tetrahydro-isoquinolinium, was the cationic dye and the anionic donor (forming the second layer) was copper (II) phthalocyanine-3,4',4'',4'''-tetrasulfonate (see **Figure 2-52 (1)**).

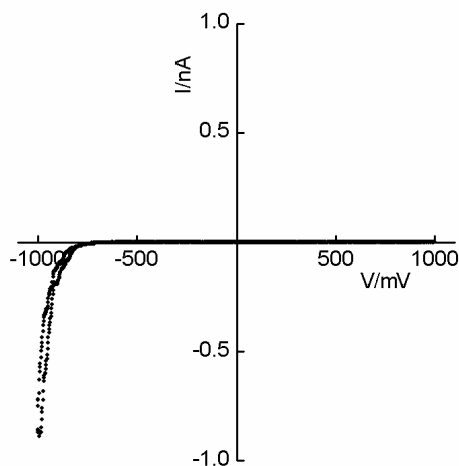


**Figure 2-53** I-V characteristic of Au-S-C<sub>10</sub>H<sub>20</sub>-A+ $\pi$ -D|D-Au structure, where the cationic moiety was 5-(4-dimethylaminobenzylidene)-5,6,7,8-tetrahydroisoquinolinium, and the anionic donor (forming the second layer) was copper (II) phthalocyanine-3,4',4'',4'''-tetrasulfonate<sup>107</sup>

Ashwell *et al.*<sup>107</sup> believed that the electrical properties of these systems were determined by the cationic dye, and in particular to the steric hindrance that effectively separated molecular orbitals localised on either acceptor or donor<sup>67</sup>. These studies also showed that the deposition of an additional layer of phthalocyanine enhanced the donor effect. Studies of two other hybrid structures<sup>107</sup> (see **Figure 2-52 (2 and 3)**) showed further evidence that rectification resulted from the hybrid structure. The structure<sup>107</sup> (see **Figure 2-52 (2)**), showed asymmetric I-V plots with RR of 15–70 at  $\pm 1$  V, whereas the same cationic moiety, without a monolayer of the phthalocyanine, showed a lack of rectification<sup>35</sup>. A significant improvement of RR was also observed for the third hybrid structure (see **Figure 2-52 (3)**), where RR increased from 50–150<sup>67</sup> to 700–900<sup>107</sup> at  $\pm 1$  V. These impressive results proved that this method may prove to be a perfect technique for incorporating successful materials into molecular electronic devices in the future.

### 2.3 Possible applications

There are a number of articles<sup>2,12</sup> and books<sup>7,108</sup> devoted to possible future applications of molecular rectifiers. They have been considered as potential materials for an electrochemical photodiode<sup>109</sup>, switches<sup>20</sup>, as liquid crystals in displays<sup>110</sup>, dye lasers,

sensors<sup>111</sup>, logic gates<sup>112</sup> and elements of memory storage<sup>113</sup>. The advantage of organic materials is that they can often be incorporated into a polymeric structure<sup>114</sup>, which can be used (for instance) to build photovoltaic cells<sup>115</sup>, diodes<sup>116</sup> and transistors<sup>20,117</sup>. However, it is not the objective of the research presented here to create a fully operational device. These few examples of possible applications are given purely to highlight the great potential behind organic materials.

## **2.4 Monolayer deposition**

To consider any organic materials for the use in a molecular electronic device, it often has to be aligned in a defined way. For this purpose, two deposition techniques (LB and SA) were implemented.

### **2.4.1 Langmuir–Blodgett technique**

The history of Langmuir films dates back to 1774, when Benjamin Franklin deposited oil on a water surface and observed its calming influence at Clapham pond<sup>118</sup>. Later, in the 1880s, Rayleigh<sup>119</sup> studied the surface tension lowering effect when oil was distributed on a water surface. Then in 1891, Pockel's studies<sup>120</sup> proved that oil formed a thin layer at the surface. Finally, joint studies by Langmuir<sup>36</sup> and Blodgett<sup>37</sup> led to the technique that allowed monolayers (called Langmuir films) to be deposited on solid substrates resulting in Langmuir–Blodgett (LB) films.

#### **2.4.1.1 Materials for Langmuir and LB films**

Organic thin films have attracted considerable attention over the past few decades for their potential applications<sup>121,122</sup> as sensors, membranes, displays, transistors etc.

The Langmuir film<sup>36,123</sup> is a monolayer formed by amphiphilic molecules trapped at an interface of two different environments, for instance: oil–water or water–air. The monolayer–forming molecules consist of two distinct groups: a hydrophilic and a hydrophobic part (see **Figure 2-54**).

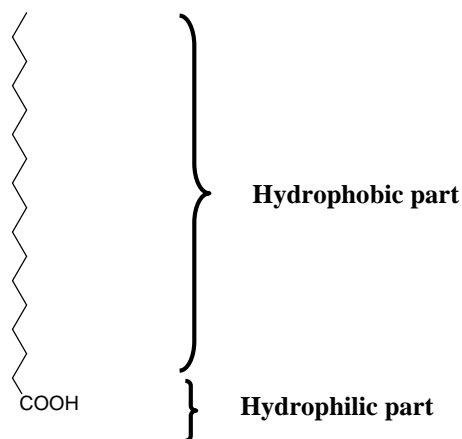


**Figure 2-54** Molecular structure of stearic acid, a typical amphiphilic molecule

The hydrophilic part is readily soluble in water, while the hydrophobic part is soluble in non-polar solvents. This specific architecture allows the molecule to be anchored at the interface of the two phases (usually water–air) and eventually form the Langmuir film. However, a correct balance between a hydrophobic and a hydrophilic part must be maintained. It was discovered<sup>122,123</sup> that  $C_{12}H_{25}$  appeared to be a critical length for the aliphatic chain. The formation of a stable monolayer was difficult to achieve with chain lengths less than this. Extensive studies<sup>13,123,124</sup> of amphiphilic molecules also revealed that any changes implemented to either the hydrophilic or hydrophobic part would result in changes to the material properties, alignment and structure. These are important features because they allow the production of molecules with desirable properties in a controlled way. For instance, the increase of the chain length causes a decrease in the water solubility of the molecule<sup>124,125</sup> (see **Figure 2-55**).



**Figure 2-55** Structures of anthracene derivatives studied by Stewart<sup>125</sup>

The implementation of double bonds or the replacement of an atom<sup>126</sup> is known to disrupt the geometry of the chain and so influences the packing and consequently alters the properties<sup>122,124</sup> (see **Figure 2-56**).

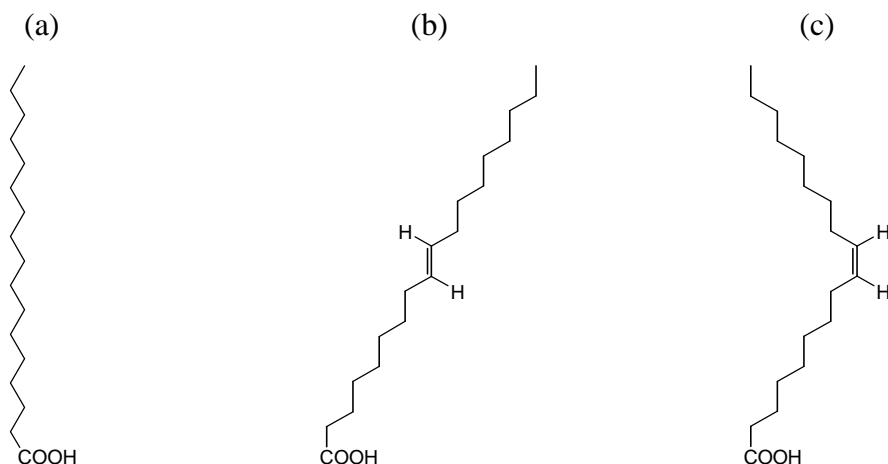


**Figure 2-56** (a) Stearic acid, (b) oleic acid, cis form, (c) elaidic acid, trans form<sup>126</sup>

The modification can also be introduced as a variation of the ‘head group’ of the amphiphilic molecule. The carboxylic group ( $-\text{COOH}$ ) could be replaced by an ester ( $-\text{CO}_2\text{R}$ ), an amide ( $-\text{CO}_2\text{NH}_2$ ), amine ( $-\text{NH}_2$ ) or alcohol ( $-\text{OH}$ )<sup>123,124</sup>.

Since the LB technique was established, a wide range of organic materials have been investigated using this method. These materials have included fatty acids and their derivatives<sup>122,124</sup>, derivatives of benzene<sup>122,125</sup>, heterocyclic compounds, dyes, liquid crystals, polymers, TCNQ derivatives, azobenzenes (and their derivatives), cyanine and merocyanine dyes<sup>124,127</sup>. Unconventional compounds such as porphyrine<sup>128</sup> and phthalocyanines (Pc)<sup>129,130</sup> have attracted much interest. They are macrocyclic compounds and are ubiquitous in nature. Although porphyrines and phthalocyanines do not possess an amphiphilic feature that is necessary for LB deposition, it is possible to generate LB film-forming derivatives by alkylation with different length hydrocarbon chains attached to the outside of the ring<sup>122</sup>. In a similar way to phthalocyanines<sup>129,130</sup> and porphyrines<sup>128</sup>, also squaraines<sup>131,132</sup>, which consist of two donor parts and one centrally located acceptor could be subjected to alkylation in order to form an amphiphilic structure (see **Figure 2-57**).

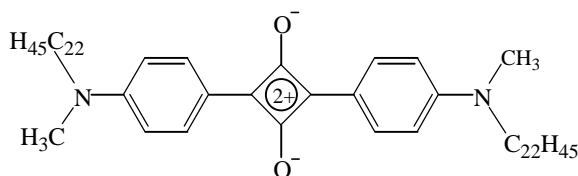


**Figure 2-57** Structure of squaraine studied by Ashwell *et al.*<sup>131</sup>

Studies<sup>131,132</sup> did confirm that these molecules formed Langmuir films and that the LB technique could be used to deposit them onto solid substrates.

A particularly unusual group of molecules that had been successfully deposited using the LB technique are fullerenes (C<sub>60</sub>, C<sub>70</sub>)<sup>133,134,135</sup>. These are not typical amphiphilic compounds, however, published results showed that pure fullerene C<sub>60</sub> or a mixture of C<sub>60</sub> with arachidic acid generated Langmuir films on a subphase<sup>133,134</sup>.

As described above, typical amphiphiles consist of a hydrophilic head and a long aliphatic chain. However, the long chain tends to act as a spacer and also increases the overall thickness of the monolayer<sup>26</sup>. Due to these factors, a lot of effort has been made to design molecules with shorter hydrocarbon chains. This research has led to a group of molecules called chevron-shaped<sup>69,92</sup>, or bent-core<sup>136,137</sup>, which are mainly known to be liquid crystals<sup>138,139</sup>.

Zou *et al.*<sup>140</sup> published studies of different chevron-shaped liquid crystals in Langmuir films (see **Figure 2-58**).

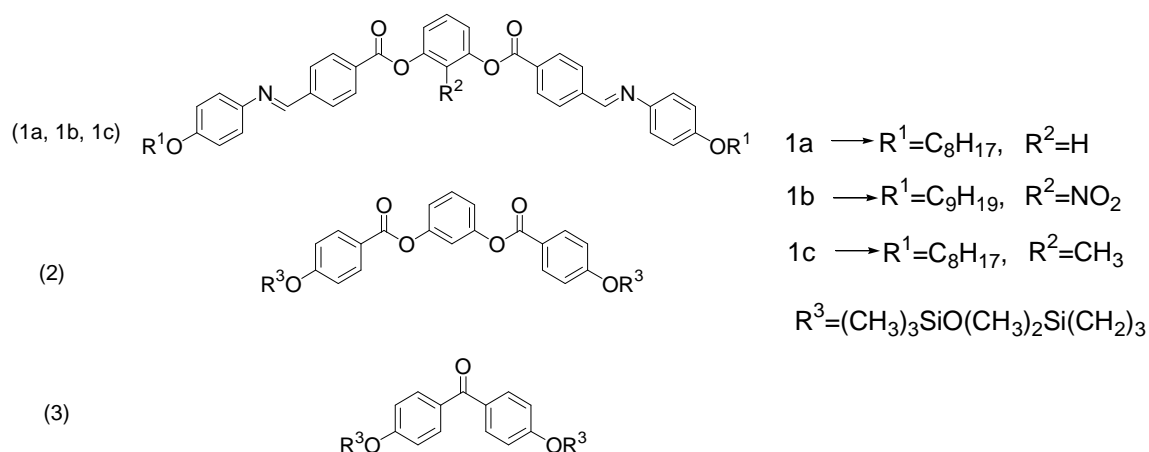


**Figure 2-58 Structures of different chevron-shaped liquid crystals<sup>140</sup>**

The hydrophobicity of both, the core and the end of the chains, were varied in order to study the molecules behaviour when deposited on a water surface. The results of five different molecules demonstrated that it was possible to form stable Langmuir

monolayers from chevron-shaped molecules. Deep analysis showed also that the properties of these layers strongly depended on the individual character of the molecule. The molecules with amphiphilic end chains were aligned flat on the air-water surface, whereas the molecules with hydrophobic chains formed a complex multilayer structure<sup>140</sup>.

Ashwell *et al.*<sup>69,92</sup> reported LB films from two different chevron-shaped molecules (see **Figure 2-37** and **Figure 2-59**).

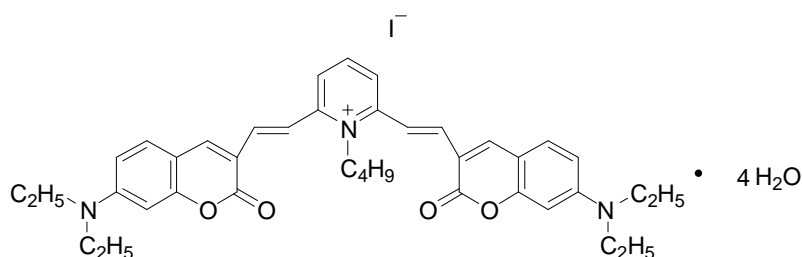


**Figure 2-59** Structure of a chevron-shaped molecule studied by Ashwell<sup>92</sup>

They have a central cationic acceptor and two  $\pi$ -bridged donor groups (D- $\pi$ -A- $\pi$ -D). The angle between the charge-transfer axes of the chevron-shaped molecule was ca. 120°. These chevron-shaped molecules represented a modified model of an Aviram and Ratner type rectifier. Published results<sup>69,92</sup> revealed that although they had short aliphatic chains it was possible to deposit them using the LB technique. It was shown that these molecules formed a non-centrosymmetric alignment and showed rectifying properties, and detailed studies are provided in a result section.

A majority of the research regarding chevron-shaped materials was based on theoretical studies of the molecules behaviour at the air-water interface<sup>141,142,143</sup>. Simulations of a chevron-shaped molecule depicted in **Figure 2-60** were carried out by Duff *et al.*<sup>141</sup>.



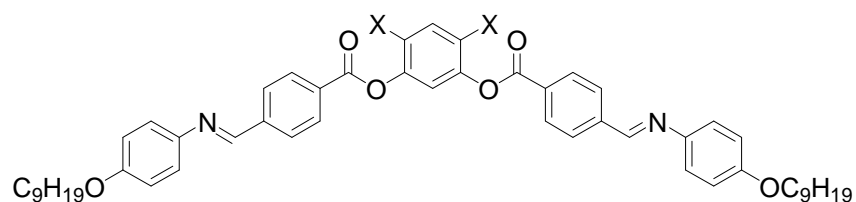


**Figure 2-60 Structure of a chevron-shaped molecule studied by Duff *et al.*<sup>141</sup>**

Calculations showed completely different molecular arrangements between films in a vacuum and films on the water surface. According to simulations the molecules aligned on the water surface in such a way that the central and outer phenyl rings tended to be flat with respect to the water surface, while the inner phenyl rings of the wings tended to take on a broad range of orientations. The studies also revealed that substitution of two hydrogen atoms on the central phenyl ring with chlorine affected the conformation significantly. AFM studies of very similar structures<sup>144</sup> to the one shown in **Figure 2-60** also revealed a strong relationship between the molecular structure and the arrangement.

#### **2.4.1.2 Pressure–area isotherm**

The isotherm is a plot of the surface pressure as a function of surface area of the water surface available to each molecule. In order to be obtained, molecules of interest are dissolved in a non-polar and volatile solvent that does not mix with the subphase<sup>36,37,124</sup>. A freshly prepared solution is then deposited drop-wise on a clean surface (usually water), which must have previously been submitted to a purification process. The solution once deposited on a water surface will spread rapidly and cover all the available area. The molecules assemble spontaneously in such a way that the polar head group are immersed in the water and the long hydrocarbon chains are pointing towards the air and the monolayer will begin to form. During the deposition process, the solvent evaporates to leave the molecules as a highly disordered film on the surface. The film is then compressed, causing the molecules to align and eventually to generate a well-packed and ordered structure that is called a Langmuir film<sup>36,124</sup> (see **Figure 2-61**).

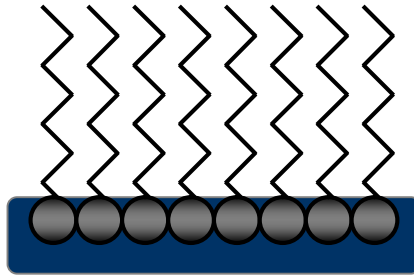


**Figure 2-61** The alignment of the amphiphilic molecules in a Langmuir film at the air–water interface

The state of the monolayer can then be characterised by controlling the changes in the surface tension<sup>124,145</sup>. The surface pressure is defined as the difference between the surface pressure of pure water ( $\gamma_0$ ) and that of the water covered by the monolayer ( $\gamma$ ):

$$\Pi = \gamma_0 - \gamma \quad (1)$$

The surface pressure measurement is recorded using Wilhelmy plates attached to a microbalance. The Wilhelmy plate is a strip of a very thin material that can be platinum, glass, quartz, mica or chromatography paper, which when suspended at an air–water interface is pulled down into the subphase by the surface tension of water<sup>145</sup> (see **Figure 2-62**).

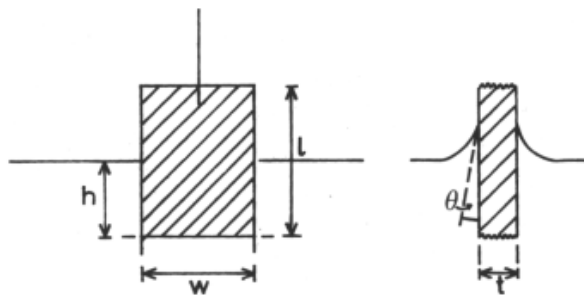


**Figure 2-62** Wilhelmy plate arrangement<sup>145</sup>

When the molecules of an organic surfactant are deposited on the surface, it results in a decrease of the surface tension. The opposing forces acting on the plate consist of gravity and surface tension acting downward, while buoyancy due to the displaced water acts upward. When a rectangular Wilhelmy plate of dimensions  $l_p$ ,  $w_p$ ,  $t_p$  and density  $\rho_p$  is immersed to a depth  $h_l$  in a liquid of density  $\rho_l$ , then the force is given by the following equation<sup>145</sup>:

$$F = \rho_p \cdot g \cdot l_p \cdot w_p \cdot t_p + 2\gamma \cdot (t_p \cdot w_p) \cdot (\cos\theta) - \rho_l \cdot g \cdot t_l \cdot w_l \cdot h_l \quad (2)$$

where  $\gamma$  is the liquid surface tension,  $\theta$  is the contact angle of the liquid on the solid plate and  $g$  is the gravitational constant.

Using equation (2) and estimating that the plate is completely wetted by the liquid (i.e.  $\cos\theta = 1$ ), the surface pressure can be determined from the following equation<sup>145</sup>:

$$\Pi = -\Delta\gamma = -\left[\frac{\Delta F}{2(t_p + w_p)}\right] = -\frac{\Delta F}{2w_p}, \text{ if } w_p \gg t_p \quad (3)$$

It is the difference in  $F$  measured for a stationary plate between a clean surface and the same surface with a monolayer present.

An isotherm is the most important indicator of the monolayer properties of an amphiphilic material. The shape of the isotherm is characteristic for the molecules that form the thin film and it provides information about the size, orientation, degree of order and stability of the compressed monolayer at high pressures<sup>36,124</sup>. In the ideal case, three characteristic phases can be observed on the isotherm: gas, liquid and solid phase (see **Figure 2-63**).

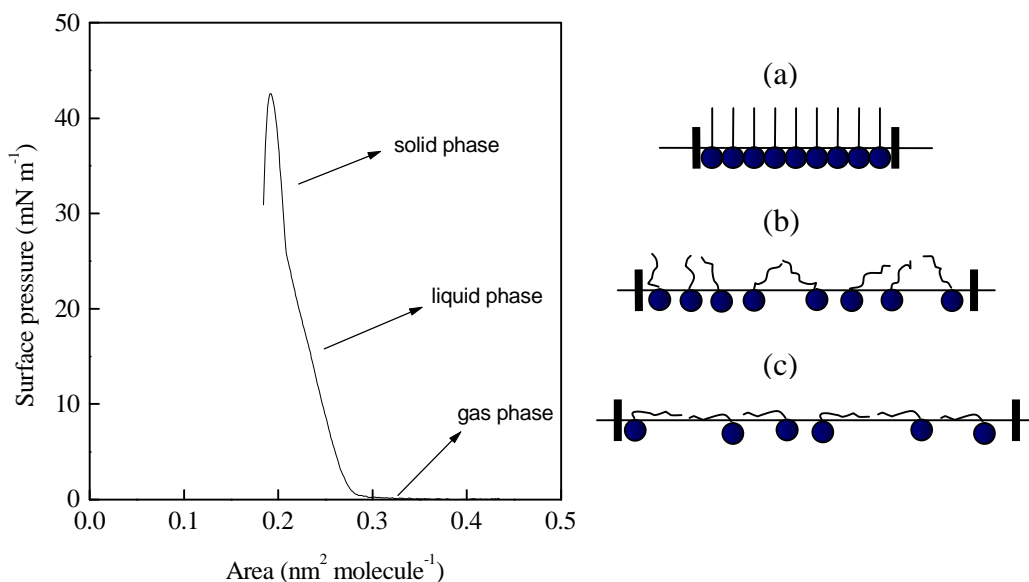


**Figure 2-63** The isotherm of stearic acid; (a) solid phase, (b) liquid phase, (c) gas phase<sup>123</sup>

In the gas phase, molecules stay highly disordered and the intermolecular distance between molecules is large and interactions between them are small. Hence, the monolayer has rather little effect on the water's surface tension and the surface pressure is very low (close to zero). As the result of a slow compression, the surface tension rises. Molecules are forced closer to each other and start forming a more ordered structure<sup>36,124</sup>. This effect is observed in the next phase and is called the liquid phase. Further compression leads the liquid phase into the solid phase. At this stage the molecules are very closely packed and interact strongly with each other and consequently the surface tension increases dramatically. The solid phase reflects the well-defined and ordered monolayer<sup>124</sup>. The film will eventually reach its collapse point when further compression is applied to the monolayer beyond the solid phase and this is characteristic for every Langmuir film. It is defined as the maximum pressure to which a monolayer can be compressed and still retain its well-ordered structure. After this point the film breaks and the surface pressure drops significantly<sup>124,36</sup>. However, instead of evenly covering the available area, molecules will often group to form domains when spread on the water surface. Therefore, the shape of an isotherm can significantly differ from the ideal. With an ideal isotherm, the boundaries of the phases are easily identifiable, but in practice, as presented in the results, these boundaries are not clearly defined and sometimes there is no observable collapse point.

#### **2.4.1.3 Experimental considerations for Langmuir and LB films formation**

The monolayers formed using the LB technique are usually of fairly high quality and great care must be taken to ensure film consistency<sup>36,124,123</sup>. The parameters to be considered involve the:

- Type of the molecules and solvents
- Chemical purity
- Subphase
- Trough
- Environment.

A crucially important factor is having a correct balance between the hydrophilic and hydrophobic parts of the amphiphile. If the 'tail group' is not hydrophobic enough, then

the whole unit may dissolve in water. On the other hand, if there is no hydrophilic part, the molecule may form a thick multilayer film on the surface. The molecules need to be dissolved in an appropriate organic solvent that is highly volatile and insoluble in water, and also chemically inert in relation to the studied material<sup>124,145</sup>. Some of the organic solvents may dissolve in water, and so the amphiphile (instead of generating the monolayer on the surface) can ‘sink’ or precipitate in the subphase. This is very common when acetone or isopropanol are used as a solvent<sup>122</sup>. The subphase that is most commonly used is water. However, there are reported cases when also mercury was utilised<sup>146</sup>. Before use, water is subjected to a purification process (double distillation) that will eliminate contamination. It is a vitally important factor that can affect the quality of the monolayer<sup>13,124</sup>. For the same reason, only the highest purity chemicals available can be used for solution preparation. The trough and substrates used for the experiment also need to be carefully cleaned. There are also constraints set for the material the trough can be made of. The requirements are quite straightforward; the material must be inert and must not release impurities into the subphase. It should be able to withstand organic solvents as well as inorganic acids. A clean-room environment also needs to be provided. Any contaminants, even very small amounts can be easily incorporated into a generated monolayer, which can significantly alter the area per molecule and change the properties of the monolayer formed<sup>124,122</sup>.

#### **2.4.1.4 LB film deposition**

At the appropriate target pressure (during the solid phase) the film is transferred onto a solid substrate. The substrate is immersed slowly into the subphase and passes through the Langmuir film using the dipper mechanism. During transfer of the compressed monolayer onto the substrate, the pressure is kept constant by a moving barrier. It is very important to choose the correct pressure for the deposition. It cannot be too low as the monolayer will not be well-packed, and it cannot be too high as the film can collapse while transferring onto the solid substrate. There are two methods of deposition depending on the substrate’s character. If it is hydrophilic, then the dipping direction is on the upstroke (as shown in **Figure 2-64**), if it is hydrophobic, then the deposition will be on the downstroke<sup>123,145</sup>.

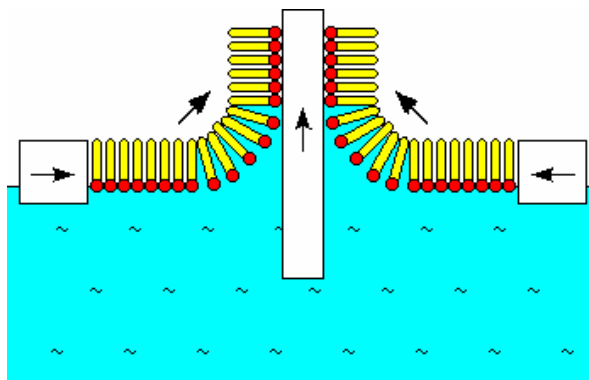


**Figure 2-64** Mechanism of deposition of the Langmuir film onto a solid substrate to form an LB film<sup>147</sup>

By utilising the LB technique it is possible to produce highly ordered and aligned monolayer or multilayer films. Depending on the orientation of the layers with respect to the substrate, and to each other, the multilayers can be aligned on the solid substrate in three different ways (an X, Y and Z – alignment)<sup>13,124</sup>. These are illustrated in **Figure 2-65**.

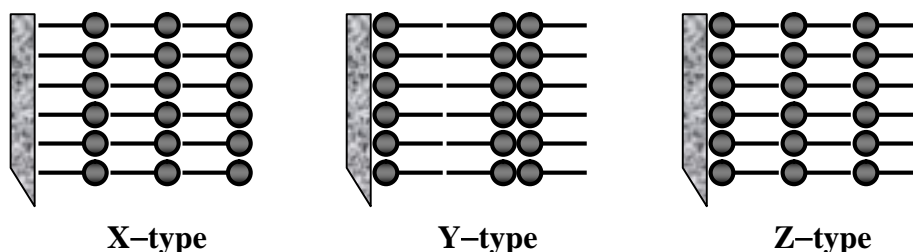


**Figure 2-65** X,Y and Z-type alignment of multilayer LB films<sup>123,124</sup>

In the X-type alignment, all layers are transferred on the downstroke. In the case of Y-type, the first layer is deposited on the upstroke and the second layer is transferred on the downstroke and this process is then repeated. In this case the layers are deposited so that they are aligned in a head-to-head and tail-to-tail arrangement. However, the most popular alignment is the Z-type, where each layer is transferred on the upstroke<sup>13,124,123</sup>.

## 2.4.2 Self-assembled monolayers

Much research has been focused around the deposition methods known as self-assembly<sup>13,148,149</sup>. This method has potential for applications in corrosion, sensors, biological applications and electronic devices<sup>13,148,150</sup>. Experiments regarding this deposition method were first reported in 1946 by Zisman<sup>151</sup>. However, interest was renewed in the early 1980's, and since then the growth in the number of published papers has been noted<sup>152,153,154</sup>. Self-assembled monolayers (SAMs) are defined as stable, well-ordered organic molecular assemblies that are formed spontaneously, either from solution or gas phase. The organic constituents are adsorbed on an appropriate substrate in an immersion process, which is based on the chemisorption phenomenon. Adsorption is driven by the formation of a chemical bond between a molecule and the substrate<sup>41,148</sup> (see **Figure 2-66**). The substrate acts as a support for the SAM. Its surface, depending on the application of the deposited SAM, can vary from planar (glass or silica covered by very thin metal films of gold, silver, copper, platinum, mercury or iron) to highly curved monostructures (colloids, nanocrystals and nanorods)<sup>40</sup>.

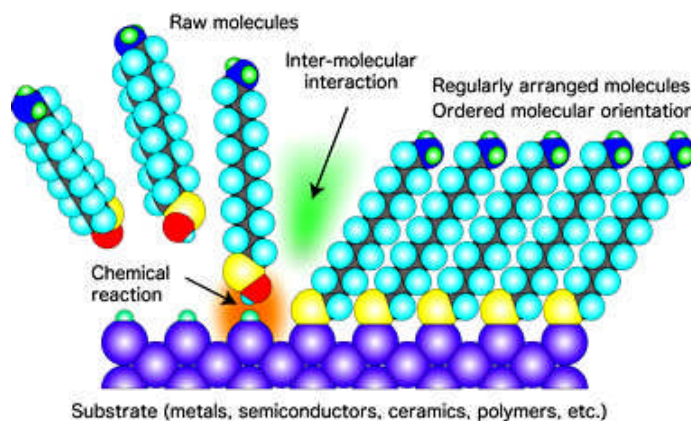


**Figure 2-66** SAM formation on a substrate<sup>155</sup>

### 2.4.2.1 Materials used in SAMs

Using this method, a wide variety of molecules can be incorporated into the structure of a SAM. These include the deposition of alcohols, fatty acids, organosilicon derivatives and organosulfur compounds<sup>13,148</sup>. Similar to molecules used in the LB technique, the organic assemblies consist of various segments (see **Figure 2-67**).





The second segment of the self-assembled molecule is the ‘body’ that can include alkyl chains and/or aromatic rings. This part of the molecule provides a well-defined thickness and also acts as a physical barrier<sup>156,157</sup>. Finally, the ‘functional group’ determines the surface properties. The terminal groups can be chosen with regards to the application of the monolayer, and can include either  $-\text{CH}_3$ ,  $-\text{OH}$ ,  $-(\text{C}=\text{O})\text{OCH}_3$ ,  $-(\text{C}=\text{O})\text{CH}_3$ ,  $-(\text{C}=\text{O})\text{CF}_3$ ,  $-(\text{C}=\text{O})\text{C}_6\text{H}_5$ ,  $-\text{COOH}$  or  $-\text{OSO}_3\text{H}$ .<sup>13,148,152</sup>

The most extensively studied compounds are organosulfur molecules<sup>153,157,158,159</sup> such as alkanethiols, disulfides or sulfides (see **Figure 2-69**).

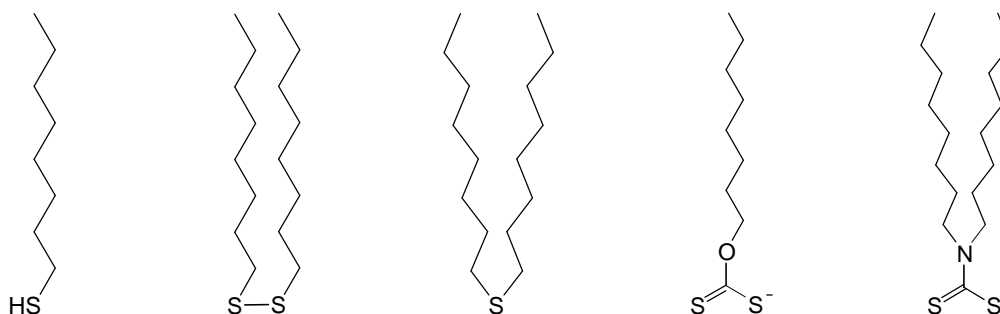


**Figure 2-69 Organosulfur compounds**<sup>156,158,159</sup>

These molecules bind to the surface of metals via the formation of a metal-sulfur bond. Due to thiols having a very high affinity to gold (a strong gold-sulfur bond is easily formed) they are known to generate well-defined and ordered monolayers. The first results referring to the deposition of organosulfur compounds on gold were published in 1982 by Taniguchi<sup>160</sup>. It was observed that pyridine disulfide spontaneously formed a SAM on gold (see **Figure 2-70**).

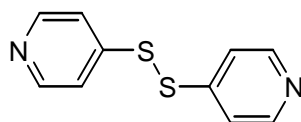
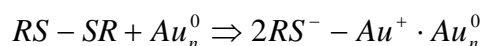


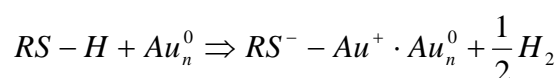
**Figure 2-70 Structure of pyridine disulfide studied by Taniguchi**<sup>160</sup>

Then in 1983, Nuzzo and Allara<sup>161</sup> reported that bifunctional disulfides formed an oriented monolayer on a gold surface. According to work reported by Bain and

Whitesides<sup>162</sup>, the chemisorption of dialkyldisulfides and alkanethiols on clean gold gave undistinguished monolayers, where Au (I) and thiolate (RS<sup>-</sup>) species were formed. It was believed that the chemisorption process of dialkyldisulfides could be described as follows\*:



As for alkanethiols, the reaction is shown below\*:



#### 2.4.2.2 Experimental considerations for SAM preparation

Similar to the LB technique, there are a few very important parameters that influence the order<sup>13</sup>, stability and the rate of the deposition<sup>153,157</sup> of the SAM<sup>163</sup>, and these include:

- Molecular structure,
- Chemical purity,
- Cleanliness of the substrate,
- Concentration of the solution,
- Immersion time,
- Temperature.

The understanding of the relationship between molecular structure and their organisation on the surface is essential. The packing and orientation of molecules affect surface chemistry and it is crucial to successfully produce monolayers with the desired properties. Therefore, several investigations of molecular arrangements of alkanethiol SAMs and in particular to those on Au (111) surfaces have been studied<sup>164</sup>. It was reported<sup>165</sup> that the n-alkanethiol molecules within the monolayer had a tendency to be tilted with respect to the surface normal, by typically 30°. Whereas, aromatic compounds, such as p-biphenylthiols, p-terphenylthiols, and oligo(phenylene ethylene)

---

\* It is an accepted way of presenting chemisorption of dialkyldisulfides and alkanethiols to gold, although the equations do not balance.

thiols appear to be bonded to the surface at different angles<sup>148</sup>. Porter *et al.*<sup>166</sup> discovered that the reduction of the alkyl chain length of n-alkylthiols leads to disordered monolayers with lower packing and coverage.

The other concern is the purity of studied molecules and solvents, and the use of a clean substrate. The formation of ordered and stable monolayers is essential for the future development of molecular devices. It is important to minimise the amount of any contamination, as it can be easily incorporated into the monolayer and consequently affect the structure and properties<sup>148,167,168</sup>. The most common solvent used to prepare the SAM is ethanol. The reason it is used so widely is that it dissolves a variety of alkanethiols with varying degrees of polar character and chain length. It is also available with high purity and shows low toxicity<sup>13</sup>.

The concentration and the duration of immersion play important roles in the adsorption process and they are inversely related. The lower the concentration of the adsorbate solution, the longer the immersion time required for the deposition. Additionally, increasing the individual immersion time reduces the number of multiple immersions and consequently reduces the overall time required for the process of monolayer formation<sup>153,158</sup>.

It was also noted that the SAMs formed at temperatures above 25°C exhibited higher order due to the improvement in kinetics. The higher temperature also increased the rate of desorption for adventitious materials and solvents physisorbed on the surface<sup>13,153</sup>. Uosaki *et al.*<sup>101</sup> believed that the temperature effect is particularly important during the first few minutes of the deposition, when the adsorption and reorganisation is taking place.

#### **2.4.2.3 SAM deposition**

There are several reasons why the self-assembly method became so popular. First of all, it is easy to prepare and it does not need a ultrahigh vacuum or complicated and expensive equipment. Moreover, the monolayers can be formed on objects of all shapes and sizes.

The deposition procedure to form a SAM is very simple<sup>13,41</sup>. The molecules are dissolved in an appropriate solvent, which is usually ethanol with a concentration normally being in the range of 1–10 mM. The freshly prepared solid is then immersed into the solution for certain periods of time to allow molecules to attach to the gold via a chemical bond (see **Figure 2-71**).

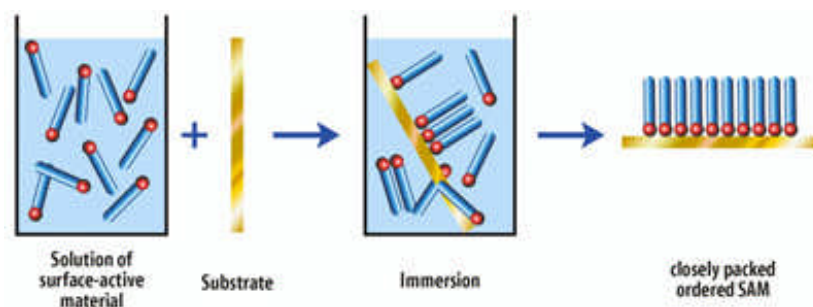


**Figure 2-71** Formation of SAMs from solution<sup>169</sup>

Between each immersion the sample is rinsed with appropriate solvents in a certain sequence to prevent physisorption of the molecules. The immersion time is individually matched to each compound studied. The total time of deposition can vary between 100 to 1000 minutes or more, as some molecules attach quicker than others.

Bain *et al.*<sup>153,157</sup> studied the kinetics of alkanethiol monolayer formation on gold. It was found that there were two adsorption kinetics. For a solution with concentrations of approximately  $10^{-3}$  M, the adsorption process occurred very rapidly during the first few minutes. During this time 80–90 % of the molecules were deposited. The kinetics then decreased significantly and the process to complete a monolayer can then take several hours.

## 2.5 Methods for monolayer characterisation

### 2.5.1 Quartz crystal microbalance

The area per molecule was determined using the QCM technique<sup>170,171</sup>. It is a well-established tool designed for monitoring the adsorption and desorption of small amounts ( $\text{ng}/\text{cm}^2$ ) of materials onto surfaces. It is widely used in drug research, development of gas sensors and thin film formation, and the detection of contamination, bacteria, etc.<sup>172,173,174</sup>. Measurements can be taken both, in a vacuum or in a normal atmosphere. It is a non-invasive technique, and together with the thickness measurements obtainable from the surface plasmon resonance (SPR) technique, a full understanding of the makeup of a molecular monolayer can be gained with insight into packing order, tilt angle, and even surface stability. The QCM consists of an AT-cut piezoelectric quartz crystal wafer. Either side of the quartz crystal are thin gold film electrodes (see Figure 2-72).

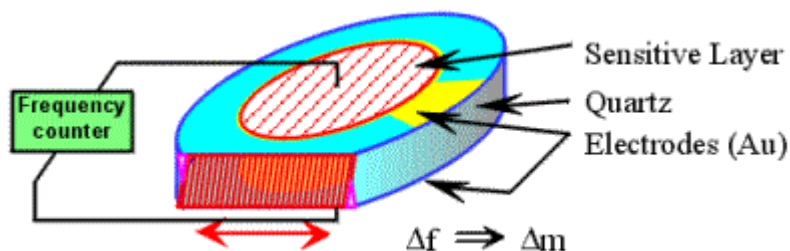


Figure 2-72 Quartz crystal microbalance structure<sup>175</sup>

The QCM is sensitive to deposition or accumulation of a surface mass and it can be used to monitor the kinetics of a deposition process in real time<sup>176</sup>. When the electrodes are connected to an oscillator and a voltage is applied over the electrodes, the quartz crystal oscillates at its resonant frequency. Mass adsorbed or desorbed causes a frequency change that can be detected at any time during the deposition process. The additional mass adsorbed causes a decrease in the oscillation frequency of the quartz crystal. Accordingly, a removal of any mass is recorded by an increase in the oscillation frequency<sup>171,173</sup>. To convert a frequency shift obtained from the experiment into a value of the mass adsorbed or desorbed from the quartz crystal, the well-known Sauerbrey equation<sup>177</sup> was utilised:

$$\Delta F = \frac{-2F_0^2}{A\sqrt{\rho_q\mu_q}} \Delta m \quad (4)$$

where  $\Delta F$  is a change in frequency (Hz),  $\Delta m$  is the mass deposited (g),  $F_0$  is the fundamental frequency of the QCM ( $10^7$  Hz),  $A$  is the area of the electrode ( $2.059 \times 10^{-5}$  m<sup>2</sup>),  $\rho_q$  is the density of the quartz ( $2.648 \times 10^6$  gm<sup>-3</sup>),  $\mu_q$  is the shear modulus of the quartz ( $2.947 \times 10^{13}$  gm<sup>-1</sup> s<sup>-2</sup>).

Changes in the oscillation frequency can be converted into changes of the disc mass:

$$\Delta m = -(9.09 \pm 0.01) \times 10^{-10} \Delta F \quad (5)$$

Finally, the area per molecule can be calculated:

$$\text{Area}_{\text{ per molecule}} = \frac{2AW}{\Delta m N_A} \quad (6)$$

where  $W$  is the molecular weight, and  $N_A$  is Avogadro's constant ( $6.023 \times 10^{23}$  molecules mol<sup>-1</sup>).

### **2.5.2 Surface plasmon resonance theory**

Surface plasmon resonance (SPR) phenomenon is a well-established and non-destructive optical method useful for investigating thin organic layers deposited on a metal surface, usually Au, Ag or Cu<sup>178,179,180</sup>. Due to the SPR method being sensitive to molecules on or near the environment of the metal film, it has become widely exploited as a sensing probe in areas such as gas sensing, biosensing, immuno-sensing and electrochemical studies<sup>181,182</sup>. It is capable of detecting small changes in the thickness and refractive index that cause a measurable change in the plasmon resonance angle. Therefore, it is often used to monitor the growth of organic monolayers on a metallic surface.

SPR is based on the total internal reflection phenomenon. Thus, if we consider light passing from a 'denser' medium (high refractive index) to a 'less dense' one (low refractive index), light will be partly reflected and partly refracted at the interface of these two different mediums. However, above a certain angle, called the critical angle, total internal reflection is observed, which means no light is refracted.

Surface plasmons are an excitation of the evanescent electromagnetic wave that travels along the interface between two mediums of different refractive index. The generated evanescent electromagnetic wave has the highest intensity at the interface and the amplitude of the wave decays exponentially with the distance from the interface<sup>179</sup>.

The SPR instrument set-up generally consists of a light source (monochromatic, p-polarised light), a prism (which represents a medium of high refractive index) and a thin (approximately 47 nm) metal film coated onto the prism and photodetector. The monolayer under study is deposited on the metal film on the opposite side of the prism<sup>183</sup> (see **Figure 2-73**).

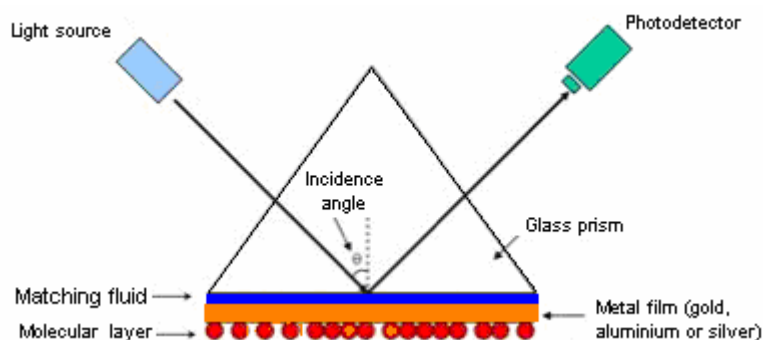


**Figure 2-73 Kretschmann configuration**<sup>184,185</sup>

Light passes through the prism (high refractive index) onto a metal film (low refractive index) at different incidence angles. Light is totally reflected from the inner face of the prism, which is coated with a metal film and the reflected light intensity is measured as a function of the incident angle (see **Figure 2-74**).

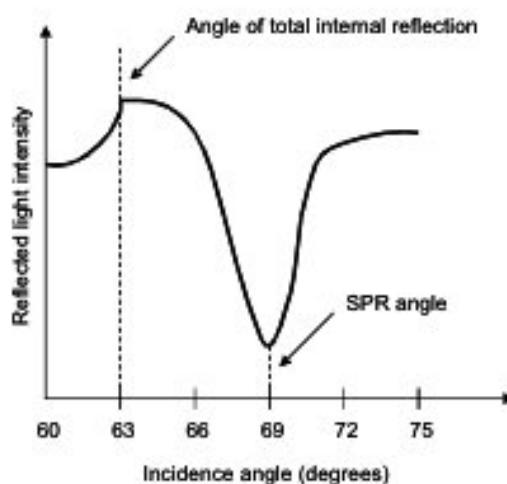


**Figure 2-74 Spectrum of reflectivity of light as a function of the incidence angle<sup>184</sup>**

At an appropriate incident angle, a deep minimum of reflected light is observed due to the resonance energy transfer between the evanescent wave and surface plasmons<sup>183</sup>. The angle strongly depends on several factors, including the characteristics of the metal film, the wavelength of incident light source, the thickness and refractive index of the molecular layer deposited onto the metal film. Consequently, if the surface is modified by the deposition of a new component then the optical properties, particularly the refractive index of the ‘new surface’ will change<sup>180</sup>.

### **2.5.3 Scanning tunnelling microscopy**

Since the vision of ‘nanodevices’ had been highlighted by Feynman, scientists have worked towards the development of tools that would be capable of investigating potential devices at the atomic scale. In the early 1980’s Binnig, Rohrer and collaborators<sup>16</sup> invented the scanning tunnelling microscope in the IBM laboratory in Zurich, for which, in 1986 they were awarded a Nobel Prize.

The scanning tunnelling microscope (STM) is a very useful, and a widely applied tool that can characterise the electrical properties of various materials, and also obtain images of surface topography at the atomic scale<sup>186,187</sup>. It allows observations of the arrangement of molecules, determining the size of compounds and their conformation. It also allows the roughness and defects of the surface to be investigated<sup>67,89,188</sup>.



The principle of the STM is simple and consists of a sharp metallic tip and a conducting sample, which is electrically biased with respect to the tip. Both the tip and the sample are working as electrodes between which a tunnelling current flows<sup>16</sup>. The main concept of a working STM is that of a tunnelling current phenomenon. It arises only when the electron orbital of the outermost atoms of the tip and the sample overlap and a voltage bias is applied between the two. The tunnelling current has a very important characteristic:

$$I = K \cdot U \cdot e^{-(k \cdot d)} \quad (7)$$

Where: K, k – constants, d – distance between tip and the surface, U–voltage, I–current. The tip is an essential part of the microscope, as it can affect the quality of the I–V characteristics and images. According to the Rohrer and Binnig design<sup>16</sup>, the tip of the microscope is manufactured in such a way that the tip is atomically sharp. A nonmetallic atom or cluster present on the tip apex can easily distort the measurements. Some common materials used for the tip are Pt/Ir alloy, tungsten or gold<sup>188</sup>. These are used due to their low reactivity and resistance to oxidation. The tip is positioned within about 1 nm distance above the studied surface to allow the tunnelling current to flow between it and the sample. The tip is attached to a piezoelectric tube, which changes shape when a voltage is applied to the circuit<sup>16,188</sup> (see **Figure 2-75**). The arising tunnelling current depends on the gap between the tip and the sample, as well as on the electronic structure of the tip.

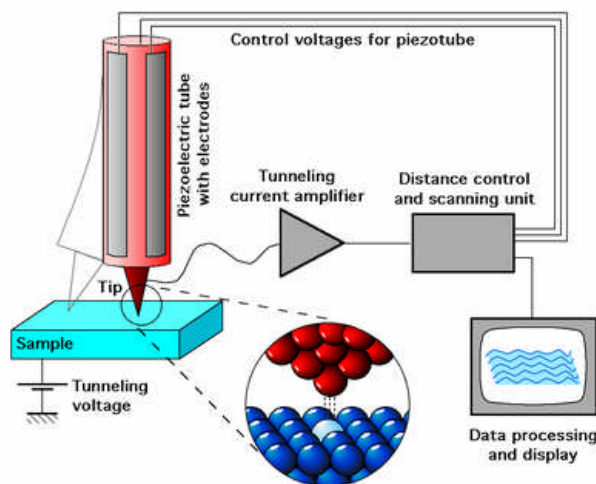


**Figure 2-75** STM apparatus<sup>189</sup>

The STM works in two different modes<sup>188</sup>: constant–height and constant–current mode. In constant–height mode the tip travels horizontally above the sample and as a result the tunnelling current is varied depending on the topography of the surface. When the STM is in constant–current mode, the tip adjusts the distance between the tip and the sample to provide a constant value of the tunnelling current at each measured point. The tunnelling current strongly depends on the precise distance between the tip and sample<sup>16,188</sup>, and it changes exponentially with the tip–sample distance. This means that very small changes in the tip–sample distance induce a large change in the tunnelling current. Increasing the gap between the sample and the tip by approximately 1 Å can cause a decrease in the value of the tunnelling current by about one order of magnitude. It is a powerful technique that permits measurements to be performed in an ultrahigh vacuum, a mineral oil or in air, and within a wide range of temperatures<sup>188</sup>.

#### **2.5.4 Second–harmonic generation**

The term ‘non-linear optics’ applies to all phenomena in which materials react non–linearly to an electric field, which includes second–harmonic generation (SHG), third–harmonic generation (THG), sum frequency generation (SFG), and difference frequency generation (DFG)<sup>190,191</sup>. For the purpose of this thesis, this section will be focused only on SHG phenomenon.

When light passes through the dielectric medium it interacts with the electrons of the matter inducing a polarisation. The polarisation<sup>190,191</sup> can be then written as:

$$P = \varepsilon_0 \chi E \quad (8)$$

where:  $\varepsilon_0$  is the permittivity of free space (constant),  $\chi$  is the susceptibility<sup>190,191</sup> (tensor) and it is related to the refractive index of the material,  $n$ , by:

$$\chi = n^2 - 1 \quad (9)$$

In most cases the polarisation is a linear function of the electric radiation. At high intensities (as can be produced by lasers) the polarisation becomes a non-linear function of the electric field<sup>191,192</sup>:

$$P = \varepsilon_0 (\chi^{(1)} E + \chi^{(2)} E^2 + \chi^{(3)} E^3 + \dots) \quad (10)$$

where:  $\chi^{(1)}$  – first order susceptibility,  $\chi^{(2)}$  – second order susceptibility,  $\chi^{(3)}$  – third order susceptibility. In theory this series goes to infinity. However, in practice, later polarisability coefficients become negligible as they fall rapidly at low light intensities. Therefore, the length of equation (10) depends strongly on the light (ie. laser) intensity. Equation (10) describes the polarisation of a bulk material. However, when considering a single molecule, the polarisation<sup>191,192</sup> can be written as:

$$P = \varepsilon_0 (\alpha E + \beta E^2 + \gamma E^3 + \dots) \quad (11)$$

where:  $\alpha$ ,  $\beta$  and  $\gamma$  correspond to first, second and third-order molecular polarisabilities respectively.  $\alpha$  and  $\beta$  are also known as first and second-order hyperpolarisabilities, respectively.

One of the non-linear processes is SHG<sup>190,191</sup>. For SHG, the light of angular frequency,  $\omega$ , is passed through a medium that then generates a beam of angular frequency  $2\omega$  (see **Figure 2-76**).

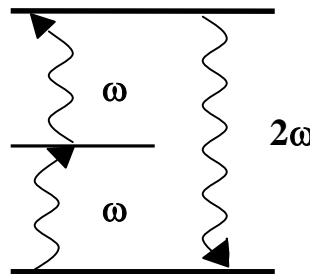


**Figure 2-76** Second-harmonic generation

The condition necessary for SHG to occur is that the medium is non-centrosymmetric, because the SHG is cancelled out by a centrosymmetric medium. If it is considered as only a second-order term from the equation (5), it gives:

$$P(x) = \varepsilon_0 \chi^{(2)} E(x)^2 \quad (12)$$

where:  $x$  represents the direction of oscillation of the dipole. If the medium is now inverted and  $(-x)$  is considered, then it can be stated that:

$$P(-x) = \varepsilon_0 \chi^{(2)} E(-x)^2 = \varepsilon_0 \chi^{(2)} E(x)^2 \quad (13)$$

Therefore:

$$P(-x) = P(x) \quad (14)$$

This is only possible when  $P(x) = 0$ , thus there is no SHG for a centrosymmetric medium.

In organic materials, atoms are connected to each other through  $\sigma$  and  $\pi$ -bonds. However, electrons forming  $\pi$ -bonds are loosely bound and hence they can be easily polarised. As a consequence, molecules containing conjugated bonds with a donor at one end and an acceptor located at the opposite end can result in large asymmetric polarisation and high  $\beta$  values when subjected to a high intensity laser beam. High  $\beta$  values for single molecules do not always mean that a bulk material will show a high value of macroscopic second-order susceptibility. The condition necessary to provide a high value of  $\chi^{(2)}$  is that the molecules are arranged in such a way that the molecular dipoles are aligned in the same direction (so they do not cancel each other out)<sup>193</sup>. Since the discovery of the LB technique, a great number of assemblies have been studied for non-optical applications<sup>194,195</sup>. In the case of thin films, second-harmonic intensity is described by the following equation<sup>193</sup>:

$$I_{(2\omega)} = \frac{(\chi_{eff}^{(2)} I_{\omega})^2}{2c^3 \epsilon_0 n_{\omega}^2 n_{2\omega}} \text{sinc}^2\left(\frac{1}{2} l \Delta k\right) \quad (15)$$

Where;

$$\Delta k = \frac{4\pi(n_{2\omega} \cos\theta_{2\omega} - n_{\omega} \cos\theta_{\omega})}{\lambda} = \frac{\pi}{l_c} \quad (16)$$

$\chi_{eff}$  is the effective susceptibility,  $l$  is the film thickness,  $n_{\omega}$  and  $n_{2\omega}$  are the refractive indices at fundamental and harmonic wavelengths respectively,  $\theta_{\omega}$  and  $\theta_{2\omega}$  are the angles of the propagating waves relative to the normal,  $l_c$  is the coherence length and  $\text{sinc}^2(1/2 l \Delta k) \approx 1$  for  $l \ll \lambda$ .

Second-harmonic intensity is directly proportional to the square of film thickness<sup>193</sup>:

$$I_{2\omega} \propto l^2 \quad (17)$$

As the thickness is proportional to the number of monolayers, therefore:

$$\sqrt{I_{2\omega(N)}} = \sqrt{I_{2\omega(1)}} N \quad (18)$$

## 3 Experimental

### 3.1 Substrate preparation

Different substrates were used with regards to the type of experiment performed. These included hydrophobic and hydrophilic glass slides, gold-coated highly oriented pyrolytic graphite (HOPG).

#### 3.1.1 Hydrophilic glass slides

Hydrophilic glass slides were used as a substrate for UV–VIS spectra of films obtained via the LB technique, and were prepared according to the following steps:

- The slides were initially examined for surface defects and wiped with dust and surfactant free tissues soaked in chloroform to remove any surface grease.
- The slides were ultrasonicated in a solution of propan-2-ol and then in ultra-pure water, for 10 minutes in each solution, and then rinsed thoroughly in ultra pure water.
- The slides were immersed in a 50:50 mixture of 30% v/v H<sub>2</sub>O<sub>2</sub> and concentrated H<sub>2</sub>SO<sub>4</sub>. This process is strongly oxidising and exothermic and takes 24 hours to complete.
- The slides were rinsed thoroughly in ultra pure water and propan-2-ol
- The slides were immersed in 30 % v/v H<sub>2</sub>O<sub>2</sub> at ca. 5°C and prior to use the slides were rinsed in ultra-pure water and finally dried in a stream of air.

#### 3.1.2 Hydrophobic glass slides

The cleaning procedure of hydrophobic glass slides (BDH) was slightly different and it involved the following stages:

- The slides were initially examined for surface defects
- The slides were ultrasonicated in a solution of chloroform and then propan-2-ol, for 20 minutes in each solution.
- The slides' surfaces were wiped with dust and surfactant free tissues soaked in acetone to remove any surface grease.

- The slides were again ultrasonicated in a solution of chloroform, propan-2-ol and ultra-pure water, for 20 minutes in each solution,
- The slides were immersed in propan-2-ol and prior to use the slides were rinsed in ultra-pure water and finally dried in a stream of air.

### **3.1.3 Highly Oriented Pyrolytic Graphite**

The Highly Oriented Pyrolytic Graphite (HOPG) was used as a substrate for I–V characterisation of the monolayers studied. The samples were purchased from *Aztech Trading*. The advantage of using graphite is that the carbon atoms create a multi–layer structure, which is flat and highly smooth. Due to its layered structure it was easy to remove the top layer and re–use the HOPG. By attaching a strong adhesive tape to the flat surface of the HOPG, and then pulling it off to remove only the top layer, leaving a smooth and clean surface underneath, the HOPG was then ready for gold coating.

### **3.1.4 Gold coating procedure**

Clean hydrophobic glass slides and HOPG were coated with a thin gold film (approximately 47–50 nm thick) for SPR and STM measurements. The coating was performed using a BOC Edwards 360 automatic coater (see **Figure 3-1**) and the gold wire (99.99 %) used as the coating material was purchased from Sigma-Aldrich Chemicals Ltd. First, the coating chamber was cleaned with isopropanol. Then substrates (slides or HOPG) and gold wire were placed on a special mask and in a molybdenum boat, respectively. Then the chamber was closed and the pressure was reduced to a value of  $1.9 \times 10^{-6}$  mbar. When the correct pressure was obtained, a current was applied to the boat to melt the gold wire. Then the deposition process was started and continued until the thickness of the gold film reached a value of 47 nm.

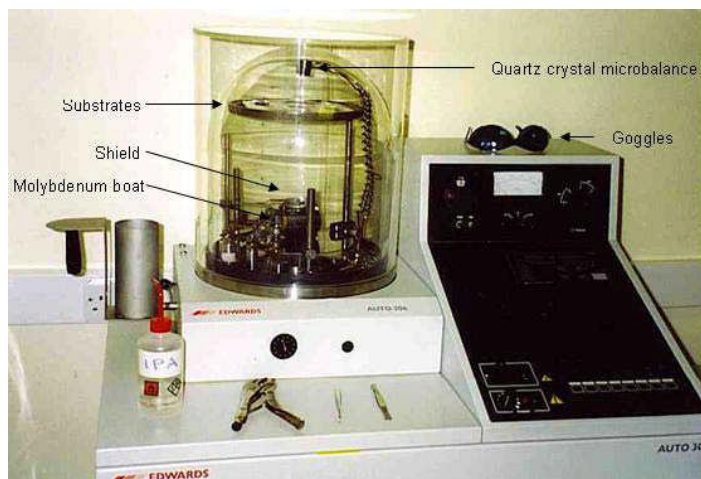


Figure 3-1 BOC Edwards 360 automatic coater<sup>196</sup>

### 3.2 Langmuir film formation and isotherms

Isotherms were obtained on a LB trough (Nima 621) (see Figure 3-2).



Figure 3-2 LB trough (Nima 621)<sup>147</sup>

It is a one-compartment rectangular trough made of PTFE that is hydrophobic, inert, and able to withstand direct contact with the subphase and other solvents used for monolayer deposition and cleaning. Prior to use, it was cleaned, first with propan-2-ol and then with chloroform. The molecules being investigated were dissolved into chloroform, with a concentration of approximately 0.1 mg/ml, and deposited onto the ultra-pure water subphase surface using a syringe (Haminton). When the desired



volume was deposited, the trough was left for 5–10 minutes in order to allow the solvent to evaporate. After this time the surface containing disordered molecules was compressed at the barrier speed of  $0.5 \text{ cm}^2/\text{s}$  to obtain an isotherm from Langmuir films of studied compounds. All isotherms presented were performed at an ambient temperature of  $22\text{--}25^\circ\text{C}$ .

### 3.3 LB deposition

The LB films were formed using a two-compartment trough (Nima 622) (see **Figure 3-3**).



**Figure 3-3** Two-compartment LB trough (Nima 622)

A dipper mechanism located in the middle of the two halves allows the transfer of Langmuir monolayers onto solid substrates. The solid substrate was placed on the dipper mechanism that rotated with a speed of  $5 \text{ mm}/\text{min}$ . At an appropriate ‘target pressure’, usually in the solid phase. The Langmuir film was transferred onto the solid substrate during the upstroke. The ‘target pressure’ was chosen individually and carefully for each studied compound. When the LB film was deposited, it was subjected to further investigations that are described in the results section.

### 3.4 SAM deposition

The deposition of the SAM was performed using a simple immersion process. A gold-coated solid substrate was immersed into the freshly prepared solution of studied molecules for certain periods of time. Between each immersion the sample was rinsed

with solvents methanol, ethanol and acetone to prevent any physisorption. When the first layer was completed, then deposition of the second layer could begin. Although the deposition of the second layer was also obtained via an immersion process, the principle of the deposition process was slightly different. While the first layer was built via formation of the covalent bond Au–S, the formation of the second layer relied on the interaction between opposite charges. The deposition of the first monolayer formed an ionic surface, which attracted oppositely charged ions or molecules. The studied molecules were dissolved in a polar solvent (ethanol or acetone) with a concentration of 0.1 mg/ml then the substrate containing the first layer was immersed in a freshly prepared solution for a set period of time. Between each immersion, samples were rinsed with solvents in the correct sequence to remove the physisorbed molecules. The deposition time altered from 600 to 1000 minutes according to the compound used.

### **3.5 QCM preparation and measurements**

QCM measurements were performed using gold-coated 10 MHz quartz crystals purchased from the International Crystal Manufacturing Company. Prior to deposition they were subjected to a cleaning procedure. First they were cleaned using the plasma cleaner, PlasmaPrep2, Gala Instrumente. Afterwards, each crystal was rinsed thoroughly with solvents in a suitable sequence: ethanol, ultra-pure water, ethanol, methanol, chloroform, methanol and ethanol, then dried in a stream of cold air. Then, the frequency of the crystal was measured. The procedure of rinsing with solvents was repeated several times until the difference in the value of subsequent frequency measurements prior to deposition of the studied molecules was not higher than 1 Hz. The crystals were then ready for sample deposition. The deposition was performed on a circular trough, Nima 2000 (see **Figure 3-4**), and the conditions for LB deposition are described in section 3.3.

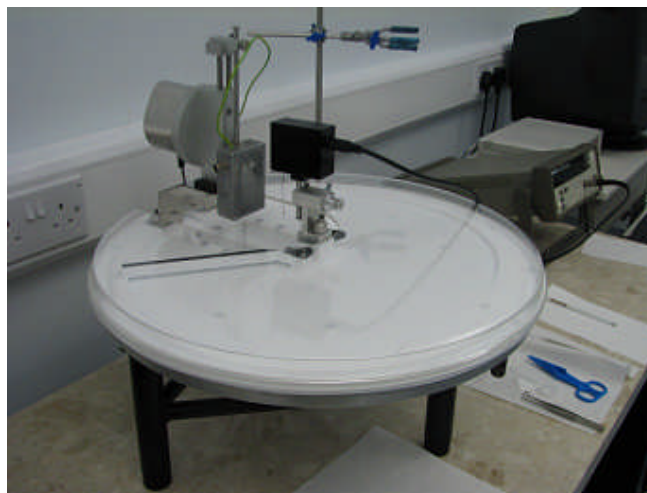


**Figure 3-4 Circular LB trough, (Nima 2000)**

After deposition, the frequency of the crystal coated with the monolayer of the investigated compound was measured again to determine the difference in the frequency before and after deposition. This was then converted into the molecular area using the Sauerbrey equation (4).

The deposition of the SAM required multiple immersions. Following each immersion the sample was rinsed with solvents and then a measurement of the crystal frequency drop was recorded. Deposition curves obtained by QCM analysis tend to flatten out toward the end of deposition, giving a useful indicator as to when the deposition was complete. All measurements were recorded using the Hewlett Packard 53131A 225 MHz Universal Frequency Counter and Thandar TS3021S power supply (see **Figure 3-5**).



**Figure 3-5 QCM setup**

### 3.6 SPR measurements

The thickness and dielectric permittivities of the LB films investigated were determined by SPR measurements (using the Kretschman configuration<sup>185</sup>). The monolayer of interest was deposited onto gold-coated glass slides. Measurements were performed using two different laser beams: 532 nm, *frequency doubled Nd:YAG laser* and 632.8 nm, *HeNe laser*. The laser beam passed through a p-polariser to remove any vertical s-polarised light. Then, only p-polarised light was passed through a chopper. The laser beam was then split in half. One half of the chopped laser beam was recorded by a reference photodetector, and the other half of the laser beam passed through the 60° BK7 prism to which a gold-coated slide was attached (see **Figure 3-6**).

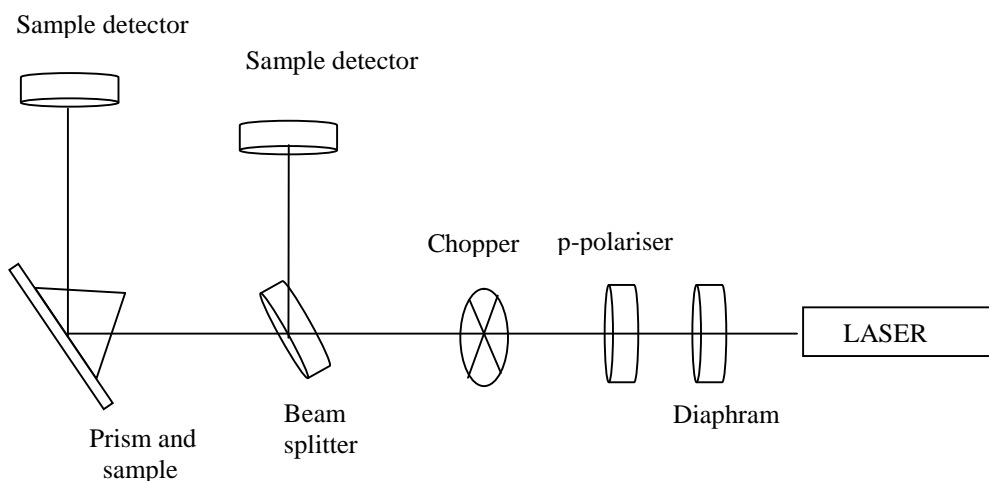


**Figure 3-6** SPR setup

The slide with the gold film deposited on the opposite side was attached to the prism using methyl benzoate as an index matching fluid to reduce interference by the interface between prism and the slide (see **Figure 2-73**). The prism and slide were placed on a rotating stage, which during the experiment was rotated by a suitable angle with respect to the laser beam. The incident angle varied from 38°–50°, this was due to the critical angle of BK7 glass being approximately 41° and so the SPR angle occurred above this angle. Both signals from sample and reference photodetectors were ratioed and analysed using software<sup>197</sup>. The fitting program uses equations by Fresnel and Maxwell to

generate an error–minimised fit of measured curves to theoretical curves predicted by the equations. It returns likely values for the real and imaginary components of the refractive indices of all layers (usually two: gold and the sample), along with thickness measurements.

### 3.7 STS measurements

I–V characteristics and images of the surface were obtained by using a Digital Instruments Multimode STM with a Nanoscope (IV) control box (see **Figure 3-7**).



**Figure 3-7 Digital Instruments Multimode STM**

The microscope is a very sensitive tool and therefore prior to measurements, it was placed on a special vibration–isolation table to prevent vibrations that could affect the measurements. All measurements were obtained by STM with the Pt/Ir tip. The tip position was set to provide a current of 200–1000 pA at a bias of 50–1000 mV. The rectification ratio (RR) at the applied voltage  $V_0$  was calculated from equation (19):

$$RR = \frac{\text{current\_at\_}V_0}{\text{current\_at\_}(-V_0)} \quad (19)$$

### 3.8 SHG measurements

In this project the SHG was measured using a Nd:YAG, p-polarised laser ( $\lambda=1064$  nm). The wavelength of the laser beam was shortened from 1064 nm to 532 nm by the organic molecules studied. These compounds were deposited onto hydrophilic slides using the LB technique. The laser beam was reflected onto a mirror and then passed through a beam splitter to split the beam into a sample and a reference beam. The sample was positioned at  $45^\circ$  relative to the beam. A quartz slide was used as a reference in the experiment (see **Figure 3-8**).

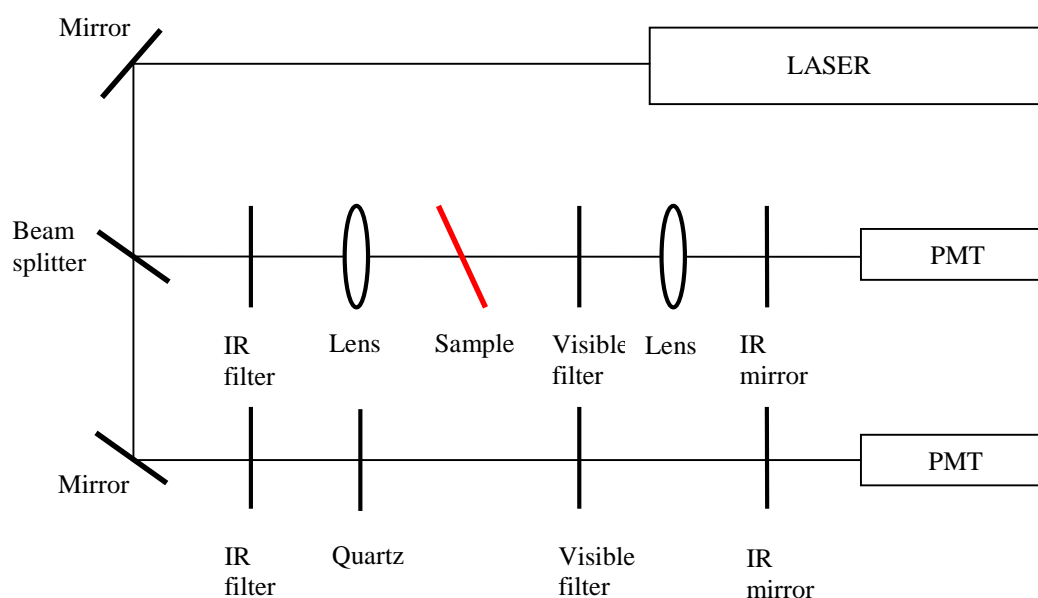


**Figure 3-8 SHG setup**

During the experiment, an average of 5 readings were taken at different positions on the slide. The sample was then replaced by a matched quartz slide and 5 readings were taken again. Photo multiplier tubes were used to monitor the reference and sample beams and the resulting signals were sent to a computer and analysed. This method allowed the control of orientation and order of the molecules in the thin film studied and also reflected the stability of the layer formed.

### 3.9 Chemical characterisation techniques

The reagents and solvents used in the experiments were purchased from *Aldrich Chemical Company* (Gillingham, UK), *Avocado Fine Chemicals* (UK), *VWR* (UK) and *Surechem* (UK). These were used as supplied without further purification. Organic compounds synthesised at Cranfield University were characterised using various techniques to confirm the structure and purity of the dyes. The techniques used included differential scanning calorimetry used to determine the melting points and purity of the dyes. The samples were placed in special crucibles that were heated from 25° C to 400° C in 10° C increments.

Mass spectroscopy was performed at the University of Wales, Swansea by the EPSRC National Mass Spectrometry Service Centre.

Hydrogen nuclear magnetic resonance spectra (NMR) were recorded at Hull University on a 250 MHz instrument.

#### 3.9.1 UV–VIS spectroscopy

Ultraviolet-visible spectra of dyes in solution were obtained using a CECIL CE 9000 series spectrophotometer, with spectra being obtained between wavelengths of 250 and 800 nm. It is a double-beam instrument; the light is split into two beams before it reaches the sample. One beam is used as the reference, while the other beam passes through the sample. The instrument has two detectors (photodiodes), and the sample and reference beam are measured at the same time. Liquid samples were placed in quartz cells with path lengths of 10 mm. The reference cell was filled with pure solvent and the sample with a dilute solution of the dye. The spectrophotometer measured the intensity of light passing through a sample ( $I$ ), and compared it to the intensity of light passing through the reference cell ( $I_0$ ). The ratio  $I / I_0$  is called the *transmittance*, and is usually expressed as a percentage (%T). The absorbance,  $A$ , is based on the transmittance:

$$A = -\log_{10}(\%T) \quad (20)$$

The spectra of films on glass slides were performed using a Perkin Elmer Lambda 7 spectrophotometer.

### 3.10 Synthesis

#### 3.10.1 1-Hexyl-2,6-dimethyl-pyridinium iodide<sup>193</sup>

To a solution of 2,6-Dimethyl-pyridine (1.02 g, 9.5 mmol) in methanol (~50 ml), was added hexyl iodide (2 g, 9.5 mmol). The resultant mixture was stirred at reflux for 5 days. After this time, the mixture was allowed to reach room temperature, and the solvent was then reduced to approximately 10 ml. About 100 ml diethyl ether was added to extract the product; a pale yellow precipitate which was filtered and left to dry, (yield 34 %). The reaction scheme is depicted in **Figure 3-9**.

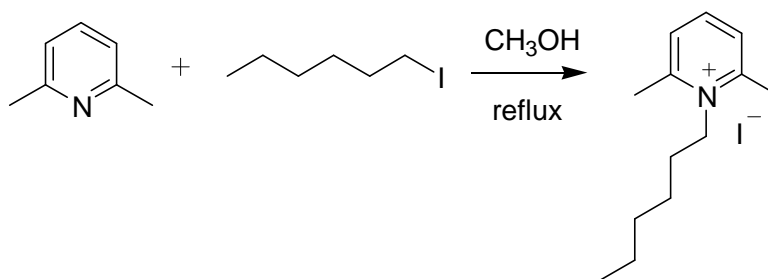


**Figure 3-9** Reaction scheme of 1-Hexyl-2,6-dimethyl-pyridinium iodide

#### 3.10.2 1-hexyl-2,6-bis-[2-(4-dibutylaminophenyl)-vinyl] pyridinium iodide (dye 8)

To a solution of 1-Hexyl-2,6-dimethyl-pyridinium iodide (0.492 g, 1.55 mmol) in methanol (~50 ml), was added 4-dibutylamino-benzaldehyde (0.7 g, 3.05 mmol) and finally piperidine (0.2 ml). The resultant mixture was heated at reflux and stirred for four weeks. Upon cooling the solvent was evaporated in a vacuum and purified by silica gel flash chromatography using chloroform and chloroform/methanol mixture (90:10 v/v) as eluent. The reaction scheme is depicted in **Figure 3-10**



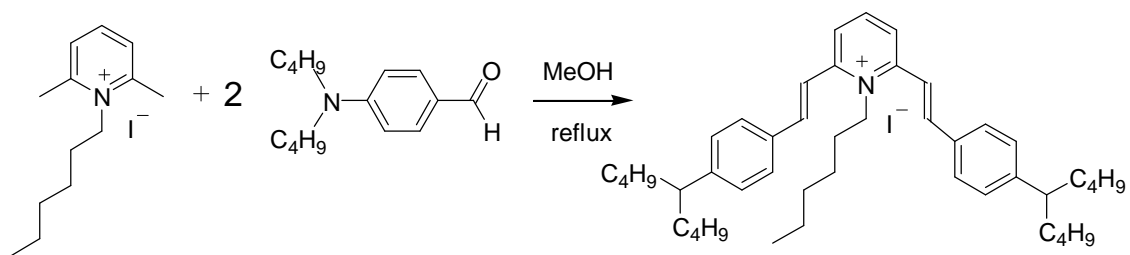


**Figure 3-10** Reaction scheme of 1-hexyl-2,6-bis-[2-(4-dibutylaminophenyl)-vinyl] pyridinium iodide (dye VI)

The final product was obtained as a dark red solid: 0.105 g, yield (12 %), mpt 170–175<sup>0</sup>C;  $\lambda_{\text{max}}(\text{CHCl}_3) = 562 \text{ nm}$ ;  $^1\text{H-NMR}$  ( $\text{CDCl}_3$ , 250 MHz, J/Hz): 0.069 (s, 15 H, ( $\text{CH}_3$ -) x 5), 0.84–0.87 (m, 10 H, ( $\text{CH}_3$ - $\text{CH}_2$ -) x 5), 0.87–0.98 (m, 2H, N- $\text{CH}_2$ - $\text{CH}_2$ -), 1.25 (s, 5H, N- $\text{CH}_2$ - $\text{CH}_2$ - $\text{CH}_2$ - $\text{CH}_2$ - $\text{CH}_2$ - $\text{CH}_3$ ), 1.33–1.41 (m, 2H, N- $\text{CH}_2$ ), 1.57 (s, 16H, ( $\text{N}^+$ - $\text{CH}_2$ - $\text{CH}_2$ -) x 4), 6.66–6.80 (m, 2H, (Ar- $\text{H}$ ) x 2), 7.0–7.12 (m, 2H, (Ar- $\text{H}$ ) x 2), 7.49 (d, 4H, (trans alkene- $\text{H}$ ) x 4), 7.51–7.52 (m, 4H, Ar- $\text{H}$ ) x 4), 7.88 (d, 2H, (Py- $\text{H}$ ) x 2), 8.20 (t, 1H, Py- $\text{H}$ ); m/z ( $\text{ES}^+$ ):622.5 ( $[\text{M}-\text{I}]^+$ ), 100%, ( $\text{ES}^-$ ):126.9 ( $[\text{I}]^-$ ), 100%.

### 3.10.3 1-Butyl-2,6-dimethyl-pyridinium iodide<sup>69</sup>

To a solution of 2,6-dimethylpyridine (1.7 g, 15.9 mmol) in methanol (~30 ml) was slowly added butyl iodide (3.02 g, 16.4 mmol). The resultant mixture was transparent in colour and was stirred at reflux for five days. After this time the mixture changed colour to a pale yellow. Upon cooling the solvent was eliminated using rotary evaporation at ambient temperature to leave ~10 ml of solvent. At the next stage ~100 ml of diethyl ether was added to extract the product, a pale yellow precipitate that was filtered and left to dry (yield 22 %), m.p. 187°C. The reaction scheme is depicted in **Figure 3-11**.

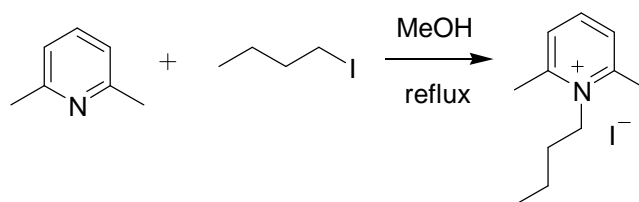


Figure 3-11 Reaction scheme of 1-Butyl-2,6-dimethyl-pyridinium iodide<sup>69</sup>

### 3.10.4 1-Butyl-2,6-bis-[2-(4-dimethylamino naphthalen)-vinyl] pyridinium iodide (dye 11)

To a solution of 4-dimethylamino-naphthalene-1-carbaldehyde (0.409 g, 2 mmol) in methanol (~ 30 ml) was added 1-Butyl-2,6-dimethyl-pyridinium iodide (0.29 g, 1 mmol) and piperidine (~0.3 ml). This was heated at reflux for three weeks. After this time the mixture was cooled and solvent was eliminated using rotary evaporation. The resultant product was extracted and purified by silica gel flash chromatography using chloroform and chloroform/methanol mixture (90:10 v/v) as eluent. The reaction scheme is depicted in Figure 3-12.

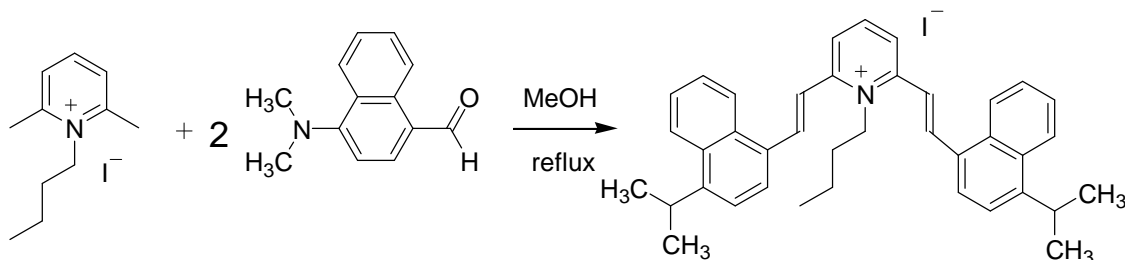


Figure 3-12 Reaction scheme of 1-Butyl-2,6-bis-[2-(4-dimethylamino naphthalen)-vinyl] pyridinium iodide (dye VIII)

The final product was obtained as a pale yellow solid: 0.2398 g, yield (49%), mpt 183<sup>0</sup>C,  $\lambda_{\text{max}}(\text{CHCl}_3)$ =360 and 490 nm; m/z (ES<sup>+</sup>):526.5 ([M-I]<sup>+</sup>), 30%, (ES<sup>-</sup>):126.9 ([I<sup>-</sup>]), 100%, no <sup>1</sup>H-NMR available.

## 4 RESULTS AND DISCUSSION

Chemical nomenclature of studied dyes is provided in a list section of the thesis.

### 4.1 Acceptor– $\sigma$ –Donor structures

#### 4.1.1 Dye 1

The first studied molecule, dye 1 depicted in **Figure 4-1** was provided by Professor D.J. Sandman at the University of Massachusetts, US.

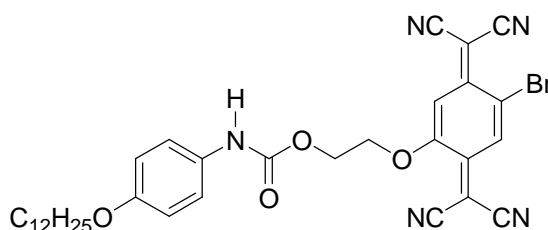


**Figure 4-1** Structure of dye 1

The molecule represents an D– $\sigma$ –A structure as proposed by Aviram and Ratner<sup>1</sup>, with the dodecyloxyphenyl group acting as an electron–donor and TCNQ as an electron–acceptor. The long aliphatic chain (C<sub>12</sub>H<sub>25</sub>–), typical for LB film–forming molecules, allowed the formation of a structure at the air–water interface. Previous studies of this compound were reported by Sambles, Mattern and Sandman<sup>28,59</sup>. Despite the D– $\sigma$ –A structure, the obtained results did not prove the concept set by Aviram and Ratner<sup>1</sup>. One of the electrodes (Mg) used is known to oxidise easily, and therefore the main reason of rectification was associated with the formation of a Schottky barrier<sup>31,32</sup>. Additionally, the electrodes used in the experiment had different work functions (3.66 and 5.65 eV)<sup>28,59</sup>, and therefore it was believed that it might also lead to asymmetrical I–V plots. For these reasons, the molecule was reinvestigated and studies of the molecule sandwiched between non–oxidisable electrodes were performed.

The conditions used to obtain isotherms and to generate the LB film were kept as close as possible to the published method<sup>28</sup>. The concentration ( $c$ ) of the solution under study was  $c=0.165$  mg/ml (see **Figure 4-2**, black curve). The isotherm yielded an area of  $A_0= 0.60$  nm<sup>2</sup>/molecule at zero pressure and  $A_c= 0.26$  nm<sup>2</sup>/molecule at 45 mN/m, which corresponded to the collapse point of the monolayer.

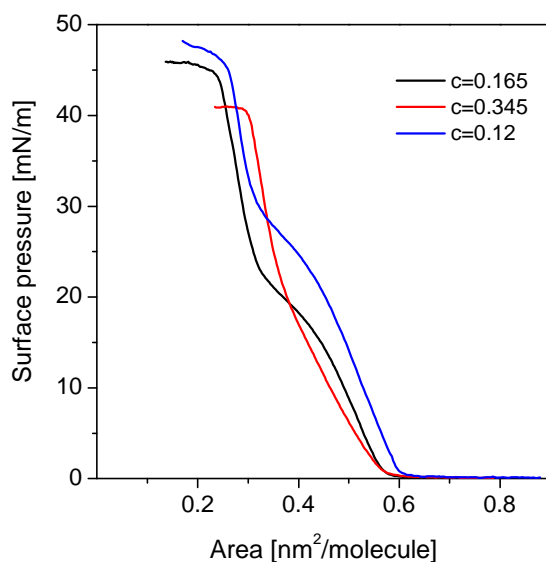


**Figure 4-2 Isotherms of dye 1**

The shape of the isotherm was similar to the one obtained 15 years ago, however some differences were observed. A region of slowly increasing pressure was observed between 17 to 22 mN/m (current data), while the original isotherm<sup>28</sup> showed that this equivalent region had a lesser gradient and occurred within the range of 21–27 mN/m. Moreover, isotherms obtained from solutions of different concentrations of 0.12, 0.165 and 0.35 mg/ml (see **Figure 4-2**) revealed different shapes in relation to each other and compared to that obtained by Sandman *et al.*<sup>28</sup>. This suggested that the molecules might have adopted different orientation at the air–water interface, or form aggregates according to concentration.

The Langmuir film of dye 1 was successfully transferred onto solid substrates, which was confirmed by its UV–VIS spectra. The UV–VIS spectrum of dye 1 in a solution of chloroform showed two bands, at 423 nm and at 401 nm (see **Figure 4-3 (a)**), whereas the

LB monolayer on a glass slide showed a broad band at a maximum absorbance between 425–430 nm (see **Figure 4-3 (b)**).

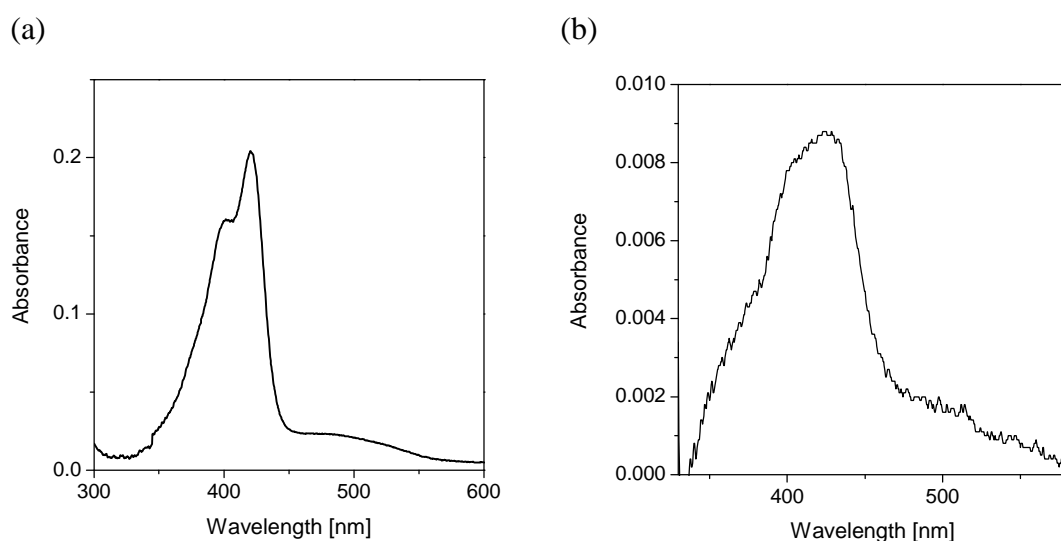


**Figure 4-3** UV–VIS spectra of dye 1; (a) in chloroform solution, (b) an LB monolayer on glass slide

The monolayers were deposited on the upstroke at different target pressures (10, 15, 20, 25, 30 and 35 mN/m), and for each deposition pressure, the isotherm (see **Figure 4-1**, black curve) showed different values of area per molecule. These values were then confirmed by QCM measurements (see **Table 4-1**).

**Table 4-1** Area per molecule of dye 1

Deposition pressure [mN/m]	Area [nm <sup>2</sup> /molecule] estimated from the isotherm*	Area [nm <sup>2</sup> /molecule] calculated from QCM measurements†
35	0.28	0.26
30	0.29	0.27
25	0.32	0.32
20	0.36	0.39
15	0.43	0.48
10	0.50	0.52

\* Diviation ( $\pm 0.2$  nm<sup>2</sup>/molecule)

† Diviation ( $\pm 0.1$  nm<sup>2</sup>/molecule)

The data revealed that the molecular area was found to be dependent on the transfer pressure used for deposition. As expected the area per molecule decreased with the increase of deposition pressure. Small areas per molecule were obtained at 35, 30 and 25 mN/m that suggested that the monolayer of dye 1 had formed a bilayer above 20 mN/m.

The main part of the investigation was focused on STS measurements. A series of samples of dye 1 were prepared and the studies provided interesting, although difficult to explain results (see **Figure 4-4**)\*. To eliminate the Schottky barrier effect<sup>31,33</sup>, non-oxidisable gold and PtIr electrodes with very similar work functions were used. Moreover, to avoid short-circuit problems associated with the evaporation of the top electrode onto a monolayer<sup>63</sup>, an STM tip was used to contact the sample. The results showed a variety of I-V characteristics, which included asymmetric and symmetric curves. The asymmetric curves had rectification values from 6–20 at  $\pm 1$  V with some showing high current in the positive quadrant and some showing high current in negative quadrant of the I-V plots. It was assumed that the molecules aligned at the air-water interface with a partly hydrophilic part pointing downwards, and a hydrophobic part directed upward. It was hoped that this alignment would be maintained when the Langmuir film was transferred onto a gold-coated substrate. However, the variety of I-V curves observed suggested a discrepancy in the orientation and alignment of the molecules on the surface, and consequently when it was transferred onto a gold-coated HOPG.

---

\* The results were reproducible and the showed I-V characteristics are representative.

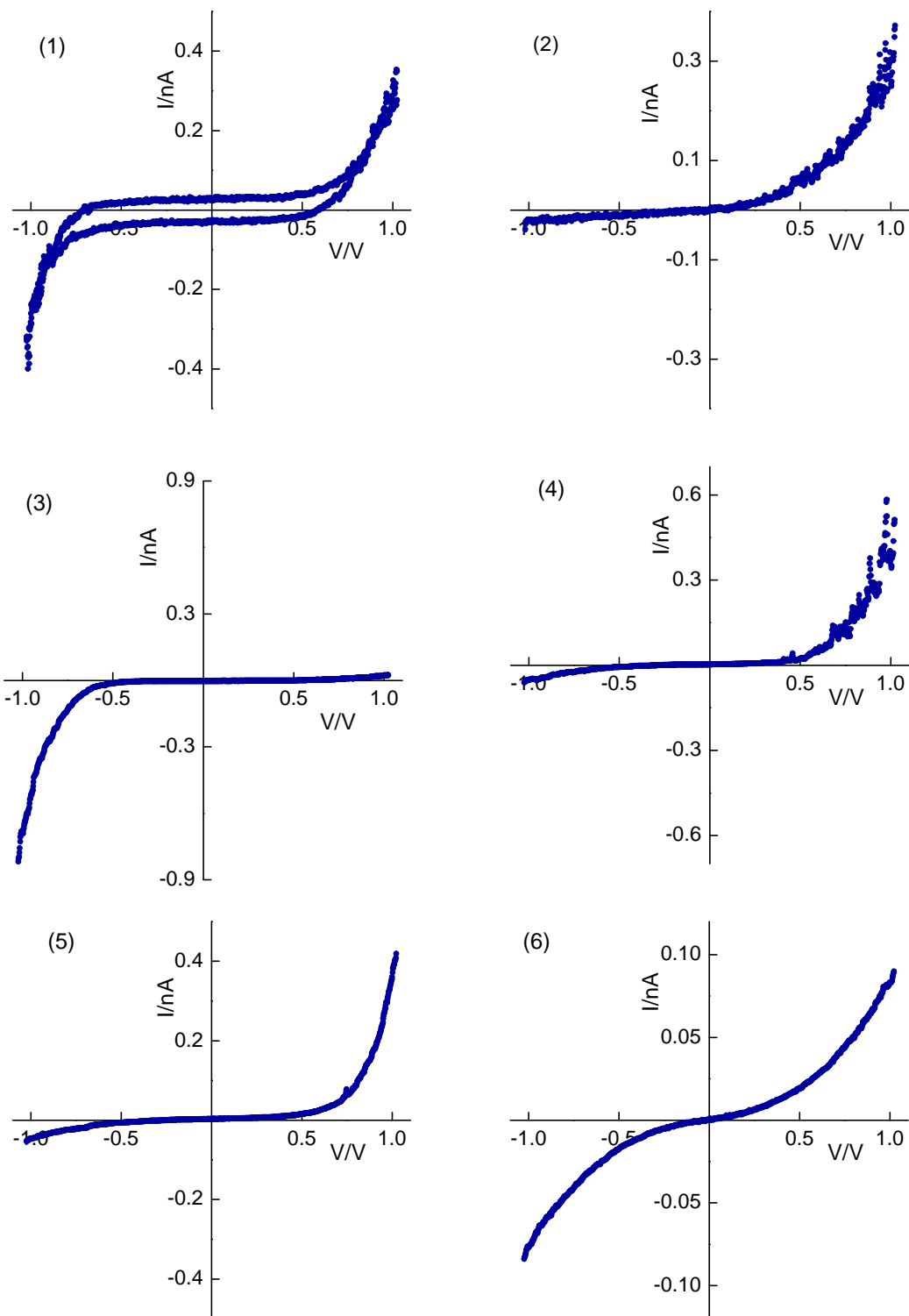


**Figure 4-4** I–V characteristics of Au |dye 1| PtIr; dyeI was deposited at different pressures; (1) 10 mN/m, (2) 13 mN/m, RR=6 (3) 16 mN/m, RR=20 (4) 17 mN/m, RR=8 (5) 19 mN/m, RR=8 (6) 20 mN/m

As depicted in **Figure 4-4** (1), the I–V plot showed hysteresis when the dye was deposited at a low pressure of 10 mN/m. The hysteresis was also observed in the original

work<sup>28,59</sup>. However, there was a difference in shape of the hysteresis observed 15 years ago and that shown in **Figure 4-4 (1)**. It was very likely that this hysteresis was caused by a very low deposition pressure and as a consequence led to the formation of an incomplete monolayer. Increasing the pressure to 13 mN/m gave slightly asymmetric curves with rectification of approximately 6 at  $\pm 1$  V with a higher current being observed in the positive quadrant of the I–V plot (see **Figure 4-4 (2)**). This implied that the preferential electron flow was from the tip through the organic monolayer to the bottom electrode. This would suggest that the molecules aligned with the acceptor (hydrophilic) located close to the tip and the donor (hydrophobic) close to the substrate. However, this is unexpected as the LB deposition on the upstroke implied the opposite orientation of the molecule. In contrast, the transfer of the monolayer at a higher deposition pressure of 15 mN/m led to asymmetric I–V curves with a high RR of 20 at  $\pm 1$  V. The direction of electron tunnelling at forward bias was from the substrate to TCNQ acceptor and simultaneously from dodecyloxyphenyl donor to the probe, followed by electron movement from the acceptor to the donor (see **Figure 4-4 (3)**). This was consistent with the direction predicted by the Aviram and Ratner model<sup>1</sup>. Unfortunately, STS measurements of other samples, which were deposited at 17 mN/m, and 19 mN/m showed again that the molecules of the dye were aligned on the solid surface in a very similar way to that of the sample deposited at 13 mN/m (see **Figure 4-4 (4 and 5)**). Finally, symmetric I–V characteristics were obtained for a film deposited at 20 mN/m (see **Figure 4-4 (6)**), and it suggested that a bilayer had formed.

The variety of I–V plots obtained for the Au | dye 1 | PtIr system revealed a relationship between rectification and the deposition pressure used to form the monolayer. These results suggested that molecules, at different deposition pressures, adopted different molecular arrangements on the subphase while being compressed and during transfer onto the gold-coated HOPG. The behaviour obtained from dye 1 was probably a consequence of the weak hydrophilic character of TCNQ, and the high flexibility of the long aliphatic chain and  $\sigma$ -bridge<sup>34,63,64</sup>. Due to the flexibility of the structure, it was thought that the molecule might adopt a scorpion-like arrangement, with the acceptor arching over the donor and SPR results seemed to confirm this concept. The significantly lower thickness obtained here ( $1.5 \pm 0.2$  nm), compared to the value



published<sup>28,59</sup> (2.2 nm) clearly indicated that the long aliphatic chains, were tilted or bent, instead of pointing upright, and thus the molecules very likely did not form an ordered monolayers.

#### 4.1.2 Dye 2

Another example of Aviram and Ratner model<sup>1</sup> is depicted in **Figure 4-5**. Dye 2, supplied by D. Mattern, comprises of the dinitrophenyl group acting as an acceptor, while pyrene was the donor. It also had a typical LB molecule structure with a long aliphatic chain ( $C_{12}H_{23}$ ) that pointed upwards when deposited at the air–water interface. The  $C_{12}H_{23}$ –chain required for the LB deposition was chosen for its ability to form densely packed monolayers<sup>62</sup>.

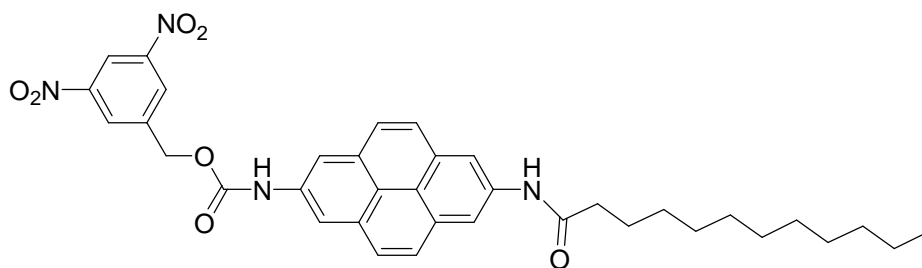


**Figure 4-5 Structure of dye 2**

The same compound, but with a shorter ( $C_6H_{13}$ ) hydrocarbon chain was previously studied by Sambles *et al.*<sup>62</sup> and the results were published. According to the publication<sup>62</sup>, the I–V characteristics obtained from the five-layered film of  $C_6H_{13}$ –analogue showed rectification in excess of 100. However, higher current was observed to flow in the opposite direction to that suggested by the Aviram and Ratner model<sup>1</sup>. Due to the oxidisable electrodes used in the experiment, the high rectification observed was associated with the Schottky barrier<sup>33</sup> created at the interface: D– $\sigma$ –A | Mg, Al, rather than the molecular structure itself.

Prior to the investigation of electrical properties of dye 2, an isotherm was produced in order to provide data about the alignment of the molecules at the air–water interface (see **Figure 4-6**). The isotherm of dye II did not show a distinct collapse point. The

chosen pressure for deposition was estimated to be 26 mN/m and based on the isotherm, the area obtained at this deposition pressure was 0.47 nm<sup>2</sup>/molecule. A lower area of 0.28 ± 0.1 nm<sup>2</sup>/molecule was found by applying the Sauerbrey equation to the frequency data when dye 2 was deposited at 26 mN/m onto 10 MHz quartz crystals. This difference could be associated with the different arrangement of the molecules at the air–water interface and on the quartz crystals.

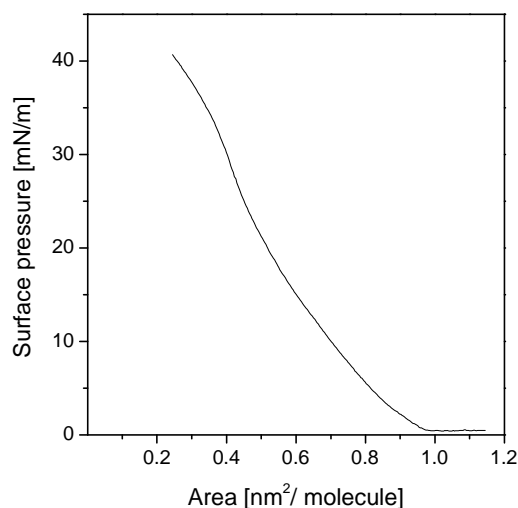


**Figure 4-6 Isotherm of dye 2**

The UV–VIS spectrum from chloroform solution revealed absorbance maxima at 270, 315, 346 and 390 nm (see **Figure 4-7**). Attempts to obtain the spectrum of dye 2 on a glass slide failed, as the spectrum did not reveal any absorbance peaks. It was most likely caused by the poor molecular attachment to the glass slide and therefore absorbance peaks could not be distinguished from the spectrum.

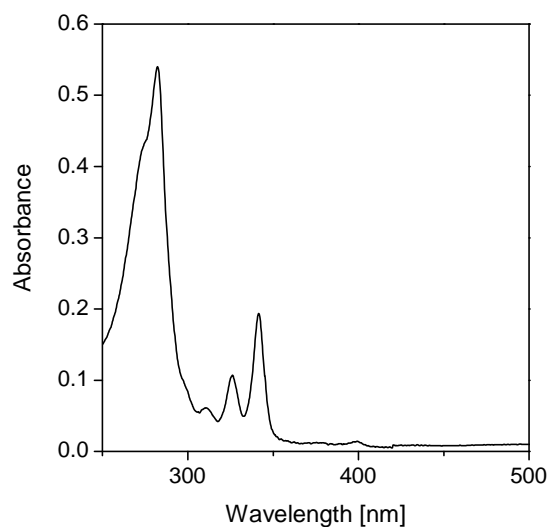


**Figure 4-7 Spectrum of dye 2 in chloroform solution**

Analysis of I–V characteristics of dye 2 provided interesting information regarding the alignment, stability and electron transport through the monolayer of dye 2 deposited between non-oxidisable electrodes. STS studies showed two types of curve, with one being almost symmetrical with a low RR of 1.5 at  $\pm 1$  V, and the other being asymmetrical with the higher current in the negative quadrant of the plot and RR up to 6 at  $\pm 1$  V (see **Figure 4-8**).

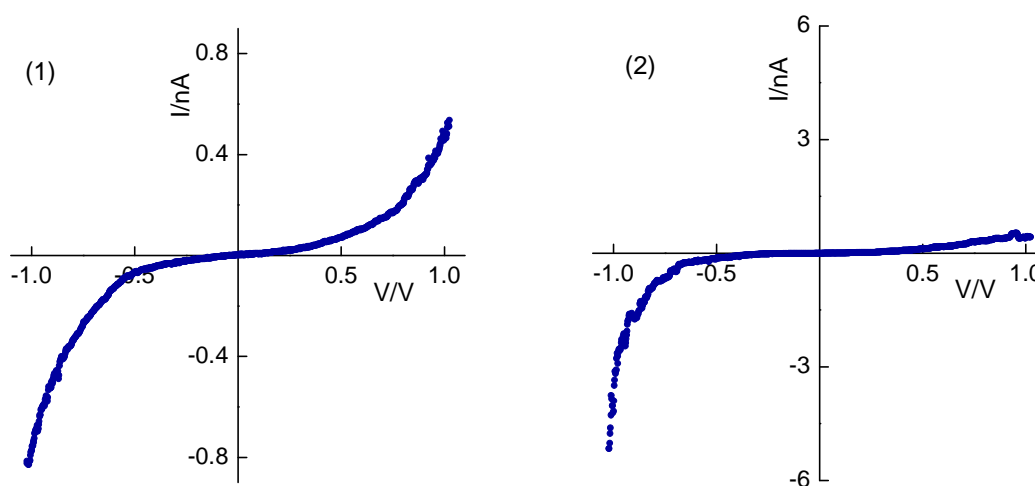


**Figure 4-8 Representative I–V characteristics of Au | dye 2 | PtIr; (1) RR=1.5 at  $\pm 1$  V, (2) RR=6 at  $\pm 1$  V**

Although, it is known that the LB molecules form usually densely-packed films, they are attached to the substrate via weak van der Waals bonds<sup>39,123,124</sup>. Therefore, when a voltage bias was applied to the system, it could lead to the reorientation of the molecules within the monolayer<sup>52,54,63</sup> and thus the two types of curves could be observed. The differences of the I–V characteristics could also be a consequence of defects at the gold surface<sup>167,168</sup>, which are believed to strongly determine the arrangement of the molecules.

The experiment was performed to test the concept proposed by Aviram and Ratner<sup>1</sup>. Due to the fact that the LB film was deposited on the upstroke, it was assumed that the hydrophilic part (acceptor) would have been located closer to the bottom electrode, while the donor (pyrene with long chain) will be closer to the tip. The higher current observed in the negative quadrant indicated that electrons were travelling from the bottom electrode through the acceptor and donor to the top electrode, and this agreed with the Aviram and Ratner concept<sup>1</sup> of the molecular rectifier. Some researchers<sup>75</sup> suggested, that using electrodes with different work functions could lead to an asymmetry of the I–V plots. However, due to the low difference in the work function values of Au (5.5 eV)<sup>28</sup> and PtIr (5.2 eV)<sup>75</sup>, it was assumed to have no influence on rectification. The presence of the long aliphatic chain (C<sub>12</sub>H<sub>23</sub>–) also indicated that the system had a geometrical asymmetry because the active part of the dye was closer to the gold electrode than to the tip, which according to Krzeminski<sup>83</sup> and Kornilovitch<sup>84</sup> this is the main factor causing rectification. Therefore, although the Au | dye 2 | PtIr system shows asymmetric I–V characteristics, it was still difficult to unequivocally determine the cause of the rectification.

## **4.2 Acceptor– $\pi$ bridge–donor structures**

### **4.2.1 Dye 3**

In order to provide more information regarding alignment and the mechanism of electron transport through the metal | D–electron bridge–A | metal system, a subsequent molecule with a strong acceptor (bipyridinium) and a dialkylamino donor group was subjected to investigation. The structure of the compound supplied by Danika Locatelli

from Milan University, Italy is depicted in **Figure 4-9**. The molecule did not represent the typical Aviram and Ratner structure<sup>1</sup>. In this case, instead of a  $\sigma$ -bridge, a twisted  $\pi$ -bridge was used to provide a non-planar structure, and thus effectively separate the molecular orbitals of the acceptor from the donor subunit.

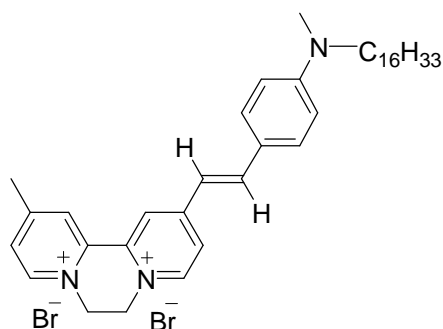


**Figure 4-9 Structure of dye 3**

The isotherms obtained revealed unusual behaviour of the molecules at the air-water interface (see **Figure 4-10**). It has been noted that there was a discrepancy in the position of the isotherms produced from the same solution in relation to each other.

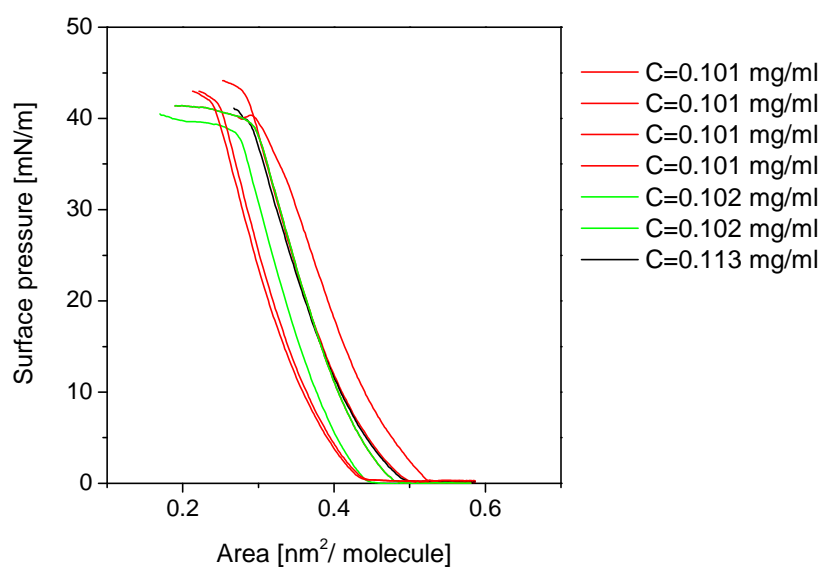


**Figure 4-10 Isotherms of dye 3**

The isotherms showed a phase transition in the range of 38–43 mN/m, and the measured area at the transfer pressure of 33 mN/m was  $A_t = 0.29\text{--}0.39 \text{ nm}^2/\text{molecule}$ . QCM measurements were performed to verify the values of the molecular area obtained from the isotherms, which yielded a value of  $0.53 \pm 0.15 \text{ nm}^2$ . A variety of values obtained from the isotherms and QCM measurements could imply that the molecules might have adopted different alignments for each deposition onto the aqueous subphase and during the transfer onto a solid substrate. As the monolayer was prepared from an aqueous subphase, ionic exchanges<sup>92</sup>, as well as a solvent trapping process<sup>198</sup> in the formed monolayer may have occurred to impair close packing within the film.

To obtain a better understanding of the molecular arrangement on the surface, SPR measurements were carried out to determine the thickness of the monolayer. The measurements provided a thickness of  $1.9 \pm 0.2 \text{ nm}$ , which suggested that the long tail was tilted, or bent in relation to the gold surface.

UV–VIS spectra from chloroform solution and the LB film on a glass slide were recorded to reveal absorbance maxima (see **Figure 4-11**).

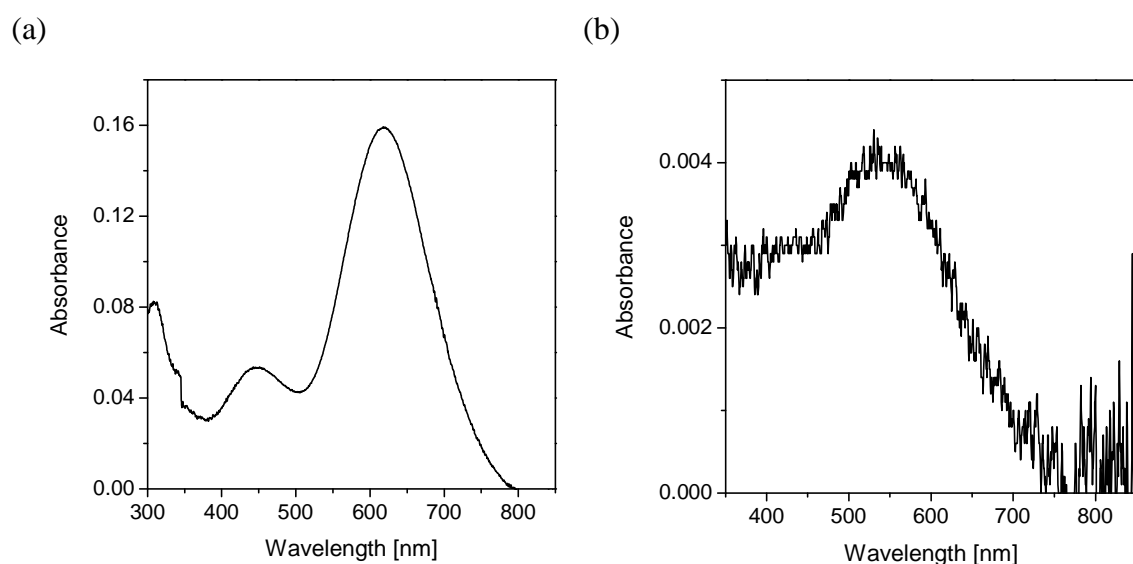


**Figure 4-11** UV-VIS spectra of dye 3; (a) in chloroform solution, (b) LB film on a glass slide

The compound showed maximum absorbance at 310, 450 and 630 nm when dissolved in chloroform solution and 420 and 540 nm when deposited as the LB film on a glass

slide. There was a large shift in the position of maximum absorbance from 630 nm to 540 nm. According to previous studies<sup>199,200</sup> this shift was caused by the alignment of dipoles in the same direction.

To investigate the electrical properties of this material, several samples were prepared for STS analysis. Monolayers were deposited on gold-coated HOPG and contacted via a PtIr tip. The measurements yielded rectifying plots from the film with rectification from 3.4 to 16 at  $\pm 1$  V (see **Figure 4-12**).

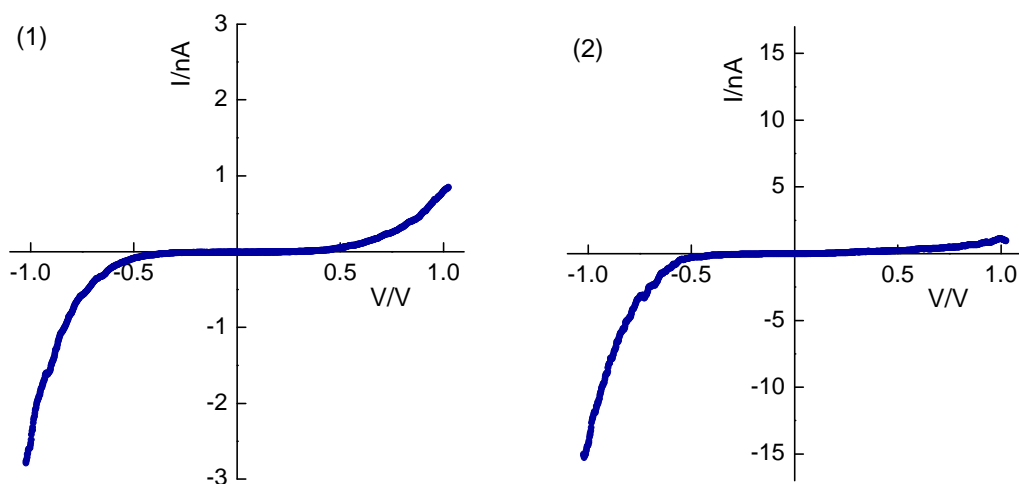


**Figure 4-12** Representative I–V characteristics of Au | dye 3 | PtIr; (1) RR=3.4 at  $\pm 1$  V, (2) RR=16 at  $\pm 1$  V

The higher current was observed in the negative quadrant of the I–V plot, which implied that the preferential direction for electron flow was from the bottom electrode to the tip of the microscope. Additionally, the I–V curve depicted in **Figure 4-12**, showed high current value of 15 nA. Due to the structure of the molecule, a hydrophilic acceptor and a hydrophobic donor, it was assumed that molecules at the air–water interface would align with the acceptor immersed in the subphase, and the long aliphatic chains pointing upright. The same arrangement was believed to be maintained when the Langmuir film was transferred onto a solid substrate. A discrepancy in RR values could be the effect of the electrical field applied to the system, which by interaction with the molecular dipoles could lead to the movement of the molecules under the tip<sup>52,63</sup>. Although, the results were consistent with the Aviram and Ratner concept<sup>1</sup>, the

geometrical asymmetry resulting from the presence of the hydrocarbon tails in the structure added ambiguity to the origin of rectification.

#### 4.2.2 Hybrid structure 1: Au-S-CH<sub>2</sub>CH<sub>2</sub>CH<sub>2</sub>-SO<sub>3</sub><sup>-</sup> / dye 4

In order to investigate the influence of the aliphatic chain on rectification, the same chromophore but with short (C<sub>4</sub>H<sub>9</sub>-) chains was studied. The attempts to deposit this compound as an LB film were unsuccessful. Due to the high affinity of the acceptor to water, and the low hydrophobic character of the donors, the molecules ‘sank’ into the water subphase and thus they were not able to form a Langmuir film at the air–water interface. Consequently, an alternative deposition technique was used to form a monolayer of dye 4 and it was achieved by the creation of an ionically assembled structure (see **Figure 4-13**).

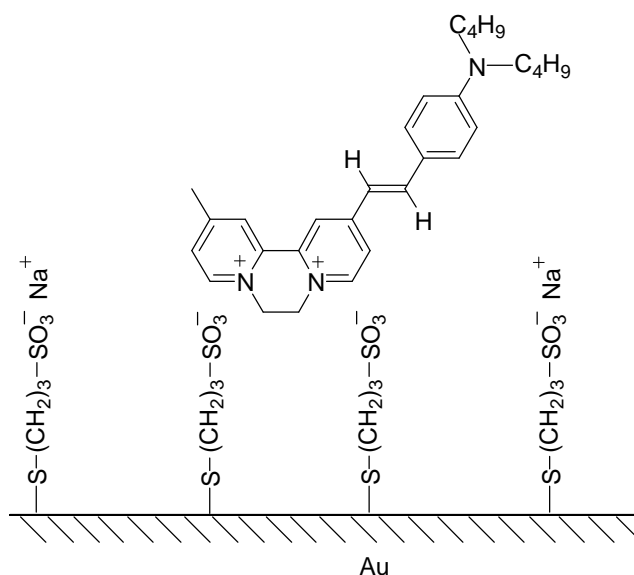


**Figure 4-13 Hybrid structure 1**

The structure was formed in two steps. The bottom monolayer was formed by the deposition of sodium 3-mercaptopropionate, shown in **Figure 4-14**, onto a gold-coated substrate. Thiols are known to produce well-packed and stable layers, due to the van der Waals interaction between the alkyl chains<sup>13,166</sup>. The thiol used possessed a sulfonate group, which was utilised to generate an anionic surface.



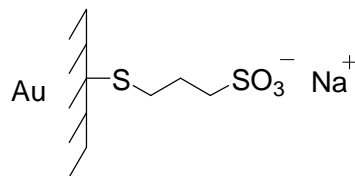


**Figure 4-14 Structure of sodium 3-mercapto-1-propanesulfonate on the gold surface**

The thiol was dissolved in methanol with the resultant solution possessing a concentration of 0.65 mg/ml. The deposition process took a total of approximately four hours. Every thirty minutes the sample was rinsed with methanol, ethanol, and acetone to remove physisorbed material. The whole process was controlled by monitoring the frequency change during deposition onto the quartz crystal. The final mean area of approximately  $0.3\text{nm}^2/\text{molecule}$  for  $\text{Au-S-(CH}_2\text{)}_3\text{-SO}_3^- \text{Na}^+$  was obtained, and this value implied a closely packed arrangement, as the cross-sectional area of the molecule approximates to the area per molecule obtained from QCM (see **Figure 4-15**).

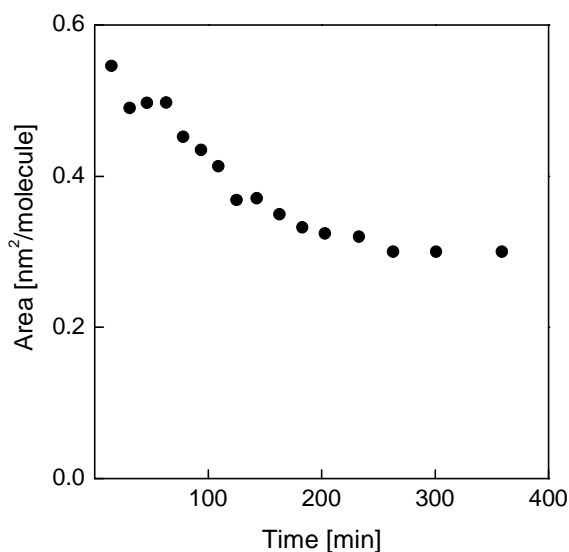


**Figure 4-15 Thiol deposition onto QCM**

SPR studies were performed and provided a thickness of  $0.6 \pm 0.05$  nm for a monolayer of thiol, which also confirmed a well-packed structure, as this approximates to the length of the molecule. Then the substrate with the thiol monolayer was immersed into the solution of dye 4 (dissolved in ethanol to obtain a concentration of 0.1 mg/ml) in order to allow the monolayer to be formed via ionic assembly. It was assumed that

during the deposition of the second layer,  $\text{Na}^+$  ions were replaced by the cationic dye at the surface. It was also assumed that  $\text{Br}^-$  ions would remain in the aqueous subphase. The total deposition time was found to be 600 minutes and the area per molecule was calculated to be approximately  $0.4 \text{ nm}^2$  (see **Figure 4-16**).

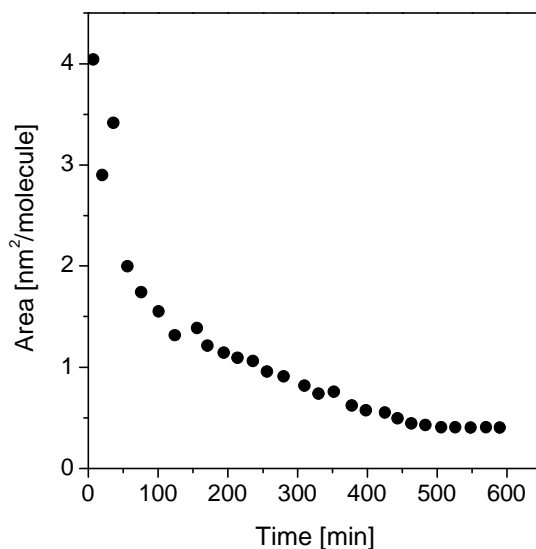


**Figure 4-16** QCM of dye 4 deposited by immersion in ethanol solution onto the thiol surface

To investigate the electrical properties, the bilayer structure was sandwiched between two electrodes: gold and PtIr tip. The STS measurements revealed three different types of I–V plots (see **Figure 4-17**). Approximately 30 % of the curves were symmetrical while the remaining 70 % showed asymmetry, with one half of these having a higher current observed in the negative quadrant of the I–V plots and RR up to 11 at  $\pm 1 \text{ V}$  and the other half having a higher current observed in the positive quadrant of the I–V plots with RR up to 4.5 at  $\pm 1 \text{ V}$ . These results were attributed to the disordered monolayer formation. It was also very likely that some amount of  $\text{Na}^+$  and  $\text{Br}^-$  ions were trapped in the film during the deposition process, and therefore could take part in the electron transport through the junction. Due to the variety of the I–V characteristics observed for this structure, the ambiguity associated with the long aliphatic chain and its contribution to rectification still remained.

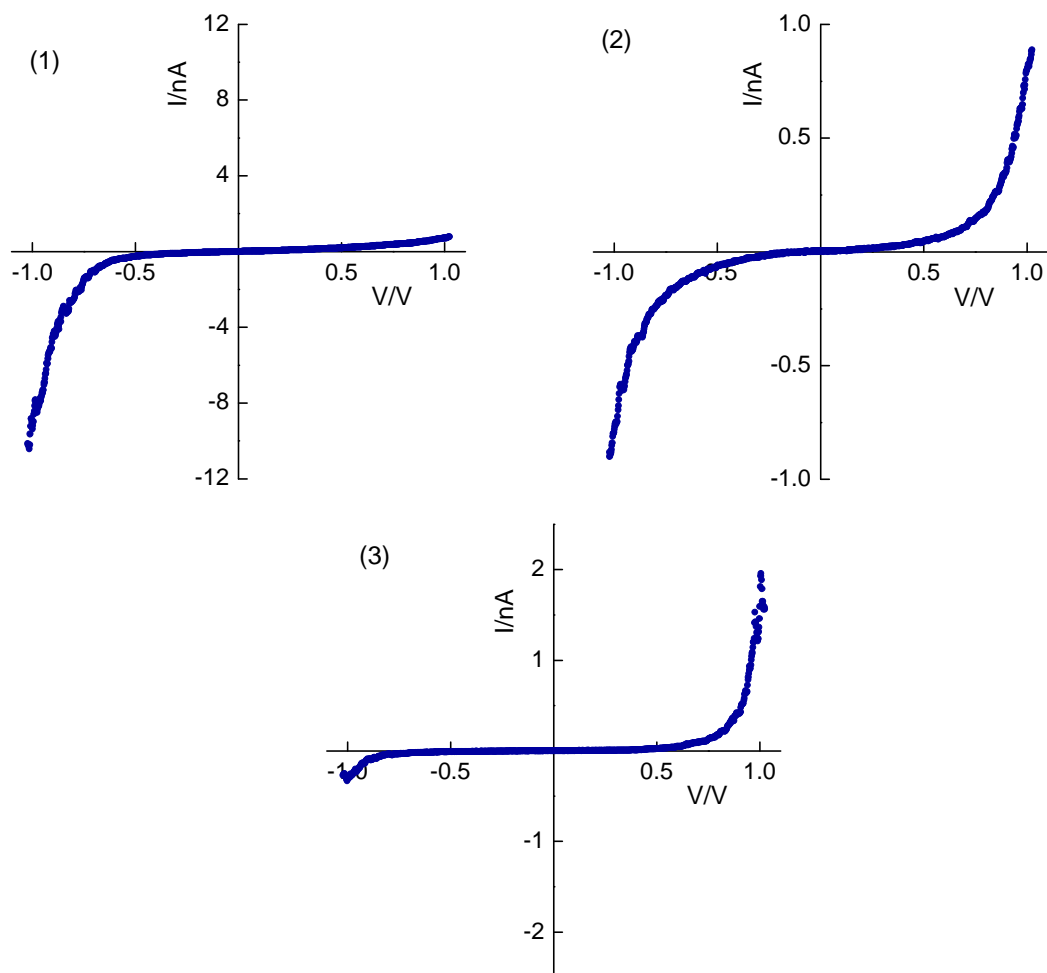


**Figure 4-17** Representative I-V characteristics of hybrid structure 1: Au-S-CH<sub>2</sub>CH<sub>2</sub>CH<sub>2</sub>-SO<sub>3</sub><sup>-</sup> / dye 4, (dye 4 was deposited as SA); (1) RR=11 at ± 1 V, (2) RR=1 at ± 1 V, (3) RR=4.5 at ± 1 V

### 4.3 Donor- $\pi$ -Acceptor- $\pi$ -Donor structures

#### 4.3.1 Dye 5 and dye 6

In order to further investigate the rectification origin for dyes 3 and 4, another two compounds supplied by Danika Locatelli from Milan University, Italy were studied (see **Figure 4-18**). These compounds, like the previous two had the same acceptor and donor with the difference of having two donor groups instead of one, and therefore formed donor- $\pi$ -acceptor- $\pi$ -donor (D- $\pi$ -A- $\pi$ -D) structures, later referred to as chevron-shaped molecules. These molecules represented a novel and unconventional

class of compounds for molecular rectification. The angle between the two charge-transfer axes of the chevron-shaped molecules is ca. 120°. The twisted  $\pi$ -bridge enforced the non-planar structure and provided effective separation between the acceptor and donors.

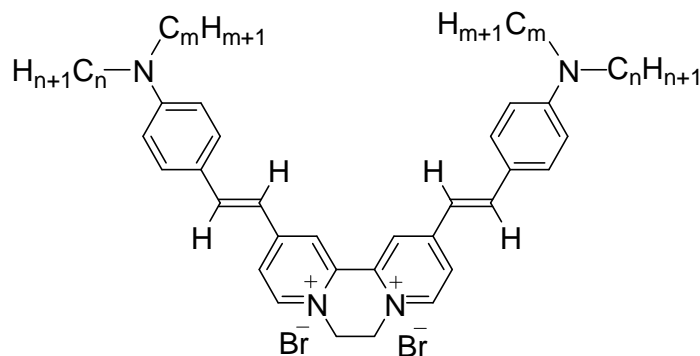


**Figure 4-18 Structure of Donor- $\pi$ -Acceptor- $\pi$ -Donor structure, dye 5 ( $n=16$ ,  $m=1$ ), dye 6 ( $n=4$ ,  $m=4$ )**

Reproducible isotherms obtained for dye 5 showed a distinct collapse point at the surface pressure of 45 mN/m and the measured areas were:  $A_0 = 1.35 \text{ nm}^2/\text{molecule}$  at a pressure of 0 mN/m,  $A_c = 0.62 \text{ nm}^2/\text{molecule}$  at 45 mN/m (collapse point), and  $A_t = 0.78 \text{ nm}^2/\text{molecule}$  at the transfer pressure of 33 mN/m. Comparing the isotherms obtained for dye 3, it seems that the presence of the 'second' donor in the structure increased the order within the monolayer at the air-water interface (see **Figure 4-19**).

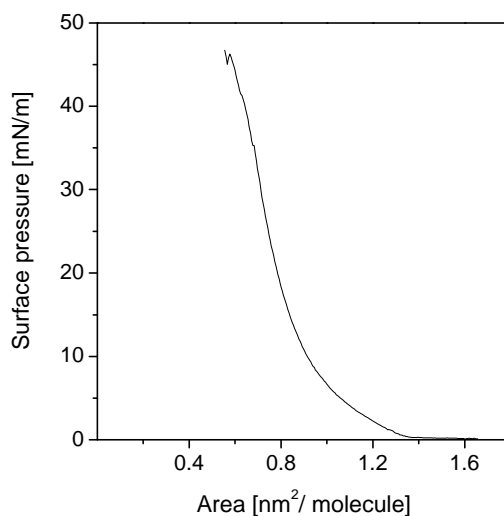


**Figure 4-19 Isotherm of dye 5**

UV–VIS spectra of the chloroform solution and the LB film (on a glass slide) were carried out to show the shift of the maxima absorbance associated with the alignment of the molecules in the same direction<sup>199,200</sup>. The spectrum in chloroform solution showed two maxima: 610–620 nm and 460 nm. As expected, the spectrum of the LB film on a glass slide also showed two maxima: 600 and 440 nm (see **Figure 4-20**).

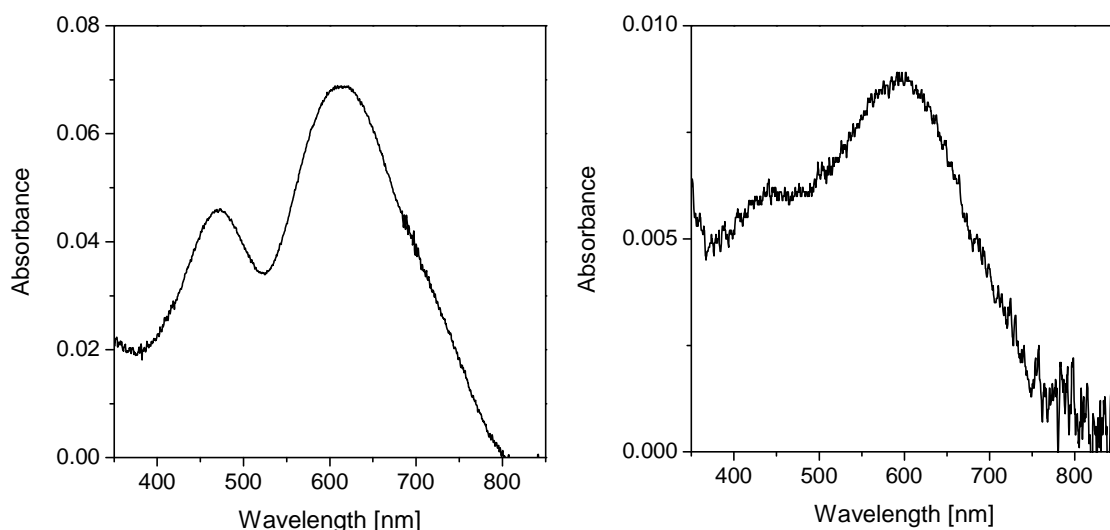


**Figure 4-20** UV-VIS spectra of dye 5; (a) in chloroform solution, (b) LB film on glass slide

QCM analysis indicated deposition to a molecular cross-section of  $0.67 \pm 0.02 \text{ nm}^2$ . SPR provided the monolayer film thickness of  $2.2 \pm 0.2 \text{ nm}$ . The calculations assumed that the  $\text{Br}^-$  counterions were retained in the deposited film, and the data confirmed the formation of a compact structure. The discrepancy between the area obtained by QCM ( $0.67 \text{ nm}^2/\text{molecule}$ ) and from the isotherm ( $0.78 \text{ nm}^2/\text{molecule}$ ) might suggest that during the monolayer transfer onto a solid substrate, part of  $\text{Br}^-$  counterions remained in the subphase.

Due to the presence of the additional donor group, it was believed that the order of the monolayer would improve, and thus also enhance the rectification. However, the I–V characteristics resulted in the same range of RR of 3.5–15 at  $\pm 1 \text{ V}$ , as for dye 3, which had only one donor group (see **Figure 4-21**).

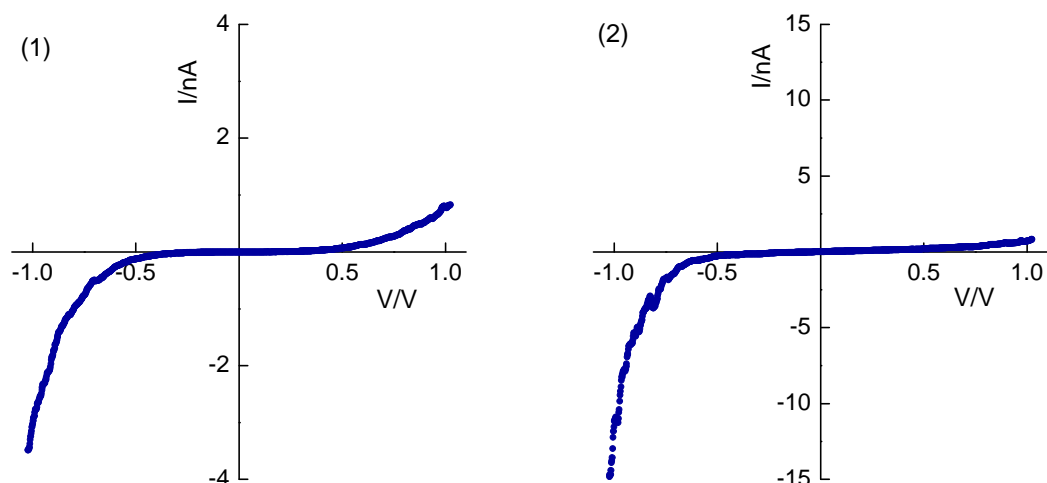


**Figure 4-21** I–V characteristics of dye 5; (1) RR=3.5 at ± 1 V, (2) RR=15 at ± 1 V

As expected, a higher current was observed in the negative quadrant of the I–V plot, which implied that the preferred movement of electrons was from the gold surface through the monolayer to the tip. This agreed with the theory proposed by Aviram and Ratner<sup>1</sup>. The variation in the observed RR values across the sample was probably due to some disorder within the monolayer. This could be caused by poor adhesion of the monolayer to the substrate or it could also be a result of defects caused by an uneven substrate surface<sup>39,167,168</sup>.

#### **4.3.2 Hybrid 2: Au-S-CH<sub>2</sub>CH<sub>2</sub>CH<sub>2</sub>-SO<sub>3</sub><sup>-</sup> /dye 6**

Dye 4, similar to dye 6, was deposited onto an anionic surface via an immersion process (see **Figure 4-22**). Formation of the thiol monolayer is described in section 4.2.2. A monolayer of dye 6 was successfully formed using a sequence of twenty-minute immersions into a 0.1 mg/ml solution in ethanol. The growth of the monolayer was monitored via frequency changes, and the deposition was obtained after approximately 660 minutes.

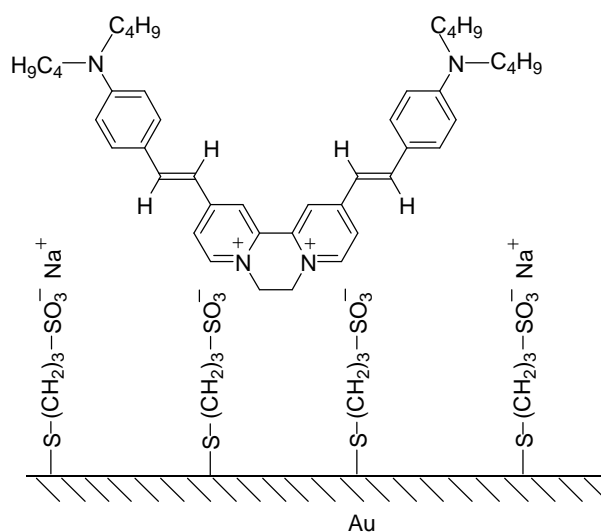


**Figure 4-22 Hybrid structure 2**

The thickness of the monolayer was found to be  $1.13 \pm 0.1$  nm. QCM studies of the complete monolayer revealed an area per molecule of  $1.14 \pm 0.1$  nm<sup>2</sup>, which surprisingly was much higher to that observed for dye 5 (with long aliphatic chains) (see **Figure 4-23**). Such a difference could have only been attributed to a greater amount of Br<sup>-</sup> ions being trapped within the monolayer of dye 6, compared to the monolayer of dye 5.

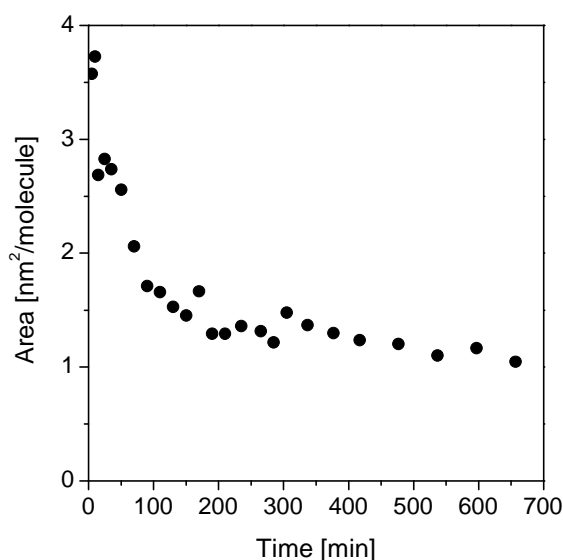


**Figure 4-23 QCM of dye 6 deposited by immersion in ethanol solution onto Au-S-CH<sub>2</sub>CH<sub>2</sub>CH<sub>2</sub>-SO<sub>3</sub><sup>-</sup> surface**

Rectification obtained from STS studies ranged from 6.5 to 21 at  $\pm 1$  V. As expected, the higher current was observed in the negative quadrant of the I–V characteristics (see **Figure 2-24**). The discrepancy in RR observed for this structure was associated with the presence of regions in the bilayer structure where molecules were more ordered than in other areas of the sample.

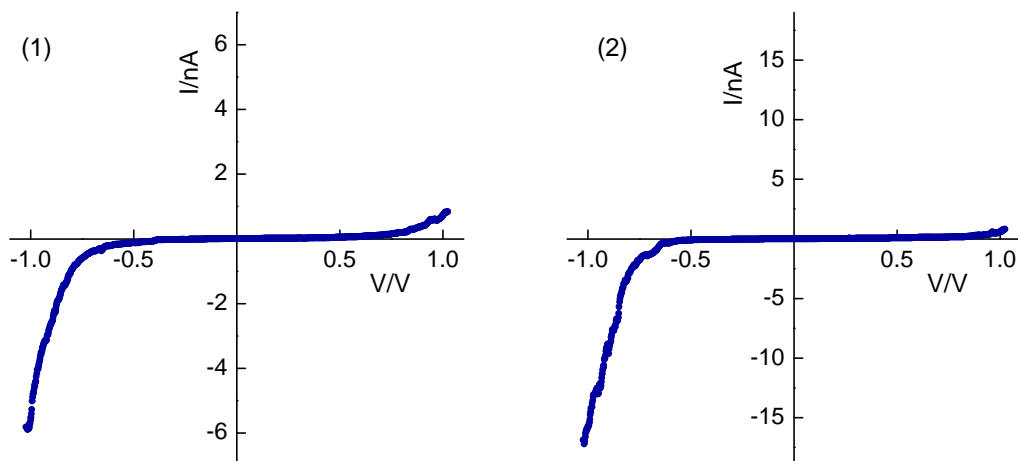


**Figure 4-24** Representative I–V characteristics of hybrid 2: Au-S-CH<sub>2</sub>CH<sub>2</sub>CH<sub>2</sub>-SO<sub>3</sub><sup>-</sup>/dye 6, (dye 6 was deposited as SAM); (1) RR=6.5 at  $\pm 1$  V, (2) RR=21 at  $\pm 1$  V

Because dye 6 with short hydrocarbon chains exhibited slightly higher rectification than dye 5, with long chains, these studies seemed to confirm that the asymmetrical position of the active chromophore between electrodes created by long aliphatic chains have an insignificant effect on the rectification compared to the D– $\pi$ –A structure. However, to provide more evidence to support this statement, further studies of molecules with short or no aliphatic chains were performed.

### 4.3.3 Dye 7

Dye 7 depicted in **Figure 4-25** is the most extensively studied chevron-shaped molecule to date<sup>69,92,93,143</sup>. It forms a non-centrosymmetric alignment and some preliminary results have been published<sup>69,92</sup>.



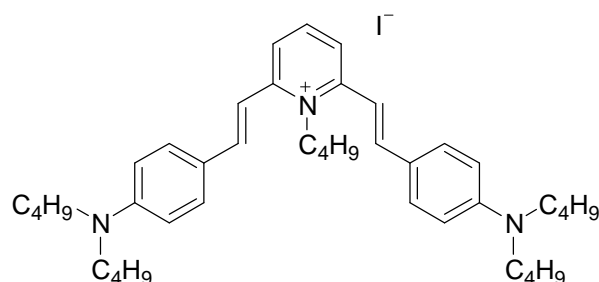


**Figure 4-25 Structure of dye 7**

The molecule consists of a pyridinium ring acceptor, which is located in the centre of two dibutylamino donor groups forming the ‘limbs’ of the compound. The long aliphatic chains, usually required for LB deposition were replaced with shorter ( $C_4H_9$ ) analogues. This was to improve the conductivity and decrease the geometrical asymmetry into the Metal | D- $\pi$ -A- $\pi$ -D | Metal system.

The isotherm confirmed that although the molecules have no significant chain, they spontaneously aligned when deposited from chloroform solution (see **Figure 4-26**). The shapes of the recorded isotherms were slightly different to that shown in the publication<sup>69,92</sup>. The original data<sup>69,92</sup> showed a collapse point at 29 mN/m, while the isotherm shown in **Figure 4-26** did not exhibit a distinct collapse point and it was assumed that the phase transition of the film occurred above 25 mN/m. These observed differences were most likely caused by a slightly different alignment adopted by the molecules at the air-water interface. In order to eliminate ambiguity resulting from the difference between the isotherms to that shown in the publication, the isotherm was repeated several times before the monolayer was deposited onto a solid substrate.

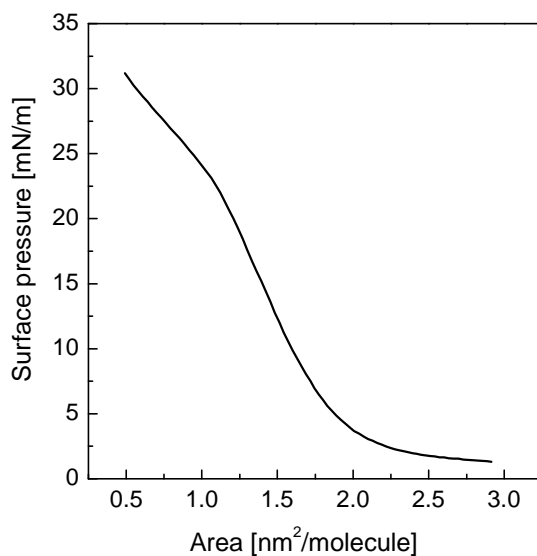


**Figure 4-26 Isotherm of dye 7**

The UV–VIS spectrum of dye 7 in chloroform solution showed a maximum absorbance at a wavelength of 490 nm (see **Figure 4-27**). The Langmuir film of dye 7 was successfully transferred onto a solid substrate at 20 mN/m and the LB film showed the maximum absorbance had shifted by 10 nm in the shorter wavelength direction.

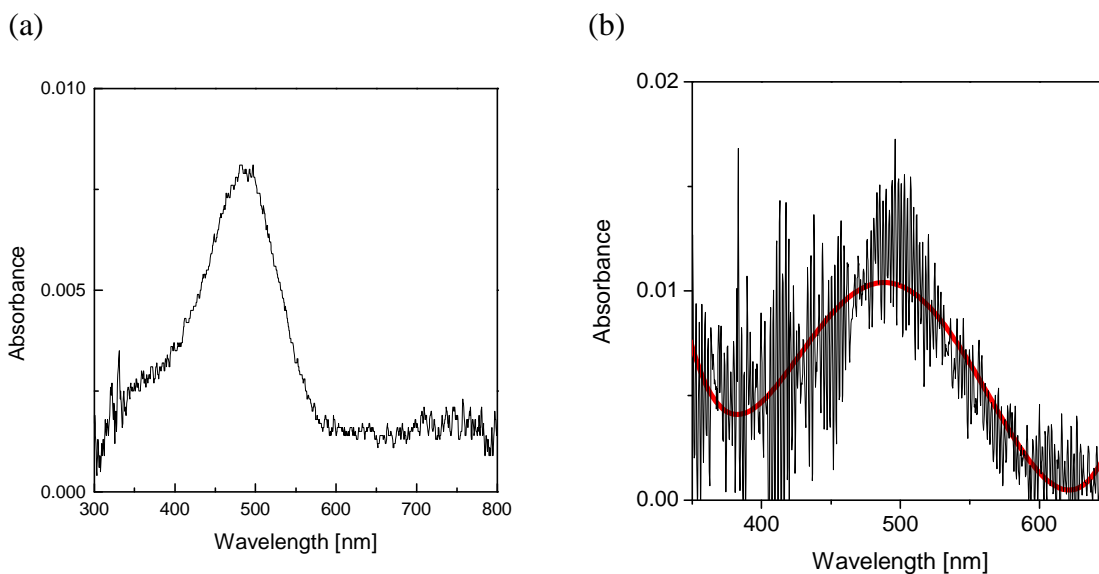


**Figure 4-27 UV–VIS spectrum of dye 7, (a) in chloroform solution, (b) on glass slide**

The monolayer of dye 7 was deposited on a gold-coated substrate in order to estimate the molecular area and thickness, which were found to be  $0.90 \pm 0.05 \text{ nm}^2/\text{molecule}$  and  $1.1 \pm 0.1 \text{ nm}$ , respectively. It should also be mentioned that the calculations assumed a presence of the iodide counterions in the deposited film. Previous studies showed that the iodide ions were partly replaced by  $\text{OH}^-$ , and because values of molecular area and thickness obtained for dye 7 were very similar to that published ( $0.95 \pm 0.05 \text{ nm}^2/\text{molecule}$  and  $1.16 \pm 0.1 \text{ nm}$ )<sup>69,92</sup>, it was also assumed that the partial ion exchange happened in this case.

It was expected that the hydrophilic part (acceptor) would be located closer to the bottom electrode when the LB film was transferred onto a solid substrate on the upstroke. However, because of the unique nature of the molecule, there was a risk that the alignment and the packing would not follow a conventional arrangement.

Asymmetric curves obtained for the Au | dye 7 | PtIr junction provided a promising result, as the calculated RR was  $30 \pm 3$  at 1 V (see **Figure 4-28**). The higher current was observed in the positive quadrant of the I-V plot, which indicated the electron flow was from the tip through the acceptor and donor of the organic monolayer to the bottom electrode. If the electron transport through the organic monolayer was ruled by the Aviram and Ratner theory<sup>1</sup>, electrons should travel from the tip to the LUMO of the acceptor (pyridinium ring) and at the same time, electrons should travel from the HOMO of the donor (dibutylamino group) to the gold electrode. This process would lead to the excited state of dye 7. Then, the electron should pass from the acceptor to the donor subunit and lead to the restoration of the molecule. However, the model proposed in 1974 really applies to  $\sigma$ -bridged compounds<sup>1</sup>, and thus the mechanism of the electron flow could be different in D- $\pi$ -A- $\pi$ -D structures.

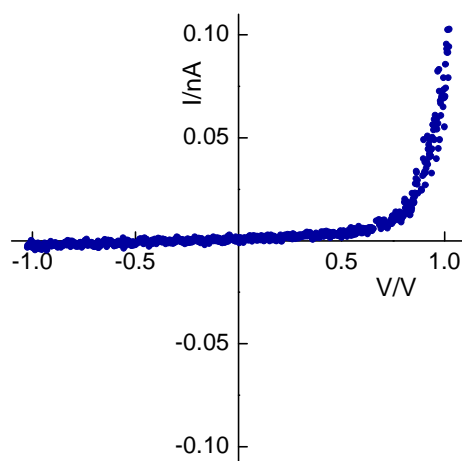


**Figure 4-28** Representative I–V characteristic of Au | dye 7 | PtIr

Previous studies<sup>69</sup> reported asymmetric I–V characteristics with an average RR of 8.4 at  $\pm 1.5$  V. Unfortunately, repeated measurements led to loss of the asymmetry, which had likely resulted from rearrangement of the molecules upon application of an electric field. Ashwell and Metzger<sup>69</sup> claimed that rectification was a result of back electron transfer from the iodide to the pyridinium. Because QCM measurements suggested presence of iodide ions in the monolayer of dye 7, it was also possible that they could significantly contribute to the rectification observed.

The results shown in this case highlighted the difficulties to unequivocally identify the molecular alignment of dye 7 on the gold-coated substrate, and consequently determine the real mechanism of the electron transport through the monolayer. The difficulty lies in whether it was the electron transport from the acceptor (pyridinium ring) to the donor (dibutylamino group), following the Aviram and Ratner model<sup>1</sup>; or charge transfer that occurred from the iodide ions to the acceptor (pyridinium ring), as was suggested by Ashwell and Metzger<sup>69</sup>.

#### 4.3.4 Dye 8

To further investigate the alignment and rectifying behaviour of chevron-shaped compounds with short aliphatic chains, dye 8 was studied (see **Figure 4-29**). It was very similar to that of dye 7, as it had the same acceptor located in the middle of the

molecule, and the same donor groups. The only difference between this molecule and dye 7 was the length of the chain attached to the pyridinium ring.

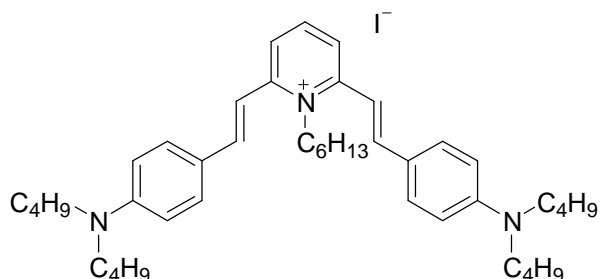


**Figure 4-29** Structure of dye 8

To produce an isotherm, the material was dissolved in chloroform and the resultant solution of concentration 0.067 mg/ml was deposited at the air–water interface and compressed at a rate of 5 mm/min to produce a Langmuir film. The shapes of the isotherms depicted in **Figure 4-30** and that of dye 7 are very similar, therefore it was assumed that the molecules were organised at the air–water interface in the same way. The isotherm yielded a phase transition of the film at 35 mN/m and an area of  $A_t = 0.67 \text{ nm}^2/\text{molecule}$  at the transfer pressure of 24 mN/m (see **Figure 4-30**).

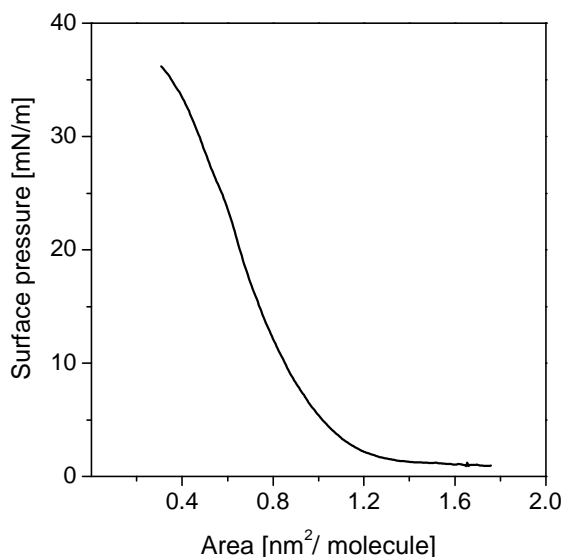


**Figure 4-30** Isotherm of dye 8

The UV–VIS spectrum of dye 8 in chloroform solution revealed that the maximum absorbance occurred at a wavelength of 562 nm (see **Figure 4-31**).

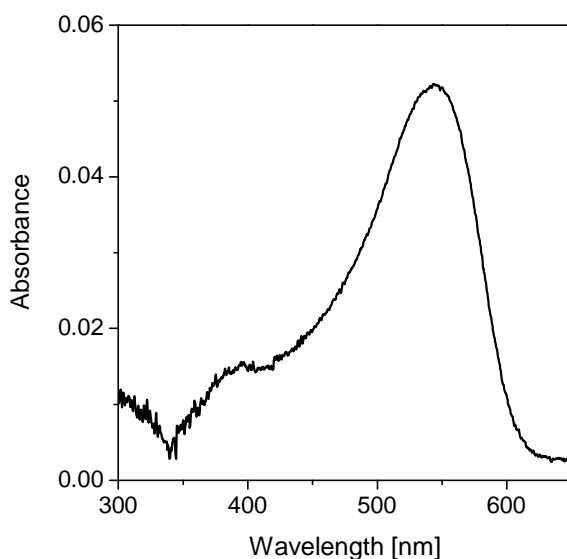


**Figure 4-31** UV-VIS spectrum of dye 8 in chloroform solution

The Langmuir film was then successfully transferred onto a solid substrate on the upstroke with a surface pressure of 24 mN/m, and subsequent QCM studies showed a molecular area of  $0.81 \pm 0.03 \text{ nm}^2/\text{molecule}$  for dye 8. This was a slightly lower value compared to the molecular area calculated for dye 7. It could suggest that some iodide ions remained in the subphase during the monolayer transfer onto a solid substrate, or they were replaced with  $\text{OH}^-$  and/or  $\text{HCO}_3^-$  at the air–water interface<sup>92</sup>. However, the latter has not been confirmed by experiment.

The main emphasis was concentrated on the STS studies to reveal electrical properties of a monolayer of dye 8 and to show whether the chain attached to the acceptor could influence the alignment and consequently rectification. For this purpose several different samples were prepared and measurements were taken in several places across each sample in order to obtain a complete picture of the monolayer properties. STS measurements revealed symmetric I–V plots (see **Figure 4-32**), whereas dye 7 did show rectifying properties with a high RR of  $30 \pm 3$  at  $\pm 1 \text{ V}$ . It was unexpected to observe completely different results from almost the same structures. Symmetric I–V plots suggested that the molecules of dye 8 very likely formed a disordered monolayer on the gold–coated substrate. This could have been the result of the rearrangement of

molecules, and in particular to highly mobile iodide ions. This could happen during the deposition process, or when an electric field was applied to the junction. Taking into account that the only difference between these two structures is the length of the hydrocarbon chain attached to the nitrogen of the acceptor, it was believed that it significantly influenced the alignment of dye 8 within the LB monolayer and consequently the rectification properties.

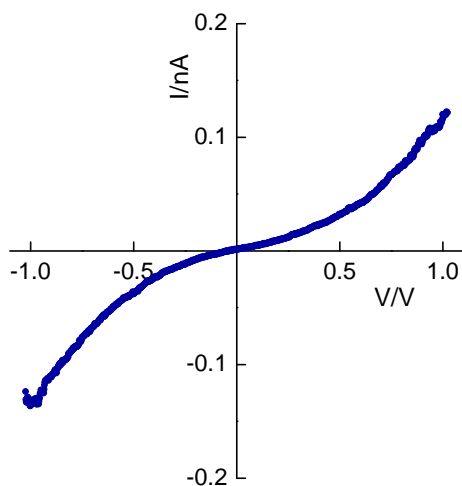


**Figure 4-32** Representative I–V characteristic of Au | dye 8 | PtIr

#### **4.3.5 Hybrid 3: Au-S-CH<sub>2</sub>CH<sub>2</sub>CH<sub>2</sub>-SO<sub>3</sub><sup>-</sup> / dye 7**

If rectification is to be assigned unambiguously to the D- $\pi$ -A- $\pi$ -D structure, an alternative method of deposition was used in order to identify the actual alignment of the molecule between the electrodes. It was believed that the formation of the hybrid structure 3: Au-S-CH<sub>2</sub>CH<sub>2</sub>CH<sub>2</sub>-SO<sub>3</sub><sup>-</sup>/dye 7 (see **Figure 4-33**) would confirm whether it was possible to force molecules to align in a defined way to produce rectification.

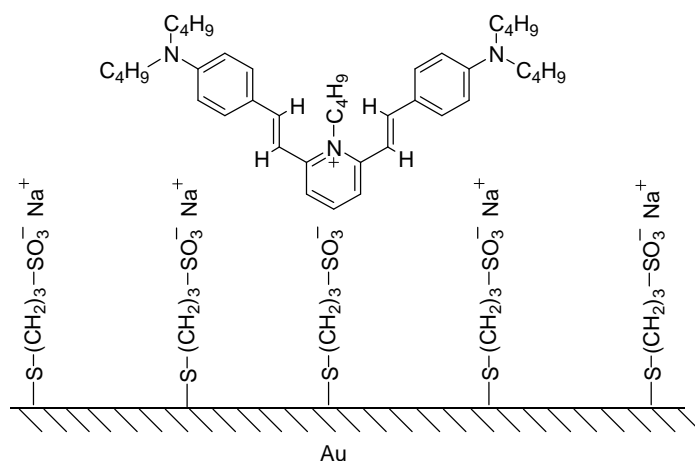


**Figure 4-33 Structure of hybrid 3: Au-S-CH<sub>2</sub>CH<sub>2</sub>CH<sub>2</sub>-SO<sub>3</sub><sup>-</sup> / dye 7**

The procedure for the hybrid formation was the same as the other examples in this thesis. A thiol monolayer was deposited onto a gold-coated substrate in order to obtain an anionic surface. A monolayer of dye 7 was successfully deposited onto an anionic surface using a sequence of one-hour immersions into a 0.1 mg/ml solution in ethanol. A complete monolayer was obtained after 1260 minutes and an area of  $0.86 \pm 0.1 \text{ nm}^2/\text{molecule}$  was determined from a Sauerbrey analysis of the frequency change<sup>177</sup> (see **Figure 4-34**). The value obtained was slightly lower compared to the molecular area observed when dye 7 was deposited onto QCM alone ( $0.95 \pm 0.1 \text{ nm}^2/\text{molecule}$ ), and it suggested that some of iodide ions were removed from the monolayer during rinsing.



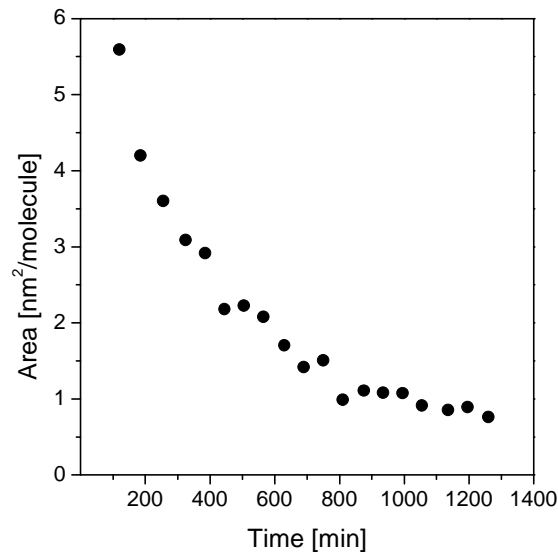


**Figure 4-34** QCM of dye 7 deposited by immersion in solution onto Au-S-CH<sub>2</sub>CH<sub>2</sub>CH<sub>2</sub>-SO<sub>3</sub><sup>-</sup> surface

The subsequent measurements taken by STS gave satisfactory results. The obtained rectification varied from 5 to 23 at  $\pm 1$  V when dye 7 was deposited onto the thiol via SA (see Figure 4-35). The higher current was observed in the negative quadrant of the I-V plots (electron flow from the bottom electrode to the tip). This was consistent with the Aviram and Ratner model<sup>1</sup>, as the molecules of dye 7 were deposited on the anionic surface in such a way that the acceptor was located close to the thiol chain and the donor groups were pointing upwards.

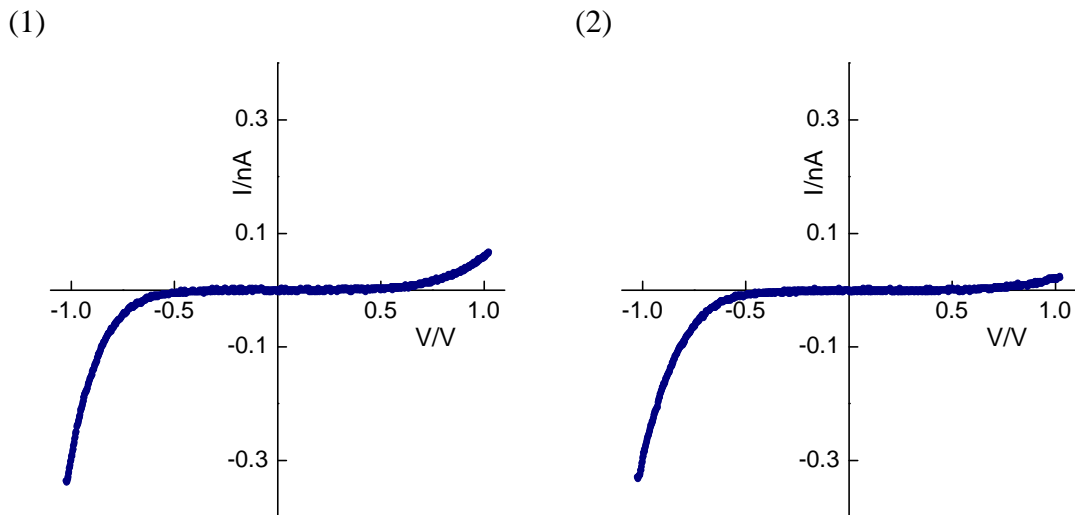


**Figure 4-35** Representative I-V characteristics of hybrid structure 3: Au-S-CH<sub>2</sub>CH<sub>2</sub>CH<sub>2</sub>-SO<sub>3</sub><sup>-</sup> / dye 7, (dye 7 was deposited as a SAM); (1) RR~5 at  $\pm 1$ V, (2) RR~23 at  $\pm 1$ V

Although the observed rectification was not as high as that achieved when dye 7 was deposited on gold by LB ( $RR=30 \pm 3$  at  $\pm 1$  V), the results were still very interesting. They clearly showed that rectification was associated with the D- $\pi$ -A- $\pi$ -D structure, as the I-V characteristics of the thiol monolayer sandwiched between electrodes showed no rectification (see **Figure 4-36**).

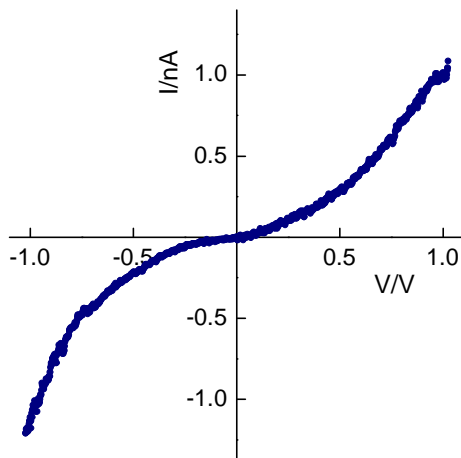


**Figure 4-36** Representative I-V characteristic of a thiol monolayer

Additionally, they demonstrated that it was possible to deposit molecules in an identifiable way, and therefore allowed better control over the alignment. They also revealed an alternative deposition method for this group of compounds. The variation in the value of RR observed across the sample indicated anisotropy of the structure. It could be a result of defects caused by an uneven substrate surface<sup>167,168</sup>, which could affect the alignment and as a consequence the electrical properties of the structure investigated.

Very surprising results were produced when dye 7 was deposited via the LB technique on the anionic surface. All I-V characteristics were symmetric (see **Figure 4-37**).

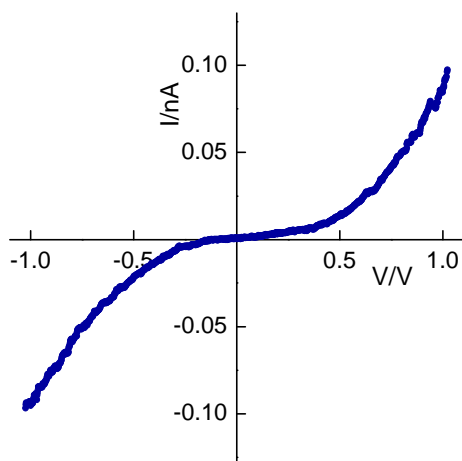


**Figure 4-37** Representative I–V characteristics of hybrid structure 3: Au-S-CH<sub>2</sub>CH<sub>2</sub>CH<sub>2</sub>-SO<sub>3</sub><sup>−</sup> / dye 7, (dye 7 was deposited as an LB film)

It would appear that when dye 7 was deposited via the traditional LB technique<sup>122,123</sup> on a gold-coated substrate, the molecules preferred to align with the donors closer to the bottom electrode and thus a high RR of  $30 \pm 3$  at  $\pm 1$  V was observed. However, when the same monolayer was aligned on the anionic surface, the interaction between the negatively charged thiol and positively charged chevron was forcing the chevron-shaped molecules to flip over and thus caused disorder within the monolayer, resulting in symmetric I–V characteristics. Additionally, QCM measurements, which provided a higher area of  $1.04 \pm 0.02$  nm<sup>2</sup>/molecule for dye 7 deposited on the anionic surface using the LB technique compared to that observed for dye 7 deposited onto QCM alone ( $0.95 \pm 0.1$  nm<sup>2</sup>/molecule) might suggest that Na<sup>+</sup> and I<sup>−</sup> were trapped within a monolayer and therefore could also affect the alignment and the STS measurements.

#### 4.3.6 Dye 9

The next structure, which was successfully deposited using the LB technique is dye 9 (see **Figure 4-38**), synthesised at Cranfield University<sup>42</sup>.

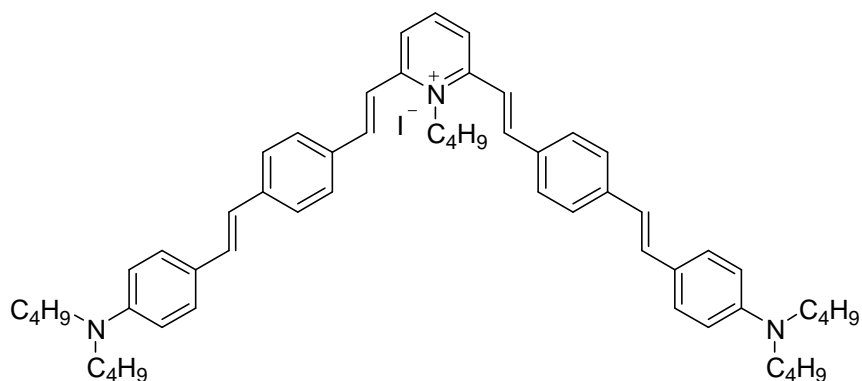


**Figure 4-38 Structure of dye 9**

According to the information obtained from the isotherm (see **Figure 4-39**), a film collapse occurred at 30 mN/m and the measured areas were:  $A_0 = 1.2 \text{ nm}^2/\text{molecule}$  at zero pressure,  $A_c = 0.5 \text{ nm}^2/\text{molecule}$  at 30 mN/m and  $A_t = 0.75 \text{ nm}^2/\text{molecule}$  at the transfer pressure of 23 mN/m. The value of the molecular area obtained was verified using the QCM technique, which provided a slightly higher area of  $0.88 \pm 0.10 \text{ nm}^2/\text{molecule}$  for the monolayer deposited at 23 mN/m. Similar to other dyes studied, the analysis assumed that the iodide counterions remained in the structure. However, QCM data suggested that the iodide ions might have been partly involved in ion exchange with  $\text{OH}^-$  and/or  $\text{HCO}_3^-$  at the air–water interface<sup>92</sup>. The molecular masses of ions  $\text{OH}^-$  and  $\text{HCO}_3^-$ , which occur naturally in the subphase, are significantly lower than that of iodide, and thus a difference between the area obtained by QCM ( $0.88 \text{ nm}^2/\text{molecule}$ ) and by isotherm ( $0.75 \text{ nm}^2/\text{molecule}$ ) was observed. Alternatively, the larger area may reflect either incomplete surface coverage, or irregular arrangement of chevron molecules upon deposition.

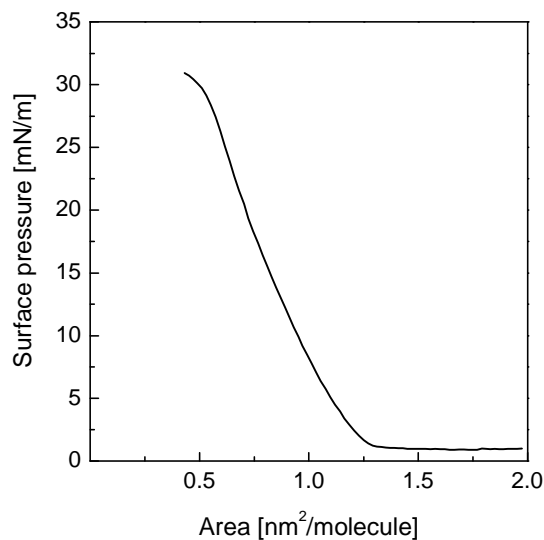


**Figure 4-39 Isotherm of dye 9**

The UV–VIS spectrum possessed two bands of absorbance, one at a wavelength 380 nm, and another more intensive at 480 nm (see **Figure 4-40**).

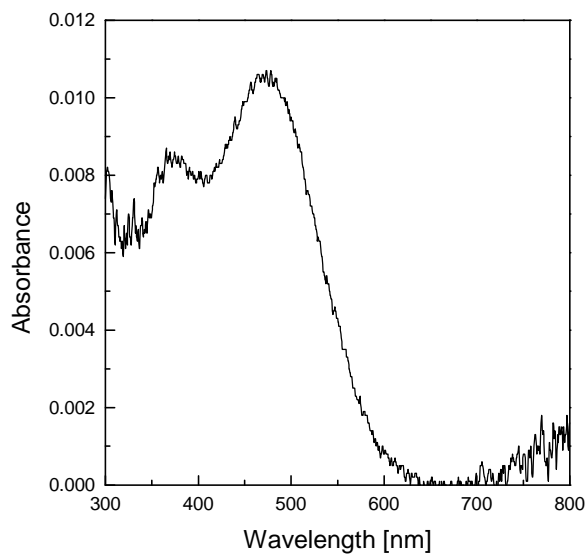


**Figure 4-40 UV-VIS spectrum of dye 9 in chloroform solution**

SPR measurements provided a thickness of  $1.95 \pm 0.05$  nm for an LB film monolayer of dye 9. This would seem to be a reasonable value, as the thickness of the monolayer of dye 7 (containing three benzene rings in the structure) was found to be  $0.9 \text{ nm}^2$ .

To study the electrical properties of the monolayer, dye 9 was deposited on a gold-coated substrate and contacted via a PtIr tip. The STS investigations revealed very interesting results. It was noticeable that dye 9, when deposited on the gold surface, seemed to be unstable after a certain period of time (approximately 3 hours). Immediately after deposition, the compound exhibited rectification with a ratio of  $16 \pm 3$  at  $\pm 1$  V (see **Figure 4-41**).

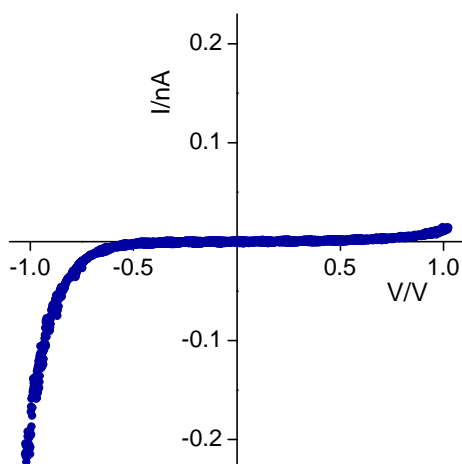


**Figure 4-41** Representative I–V characteristic of Au | dye 9 | PtIr (after deposition)

Because the monolayer was transferred on the upstroke, it was assumed that the acceptor of the molecule was attached to the gold surface, while donors were located closer to the tip. It was believed that donor groups with short butyl chains attached represented the hydrophobic part of dye 9, and thus they should point upright when deposited at the air–water interface. The higher current was seen in the negative quadrant of the I–V plot and it corresponded to electron movement from the substrate, through the acceptor, and then the donor of the monolayer to the tip. This agreed with the Aviram Ratner theory<sup>1</sup>. However, a few hours later when the measurements were repeated, the STS study showed that the RR had decreased and the I–V curves had become more symmetric (RR = 2 at  $\pm 1$  V) (see **Figure 4-42**).

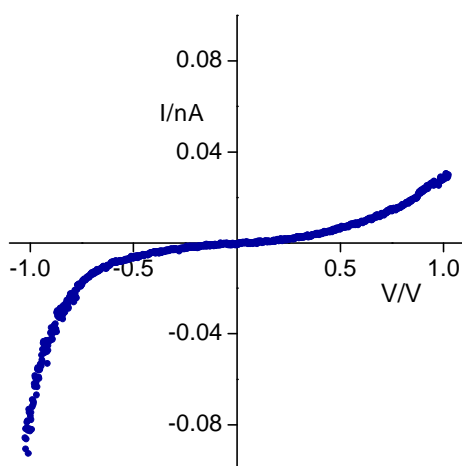


**Figure 4-42** Representative I-V characteristic of Au | dye 9 | PtIr ( 3 hours after deposition)

These results demonstrated the importance of stability and structural order of the LB film in order to generate rectification. The decrease of rectification in the Au | dye 9 | PtIr system suggested that the electric field probably interacted with the molecular dipoles<sup>61</sup> causing movement of the cationic dye and anion within the monolayer. Due to these molecules not being strongly attached to the gold surface<sup>39,63</sup>, they may have a tendency to flip over. Thus, the initial well-ordered monolayer of dye 9 became more and more disordered over a period of time, and as a result the observed rectification decreased.

Additionally, the SHG studies confirmed that dye 9 initially exhibited a non-centrosymmetric alignment. After a few hours, the SHG dropped to zero, which could be explained by a change in orientation of the molecules within the monolayer (see Figure 4-43), and resulted in a disordered alignment.

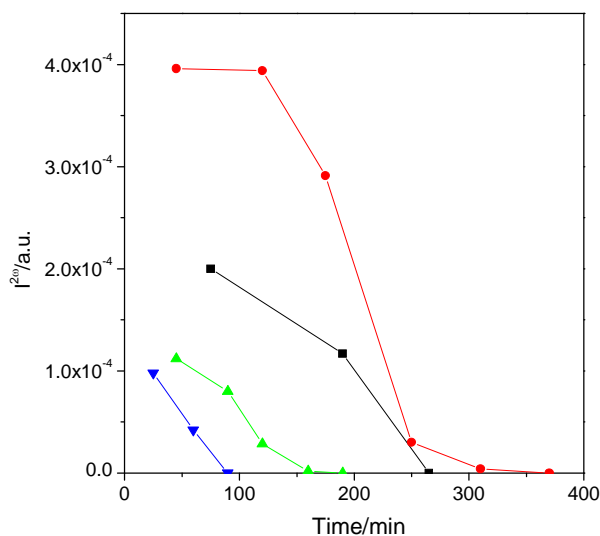


**Figure 4-43 Time dependence of the suppression of the second-harmonic intensity of four LB films following deposition on glass substrates. The different initial intensities are consistent with the film structure being inherently unstable**

The changes in the alignment of the monolayer of dye 9 were also observed in UV–VIS spectra measurements on glass slides. The monolayer showed maximum absorbance at approximately 480 nm, which is in very close vicinity with SHG signal (532 nm). Therefore, it was possible that the monolayer of dye 9 could absorb the signal, and this could consequently lead to molecular rearrangement within a monolayer. As a result, the absorption maximum at 500 nm disappeared after a few hours following deposition (see Figure 4-44).



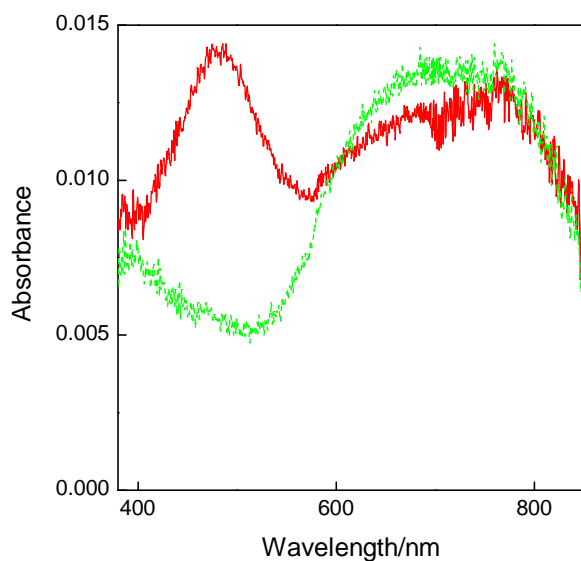


**Figure 4-44** UV–VIS spectra of a monolayer LB film of dye 9, (red curve) just after deposition, (green curve) 3 hours after the deposition

#### 4.3.7 Hybrid 4: Au-S-CH<sub>2</sub>CH<sub>2</sub>CH<sub>2</sub>-SO<sub>3</sub><sup>-</sup> / dye 9

In order to improve the stabilisation of the dye 9 monolayer, it was deposited on an anionic surface using two different methods. The first was to align the chevron-shaped molecules by simply immersing the anionically coated quartz crystal in a solution of dye 9 to obtain the hybrid structure as depicted in **Figure 4-45**.

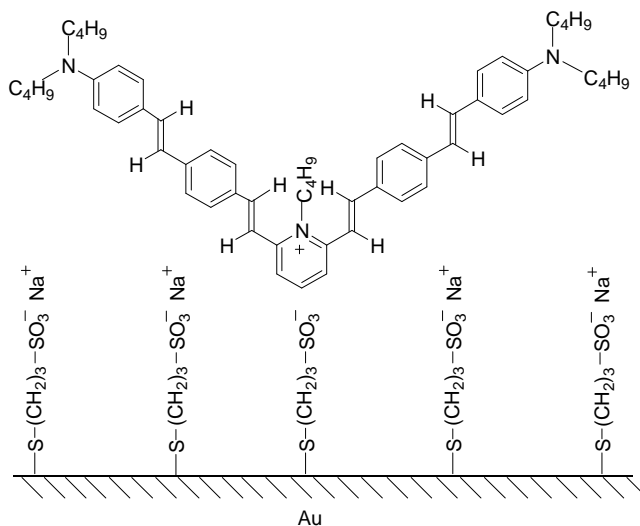


**Figure 4-45** Hybrid structure 4: Au-S-CH<sub>2</sub>CH<sub>2</sub>CH<sub>2</sub>-SO<sub>3</sub><sup>-</sup> /dye 9

The QCM measurements gave satisfactory results, implying that although dye 9 belongs to the LB film-forming group, it was possible to deposit it using the SA method (see **Figure 4-46**). A monolayer of dye 9 was successfully formed using a sequence of one-hour immersions into a 0.1 mg/ml solution of chloroform. The complete monolayer was formed after 1300 minutes. It was assumed that during the deposition of the second layer, ions of  $\text{Na}^+$  were replaced by the cationic dye at the surface. It was also suspected that iodide ions would remain in the aqueous subphase. However, the area per molecule for dye 9 was found to be  $1.01 \pm 0.10 \text{ nm}^2/\text{molecule}$  (see **Figure 4-46**), which was slightly higher than the value obtained from QCM analysis when dye 9 was deposited via the LB technique ( $0.88 \pm 0.10 \text{ nm}^2$ ). The QCM values obtained suggested the existence of a disordered monolayer and a presence of iodide ions in the second layer. These could then influence the electron transport through the bilayer structure.

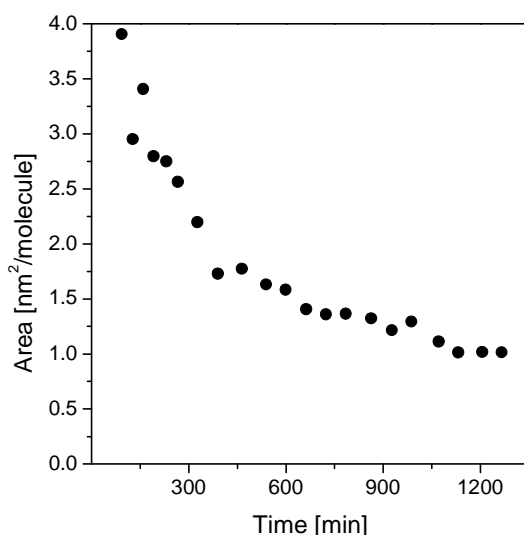


**Figure 4-46** QCM of dye 9 deposited on anionic surface by immersion in chloroform solution

Subsequent STS studies of this hybrid structure provided disappointing data, as only slightly asymmetric I–V curves with RR of only approximately 2 at  $\pm 1 \text{ V}$  were observed (see **Figure 4-47**). Moreover, the higher current was observed in the positive quadrant of the I–V plot, so the movement of electrons was from the tip through the monolayer to the bottom electrode, which was opposite to that expected. These results seemed to confirm that the presence of iodide ions in the structure and their position in relation to the cationic dye played a manipulated rectification<sup>69</sup>.

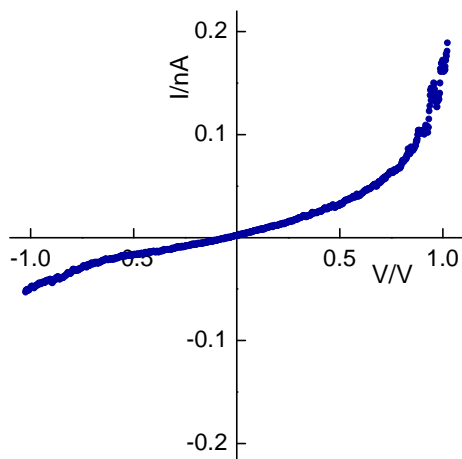


**Figure 4-47 Representative I–V characteristic of hybrid structure 4: Au-S-CH<sub>2</sub>CH<sub>2</sub>CH<sub>2</sub>-SO<sub>3</sub><sup>-</sup>/dye 9, (dye 9 was deposited as a SAM)**

Due to the disappointing results, the second deposition method of dye 9 was implemented. The chevron-shaped molecules were deposited on the anionic surface using the LB technique. The conditions for deposition were the same as described in section 4.3.6. It was very likely that some of the  $\Gamma^-$  ions could be incorporated into the structure during the deposition process as the QCM studies yielded an area per molecule of  $0.90 \pm 0.03 \text{ nm}^2$ . This value is exactly the same for the monolayer of dye 9 when deposited straight onto QCM alone. The assumption was that the interaction between thiol and dye would be strong enough to stabilise the structure, and further STS investigations confirmed this. At forward bias, which corresponds to the negative quadrant of the I–V plot, the electrons travelled from the substrate to the tip, and consistent with the Aviram and Ratner concept<sup>1</sup>, they travelled from the cathode to the HOMO of the acceptor and from the LUMO of the donor to the anode. Finally, by intramolecular tunnelling, the molecule was restored to the ground state. This meant that the acceptor, where the positive charge was located, was placed close to the thiol and the donor subunits were pointing upwards. STS studies also provided a satisfactory increase in the RR from 14 to 25 at  $\pm 1 \text{ V}$  (see **Figure 4-48**). The measurements were repeated the following day to ensure that it was not short-lived and the results showed similar curves with RR between 22–25 at  $\pm 1 \text{ V}$ .

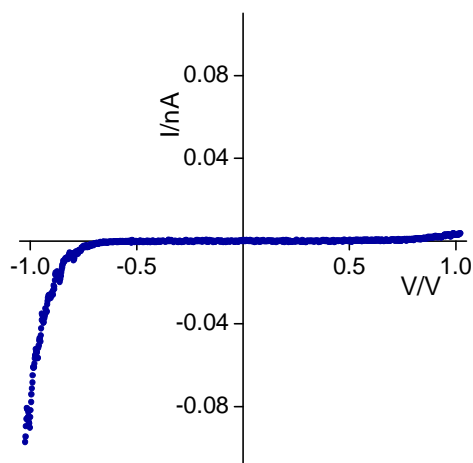


**Figure 4-48** Representative I-V characteristic of hybrid structure 4: Au-S-CH<sub>2</sub>CH<sub>2</sub>CH<sub>2</sub>-SO<sub>3</sub><sup>-</sup> /dye 9, (dye 9 was deposited as LB film)

These results showed that this simple modification of the substrate surface had a profound effect in preventing molecular realignment of the LB film-forming dye and also led to an improvement of the RR.

#### 4.3.8 Dye 10

Dye 10 is similar to the previous chevron-shaped dyes, having a D- $\pi$ -A- $\pi$ -D structure with twisted  $\pi$ -conjugated bridges to enforce a non-planar structure and to effectively separate the donor from acceptor. Professor David Lacy from the University of Hull supplied this molecule and its structure is depicted in **Figure 4-49**

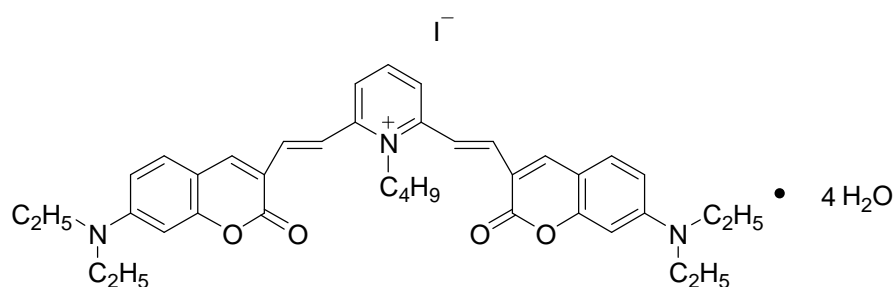


**Figure 4-49** Structure of dye 10

It is believed that the electrical properties of LB films are limited by the hydrophobic alkyl chain because it introduces an additional insulating barrier between one of the electrodes and the D-electron bridge-A in a molecular device<sup>60</sup>. Therefore, the length

of the chain was further decreased, and this structure had the advantage of shorter tails ( $\text{C}_2\text{H}_5-$ ) attached to the donor groups. This molecule had been studied previously<sup>92</sup>, and the studies had revealed a considerable amount of information about the LB monolayer of this material. However, to further identify the critical areas of interest such as the exact surface arrangement and electrical properties of this unique LB monolayer, more investigation was required. In order to obtain this information an isotherm was produced and the resultant shape is presented in **Figure 4-50**. The discrepancy observed between the shape of the published isotherm<sup>92</sup> and the isotherm obtained here was possibly due to the water molecules trapped in the structure. Due to the lack of a distinguishable collapse point it was assumed that the Langmuir film of dye 10 collapsed above 14 mN/m. The measured areas were:  $A_c = 0.87 \text{ nm}^2/\text{molecule}$  at 14 mN/m and  $A_t = 1.05 \text{ nm}^2/\text{molecule}$  at the transfer pressure of 10 mN/m (see **Figure 4-50**).

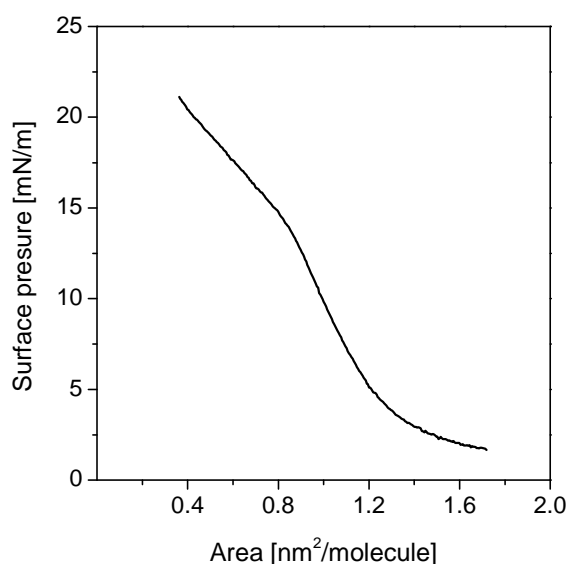


**Figure 4-50 Isotherm of dye 10**

Previous studies<sup>92</sup> on such films had revealed a molecular area of  $0.88 \text{ nm}^2$ , and a film thickness of 1.23 nm, indicating that the molecules formed a well-packed monolayer. QCM measurements of dye 10 resulted in a value of  $1.1 \pm 0.1 \text{ nm}^2$ . The SPR measurements provided a thickness of  $1.18 \pm 0.1 \text{ nm}$ . It was believed that the molecules were tilted away from the desired vertical orientation relative to the surface. The higher value of the molecular area obtained for dye 10 also confirmed the assumption that iodide ions and water may have been trapped in the structure during deposition.

UV–VIS spectrum from the LB monolayer film on a glass slide showed an absorbance maximum at 520 nm (see **Figure 4-51**) and this is consistent with the reported data<sup>92</sup>.

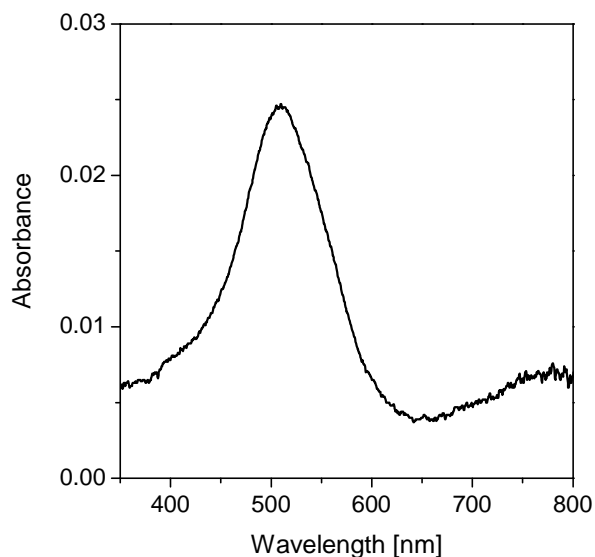


**Figure 4-51** UV–VIS spectrum of the LB monolayer of dye 10 on glass slide

The main emphasis however, was concentrated on STS investigations of dye 10. In order to obtain I–V characteristics the monolayer of dye 10 was deposited on a gold–coated HOPG and contacted via a PtIr tip. STS studies showed disappointing results. This compound did not seem to rectify, as the I–V plots were only slightly asymmetric with a very low RR approximately 1.4 at  $\pm 1$  V (see **Figure 4-52**).

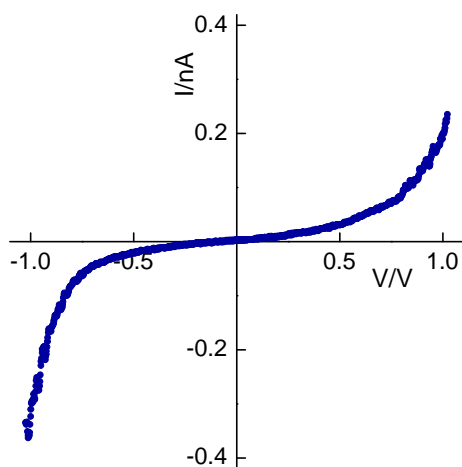


**Figure 4-52** Representative I–V characteristic of Au | dye 10 | PtIr

The very low RR observed across the sample indicated anisotropy of the monolayers studied. This could be due to the poor attachment of the molecules to the gold substrate, which could have led to the reorganisation of the molecules when a voltage was applied to the junction<sup>61,63</sup>. Moreover, the presence of  $\Gamma^-$  and water molecules trapped within the monolayer, could have disrupted the alignment of the molecules when deposited at the air–water interface, and subsequently during the transfer onto the substrate.

#### 4.3.9 Hybrid structure 5: Au-S-CH<sub>2</sub>CH<sub>2</sub>CH<sub>2</sub>-SO<sub>3</sub><sup>-</sup> /dye 10

The low rectification ratio of 1.4 at  $\pm 1$  V achieved for dye 10 led to the investigation of hybrid structure 5 (see **Figure 4-53**), which was believed to improve the order within the monolayer and consequently rectification.

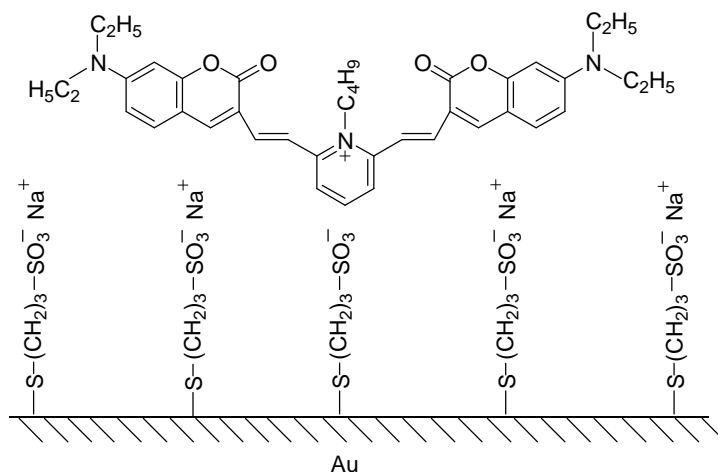


**Figure 4-53** Hybrid structure 5: Au-S-CH<sub>2</sub>CH<sub>2</sub>CH<sub>2</sub>-SO<sub>3</sub><sup>-</sup> /dye 10

STS measurements of this hybrid structure yielded asymmetric I–V characteristics with the RR of 8 at  $\pm 1$  V. A higher current was observed in the negative quadrant of the plot (see **Figure 4-54**), and this implied that the chevron-shaped molecules aligned in the desired way as depicted in **Figure 4-53** with the positively charged acceptor positioned closer to the short chains of the thiols, while the donor groups were directed upwards. The increase of the RR value from 1.4 to 8 at  $\pm 1$  V clearly indicated that the molecules of dye 10 formed a more ordered and closely–packed monolayer. The results also followed the modified Aviram and Ratner model<sup>1</sup>.

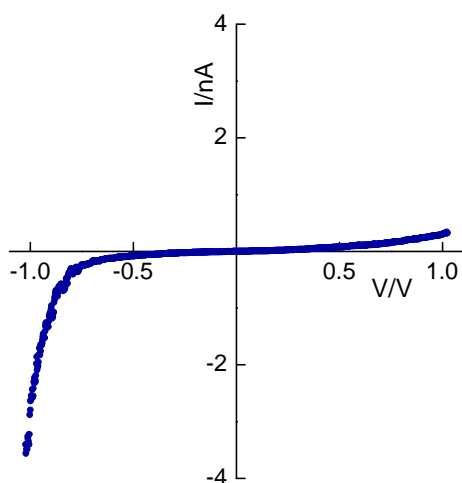


**Figure 4-54** Representative I–V characteristics of hybrid structure 5: Au-S-CH<sub>2</sub>CH<sub>2</sub>CH<sub>2</sub>-SO<sub>3</sub><sup>-</sup> /dye 10, (dye 10 was deposited as a LB)

The studies of hybrid structure 5 were continued with the monolayer now being deposited via immersion of the ionically modified substrate into an acetone solution of dye 10 (concentration 0.1 mg/ml). The deposition of the second monolayer was based on interactions between the positively charged acceptor of the dye with the negatively charged thiol. It was assumed that this interaction would be strong enough to force molecules to align in a specific way to obtain the hybrid structure as depicted in **Figure 4-53**. An optimum deposition was achieved after approximately 1000 minutes, and the resultant monolayer characterised by QCM had an area per molecule of approximately 0.4 nm<sup>2</sup> (see **Figure 4-55**).



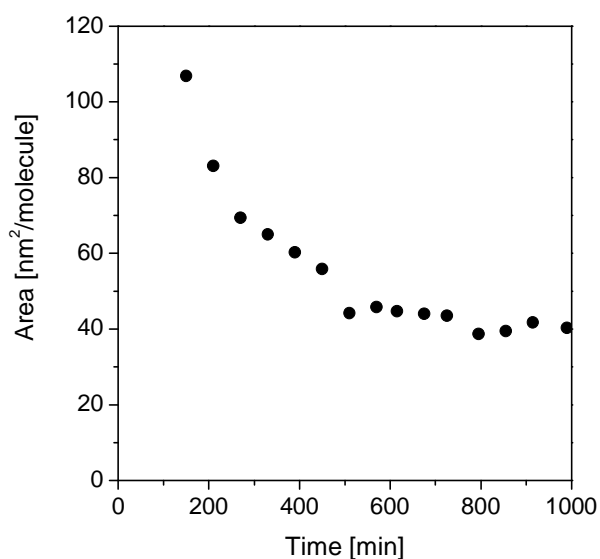


**Figure 4-55** QCM of dye 10 deposited by immersion in acetone solution onto an ionic surface

STS studies of hybrid structure 5 showed a further increase of the RR to 25 at  $\pm 1$  V (see **Figure 4-56**). The low value of area per molecule determined from a Sauerbrey analysis<sup>177</sup> of the frequency changes implied that during deposition,  $\text{Na}^+$  and  $\text{I}^-$  ions remained in the solution, and thus they had not disrupted the monolayer and consequently had not contributed to rectification. In conclusion, the rectification obtained could only have been a result of the ordered monolayer of dye 10.

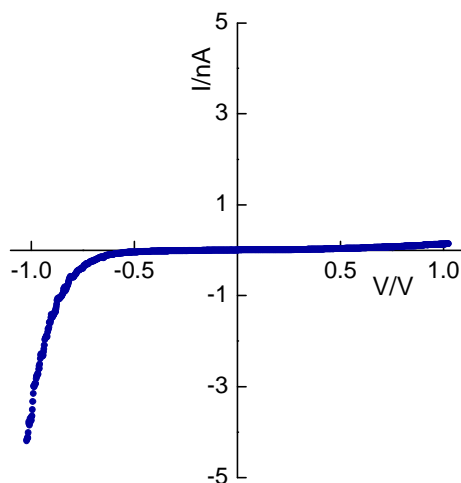


**Figure 4-56** Representative I–V characteristics of hybrid 5:  $\text{Au-S-CH}_2\text{CH}_2\text{CH}_2\text{-SO}_3^-$  /dye 10, (dye 10 was deposited as a SAM)

STS measurements of Au-S-CH<sub>2</sub>CH<sub>2</sub>CH<sub>2</sub>-SO<sub>3</sub><sup>-</sup>Na<sup>+</sup> | PtIr junction, which yielded symmetric I–V plots seemed to provide further evidence of the Aviram and Ratner mechanism<sup>1</sup> causing rectification.

These results demonstrated that it was possible to design and then enforce a desired alignment to improve the stabilisation and order of molecules within a monolayer and therefore increase the RR value.

### 4.3.10 Dye 11

To further investigate the chain length effect on the diode-like behaviour of chevron-shaped compounds another chromophore was studied. Dye 11 was synthesised by the author, and the synthesis is detailed in section 3.10.4 and the structure of the compound is shown in **Figure 4-57**.

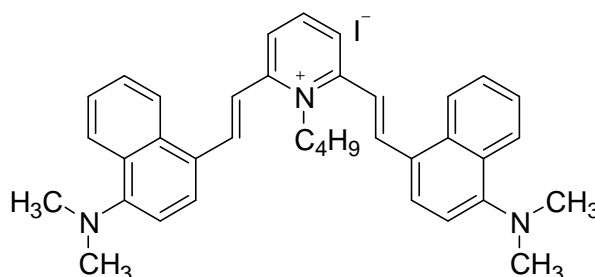


**Figure 4-57** Structure of dye 11

The compound was dissolved in chloroform and the resultant solution with a concentration of 0.1 mg/ml was deposited at the air–water interface and compressed in order to produce an isotherm. Based on the results from the obtained isotherm it was assumed that the phase transition of the film occurred above 22 mN/m and the measured areas were unexpectedly low:  $A_o = 0.13 \text{ nm}^2/\text{molecule}$  at zero pressure,  $A_c = 0.048 \text{ nm}^2/\text{molecule}$  at 22 mN/m and  $A_t = 0.07 \text{ nm}^2/\text{molecule}$  at the transfer pressure of 19 mN/m (see **Figure 4-58**).

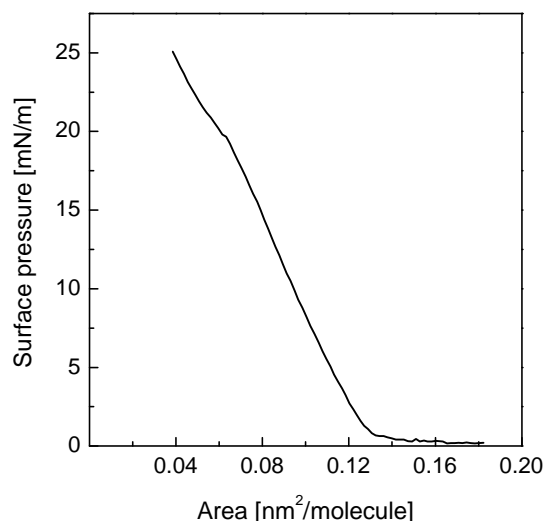


**Figure 4-58 Isotherm of dye 11**

The low areas obtained from the isotherm suggested that molecules of dye 11 overlapped during the compression process and did not result in a well-ordered Langmuir film. Consequently, it was very likely that the molecules formed very poor quality LB films. However, in order to confirm this conclusion the measurements were continued.

The UV-VIS spectrum of a chloroform solution of dye 11 showed two bands of absorbance, one at 360 nm and another at 490 nm (see **Figure 4-59 (a)**). The spectrum of an LB monolayer of dye 11 deposited at a transfer pressure of 19 mN/m on a glass slide revealed a very similar spectrum with maximum absorbance observed at the same wavelengths (**Figure 4-59 (b)**). Additionally, the spectrum of the LB monolayer of dye 11 exhibited an absorbance that was unusually high for a single monolayer. These results suggested that molecules of dye 11 overlapped and did not form a well-ordered monolayer.

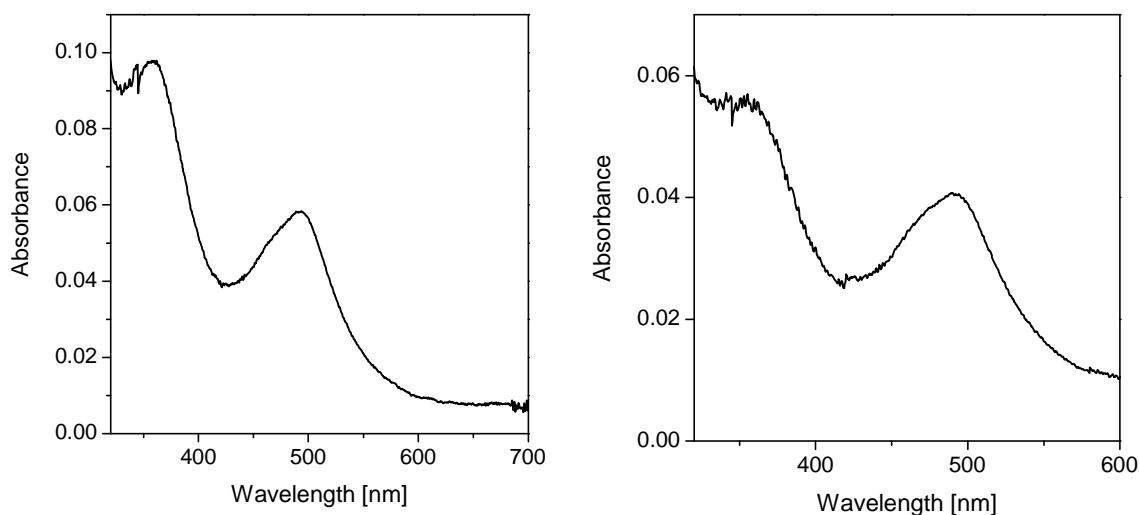


**Figure 4-59 UV–VIS spectra of dye 11; (a) in chloroform solution, (b) LB monolayer on glass slide**

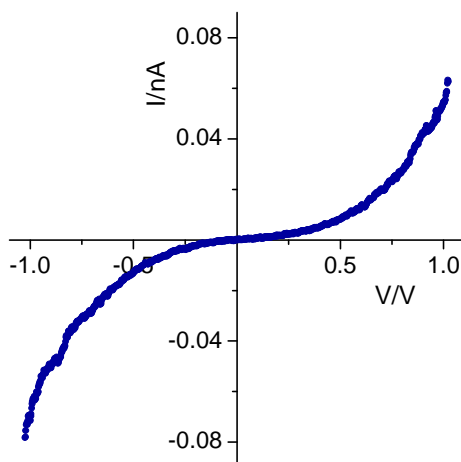
QCM (see Table 4-2) and SPR studies confirmed the results obtained from the isotherm. SPR provided a thickness for the monolayer of  $2.9 \pm 0.2$  nm, which was also found to be too high for a single monolayer. Therefore, it was assumed that during Langmuir film compression and deposition a bilayer or multilayer was formed.

Dye 11 was deposited at various target pressures in the range of 17–25 mN/m. As expected the area per molecule decreased with increasing pressure. This indicated that the higher the deposition pressure, the more compact was the resultant monolayer. However, the measurements resulted in smaller values of area per molecule than expected and this clearly indicated that a bilayer or multilayer was formed. This could be due to the chosen target pressures being too high and so leading to film breakage. This breakage may have occurred as a result of the weak hydrophobic character of the donor groups, which failed to maintain the molecules of dye 11 at the air–water interface.

**Table 4-2 Area per molecule of dye 11**

Deposition pressure [mN/m]	Area [nm <sup>2</sup> /molecule]
25	0.24
20	0.35
18	0.44
17	0.43

The results obtained from the isotherm, QCM and SPR measurements provided evidence that the film of dye 11 overlapped during compression, and therefore, it was not possible to obtain a well-ordered and stable monolayer. Also, data supplied from STS measurements confirmed this assumption because all I–V characteristics were symmetric (see **Figure 4-60**). These results showed that the advantage of having reduced alkyl chains had been balanced by the formation of a disordered monolayer.

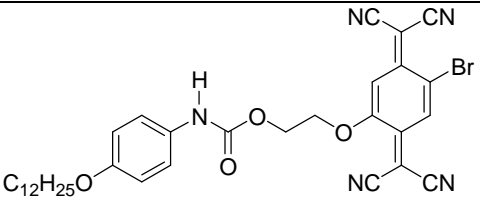
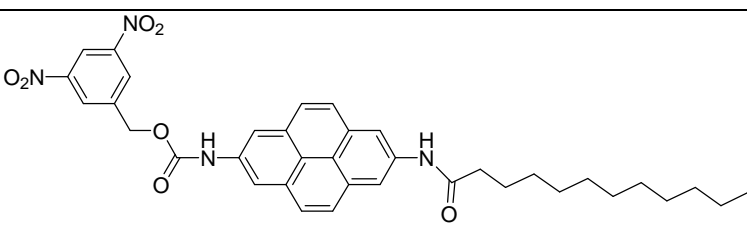
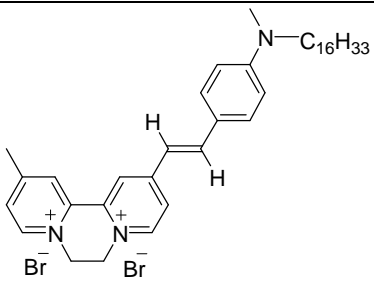


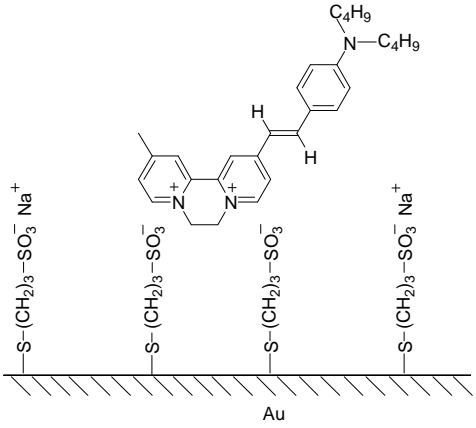
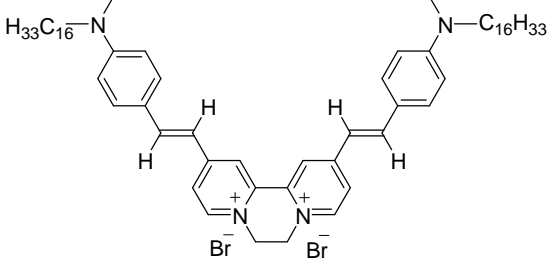
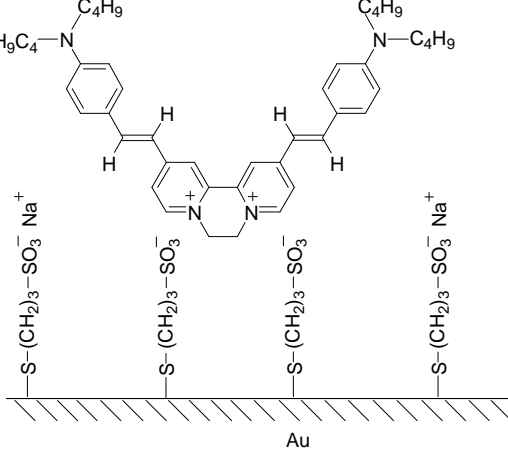
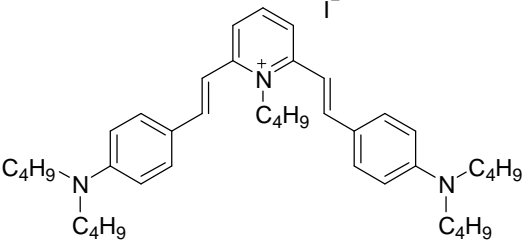
**Figure 4-60 Representative I–V characteristic of Au | dye 11 | PtIr**

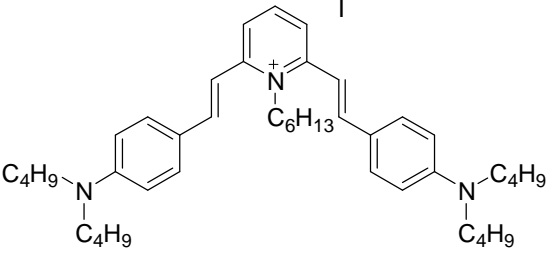
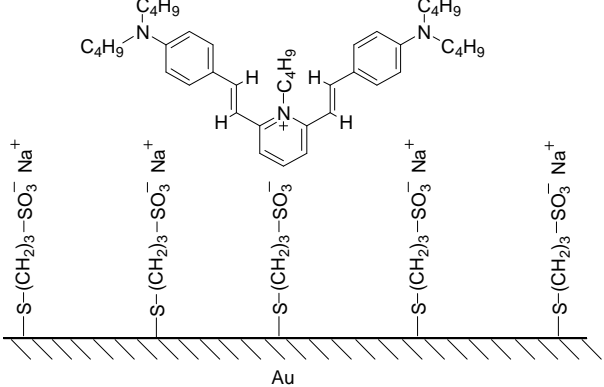
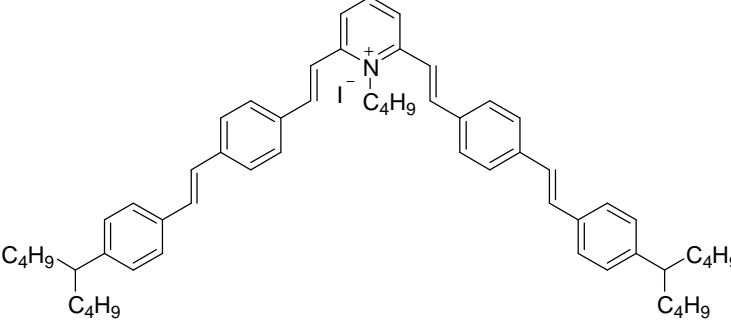
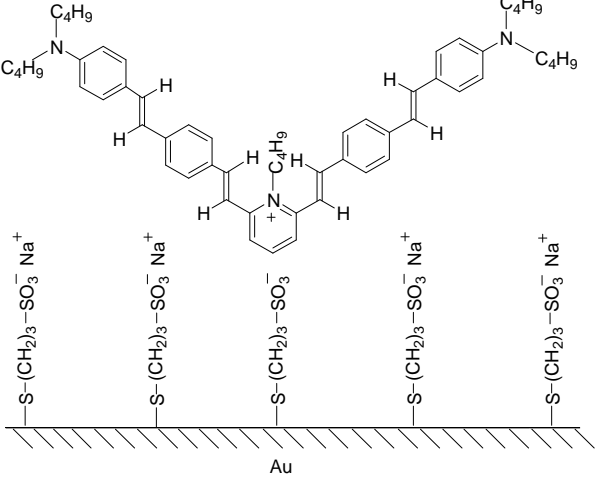
## 5 CONCLUSIONS

The main objective of this research was to investigate the alignment and electrical properties of different types of D–electron bridge–A structures when placed between non–oxidised electrodes. These included LB type compounds with a long aliphatic chain, chevron–shaped molecules, and finally hybrid structures. This research was inspired by the Aviram and Ratner proposal<sup>1</sup> of the organic rectifier. The results obtained, summarised in **table 5.1**, showed that the physical properties of thin films strongly depend not only on the molecular structure but also on the molecular–level packing, and the possible intermolecular interactions between charged species (ruled by the orientation of the molecules with respect to one another).

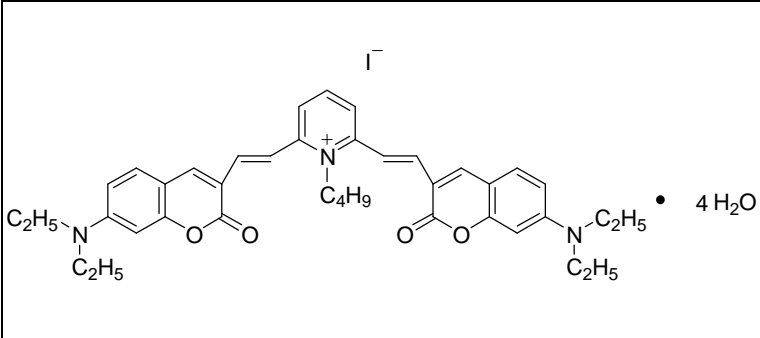
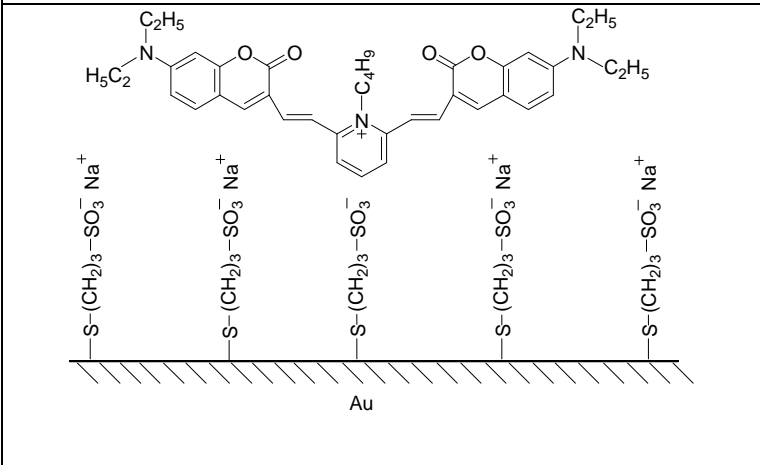
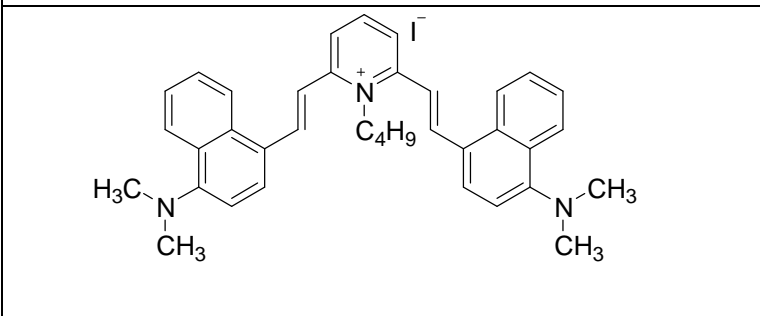
**Table 5-1 I–V characteristics of all compounds studied**

Structure	I–V characteristics
	Strong relationship between I–V characteristics and deposition pressure, RR up to 20 at $\pm 1$ V
	Symmetric and asymmetric with RR of 6 at $\pm 1$ V
	Asymmetric with RR between 3.4–16 at $\pm 1$ V

	<p>Symmetric and asymmetric curves with RR between 4.5–11 at <math>\pm 1</math> V</p>
	<p>Asymmetric with RR between 3.5–15 at <math>\pm 1</math> V</p>
	<p>Asymmetric with RR between 6–21 at <math>\pm 1</math> V</p>
	<p>Asymmetric with RR of 30 at <math>\pm 1</math> V</p>

	Symmetric
	<p>Symmetric when the second layer was deposited using the LB technique</p> <p>Asymmetric (RR between 5–23 at <math>\pm 1</math> V) when the second layer was deposited in the immersion process</p>
	Asymmetric just after deposition with RR of 16 at $\pm 1$ V, symmetric after few hours from deposition
	<p>Symmetric when the second layer was deposited in the immersion process</p> <p>Asymmetric (RR of 25 at <math>\pm 1</math> V) when the second layer was deposited using the LB technique</p>



	Symmetric
	Asymmetric (RR of 8 at $\pm 1$ V) when the second layer was deposited using the LB technique. Further increase of RR to 25 at $\pm 1$ V when the second layer was deposited in the immersion process
	Symmetric

The molecules studied were deposited onto a substrate using different techniques. The LB technique was chosen because it is known to produce well-packed structures<sup>123,124</sup>. However, as the results showed, great care was needed when the LB monolayers were formed and exploited. Studies of dye 1 revealed a strong relationship between the deposition pressure and molecular arrangement. Depending on the deposition pressure the molecules of dye 1 aligned at the surface in different ways and as a consequence a variety of I-V characteristics were observed. Dye 2 yielded two types of I-V curves: symmetrical and asymmetrical, with a higher current in the negative quadrant and low RR of 6 at  $\pm 1$  V, which seemed to follow the Aviram and Ratner theory<sup>1</sup>. Unfortunately, there had been noted difficulties over controlling the alignment of these molecules due to a flexible  $\sigma$ -bridge<sup>68</sup>. For this reason the investigation was then

focused towards a modified D- $\pi$ -A Aviram and Ratner rectifier model<sup>1</sup>, which used a twisted  $\pi$ -bridge instead of a  $\sigma$ -bridge. The implementation of a twisted  $\pi$ -bridge was believed to keep an effective separation of molecular orbitals of the donor from the acceptor, and additionally form a more rigid structure<sup>34,87</sup>, and this studies confirmed it. Studies of dye 3 and the chevron-shaped molecule with long aliphatic chains attached to donors (dye 5) showed improvement of RR values (3.4–16 at  $\pm 1$  V). The rectification observed agreed with the Aviram and Ratner proposal<sup>1</sup>. However, there was a high possibility that ions took a significant role in the electron transport. Moreover, some scientists<sup>60,83,84</sup> claimed that the long hydrocarbon chains required for the LB deposition acted as an additional tunnelling barrier and might affect electrical behaviour of the metal | monolayer | metal structures. In order to avoid the ambiguity associated with the presence of long chains in the molecular structures, a major part of the research was devoted to chevron-shaped molecules without long aliphatic chains. These materials were defined as a modified Aviram and Ratner rectifier<sup>1</sup>, which consisted of a central cationic acceptor and two  $\pi$ -bridged donor groups (D- $\pi$ -A- $\pi$ -D). Unfortunately, the results showed that the reduction of aliphatic chains was very likely balanced by the formation of less ordered or unstable monolayers. Of all the chevron-shaped molecules investigated, dye 7 revealed the highest RR of  $30 \pm 1$  V. However, the direction of the current observed from the I-V characteristics suggested a different alignment to the one expected. Dyes 8, 10 and 11 showed symmetric I-V curves. Dye 9, although showed asymmetric I-V characteristics shortly after deposition onto the gold-coated HOPG, it seemed to create an unstable alignment on the hydrophilic slide and as a consequence the rectification decayed over a period of a few hours. Due to the instability of the LB monolayers, an innovative method of stabilisation based on the layer-by-layer technique was introduced. This simple method was used to modify the substrate surface by the deposition of short chain thiols on the gold surface to generate an ionic surface. Then the second monolayer was formed via the interactions between positively charged chromophores and the negatively charged substrate. As the results showed, this method not only increased the stabilisation of LB films but also enhanced the rectification behaviour of these structures as a result of the improved molecular alignment of the unconventional LB film-forming dyes. Studies of the hybrid structure 4 (Au-S-CH<sub>2</sub>CH<sub>2</sub>CH<sub>2</sub>-SO<sub>3</sub><sup>-</sup> / dye 9) resulted in a desirable

monolayer stabilisation and an increase in RR from 16 to 25 at  $\pm 1$  V. Studies of hybrid structures 1 and 2 showed also that this technique could also be used as an alternative deposition method for the molecules which could not form a monolayer using the LB technique. The strong hydrophilic character of the acceptor compared to hydrophobic character of the donor for dyes 4 and 6 prevented the monolayer formation using the LB technique. However, the molecules seemed to be able to produce a monolayer based on opposite charge attraction. STS measurements obtained from hybrid 2 showed asymmetric curves with RR in the range of  $6-21 \pm 1$  V. Studies of the hybrid 1 structure confirmed that the formation of the monolayer of dye 4 was achievable but unfortunately it appeared to be disordered. Very satisfactory results were obtained also from hybrid structure 5, where as a chromophore, dye 10 was used. Studies showed that dye 10 formed disordered monolayers when deposited on a purely gold-coated substrate, and thus symmetric I-V characteristics were obtained. However, the RR increased to 8 at  $\pm 1$  V when the same monolayer was deposited on top of the thiol monolayer using the LB technique. A further increase of RR to 25 at  $\pm 1$  V was observed when the same monolayer was deposited on a thiol monolayer via the immersion process.

In summary, the studies presented here show that it is extremely important to understand the mechanism of the electron transport through the device and all factors that may significantly influence it. Experimental verification of the Aviram and Ratner concept proved to be difficult to achieve. Studies of D- $\sigma$ -A compounds did not yield very promising results. Although an ambiguity associated with the Schottky effect<sup>31,32</sup> and the use of the electrodes with different work functions had been eliminated, the results highlighted the difficulties of controlling the alignment of molecules with a flexible  $\sigma$ -bridge. All structures studied represented a typical or modified Aviram and Ratner molecular rectifier<sup>1</sup>. However, the mechanism of the electron transport through a metal | organic | metal junction still remains unclear. This was due to  $\Gamma^-$ ,  $\text{Br}^-$ ,  $\text{OH}^-$  and  $\text{HCO}_3^-$  ions trapped within the structures. On the other hand, this work has proved that the identification and control over the alignment of the molecules within a monolayer play a key role in the determination of rectifying behaviour of the structures studied. This research pointed out that the molecules must form stable and ordered monolayers,

which have a strong enough attachment to the substrate to be able to withstand the electric field applied to the device. The satisfactory results obtained from the hybrid structures encourage further investigation in this field. This method enabled the incorporation of additional layers, which acted as ‘stabilisers’ in order to generate an ordered and stable monolayer. It also provided a great opportunity to form desired structures from building blocks and often avoided very complicated synthesis.

Although there is still much research involved in order to fabricate a real nano-scale device, the first steps have been made to bring this idea closer to reality.

## 6 REFERENCES

---

- <sup>1</sup> A. Aviram, M.A. Ratner, *Chemical Physical Letters*, 29, **1974**, 277.
- <sup>2</sup> G. Maruccio, R. Cingolani, R. Rinaldi, *Journal of Material Chemistry*, 14, **2004**, 542.
- <sup>3</sup> D. Goldhaber-gordon, M.S. Montemerlo, J.C. Love, G.J. Opiteck, J.C. Ellenbogen, *Proceedings of the IEEE*, 85, **1997**, 521.
- <sup>4</sup> R.D. Piner, J. Zhu, F. Xu, S. Hong, C.A. Mirkin, *Science*, 283, **1999**, 661.
- <sup>5</sup> M.C. Petty, M.R. Bryce, D. Bloor, (1995), *Introduction to Molecular Electronics*, Edward Arnold, Cambridge.
- <sup>6</sup> Feynman, R.P. (1959), *There's plenty of room at the bottom*, available at: <http://www.zyvex.com/nanotech/feynman.html> (accessed 40).
- <sup>7</sup> M. Wilson (red.), (2002) *Nanotechnology: basic science and emerging technologies*, Chapman & Hall/CRC.
- <sup>8</sup> H. Ahmed, P.J. Spreadbury, (1973) *Electronics for Engineers*, Cambridge University Press, Cambridge
- <sup>9</sup> T. Duncan, (1983) *Success in electronics*, John Murray (Publishers) Ltd. London.
- <sup>10</sup> G.E. Moore, *Electronics*, 3, **1965**, 114.
- <sup>11</sup> Moore's law scheme available at: [http://www.accelerating.org/acc2003/pics/moores\\_law.jpg](http://www.accelerating.org/acc2003/pics/moores_law.jpg)
- <sup>12</sup> R.M. Metzger, *Colloids and Surfaces A: Physicochemical and Engineering Aspects*, 284, **2006**, 2.
- <sup>13</sup> A. Ulman, (1991) *An introduction to ultrathin organic films from Langmuir-Blodgett to self-assembly*, Academic Press, New York.
- <sup>14</sup> R. Tredgold, *Journal of Material Chemistry* 5, **1995**, 1095.
- <sup>15</sup> N. Robertson, C.A. McGowan, *Chemical Society Reviews*, 32, **2003**, 96.
- <sup>16</sup> G. Binning, H. Rohrer, C. Gerber, E. Weibel, *Physical Review Letters*, 49, **1982**, 57.
- <sup>17</sup> T.W. Kelley, E.L. granstrom, C.D. Frisbie, *Advanced Materials*, 11, **1999**, 261. (AFM)
- <sup>18</sup> B. Crone, A. Dodabalapur, Y.-Y. Lin, R.W. Filas, Z. Bao, A. LaDuca, R. Sapershkar, H.E. Katz, W. Li, *Nature*, 403, **2000**, 521.
- <sup>19</sup> L. Fu, L. Cao, D. Zhu, *Advances in Colloid and Interface Science*, 111, **2004**, 133.
- <sup>20</sup> C. Joachim, J.K. Gimzewski, A. Aviram, *Nature*, 408, **2000**, 541.

- 
- <sup>21</sup> A. Salomon, D. Cahen, S. Lindsay, J. Tomfohr, V.B. Engelkes, D. Frisbie, *Advanced Materials*, 15, **2003**, 1881.
- <sup>22</sup> F. Moresco, A. Gourdon; *Proceeding of the National Academy of Science* , 102, **2005**, 8809.
- <sup>23</sup> M. Hietschold, M. Lackinger, S. Griessl, W.M. Heckl, T.G. Gopakumar, G.W. Flynn, *Microelectronic Engineering*, 82, **2005**, 207.
- <sup>24</sup> H. Kuhn, *Thin Solid Films*, 99, **1983**, 1.
- <sup>25</sup> T. Bjornholm, T. Hassenkam, N. Reitzel, *Journal of Materials Chemistry*, 9, **1999**, 1975.
- <sup>26</sup> G.G. Roberts, P.S. Vincett, W.A. Barlow, *Journal of Physics C: Solid State Physics*, 11, **1978**, 2077.
- <sup>27</sup> E. Meinhard, *Journal of Applied Physics*, 35, **1964**, 3059.
- <sup>28</sup> N.J. Geddes, J.R. Sambles, D.J. Jarvis, W.G. Parker, D.J. Sandman, *Journal of Applied Physics* 71, **1992**, 756.
- <sup>29</sup> S. Chang, Z. Li, C. N. Lau, B. Larade, R. S. Williams, *Applied Physical Letters*, 83, **2003**, 3198.
- <sup>30</sup> G.J. Ashwell, J.S. Bonham, L.E. Lyons, *Australian Journal of Chemistry*, 33, **1980**, 1619.
- <sup>31</sup> J.G. Simmons, *Journal of Physics D: Applied Physics*, 4, **1971**, 613.
- <sup>32</sup> F. Flores, R. Miranda, *Advanced Materials*, 6, **1994**, 540.
- <sup>33</sup> E. Wu, F. Hellman, R.C. Dynes, (September 2003) *Anisotropic pinning and Schottky barrier of iron silicide thin films on silicon*, poster, available at: [http://www.calit2.net/calit2day/ppts/poster\\_edWu.pdf](http://www.calit2.net/calit2day/ppts/poster_edWu.pdf) (accessed 20).
- <sup>34</sup> G.J. Ashwell, J.R. Sambles, A.S. Martin, W.G. Parker, M. Szablewski; *Journal of the Chemical Society, Chemical Communications*; 70, **1990**, 1374.
- <sup>35</sup> G.J. Ashwell, W.D. Tyrrell, A.J. Whittam, *Journal of the American Chemical Society*, 126, **2004**, 7102.
- <sup>36</sup> I. Langmuir, *Journal of the American Chemical Society*, 39, **1917**, 1848.
- <sup>37</sup> K.B. Blodgett, *Journal of the American Chemical Society*, 56, **1934**, 495.
- <sup>38</sup> G.G. Roberts, *Advances in Physics*, 34, **1985**, 475.
- <sup>39</sup> I.R. Peterson, *Journal of Physics D: Applied Physics*, 23, **1990**, 379.
- <sup>40</sup> A. Ulman, *Chemical Reviews*, 96, **1996**, 1533.

- 
- <sup>41</sup> F. Schreiber, *Progress in Surface Science*, 65, **2000**, 151.
- <sup>42</sup> G.J.Ashwell, M.Sujka, A.Green, *Faraday discussions*, 131, **2006**, 2.
- <sup>43</sup> G.J. Ashwell, A. Chwialkowska, *Chemical Communication*, 13, **2006**, 1404.
- <sup>44</sup> P.Bedrossian, *Science and technology Review*, **1995**.
- <sup>45</sup> B.A.Mantooth, P.S.Weiss, *Proceedings of the IEEE*, 91, **2003**, 1785.
- <sup>46</sup> M.L. Chabinyk, X. Chen, R.E. Holmlin, H. Jacobs, H. Skulason, C.D. Frisbie, V. Mujica, M.A. Ratner, M.A. Rampi, G.M. Whitesides; *Journal of the American Chemical Society*, 124, **2002**, 11730.
- <sup>47</sup> M.A.Reed, C.Zhou, C.J.Muller, T.P.Burgin, J.M. Tour, *Science*, 278, **1997**, 252.
- <sup>48</sup> C.Zhou, M.R.Deshpande, M.A.Reed, L.Jones II, J.M.Tour, *Applied Physical Letters*, 71, **1997**, 611.
- <sup>49</sup> G.Kushmerick, D.B.Holt, S.K.Pollack, M.A.Ratner, J.C.Yang, T.L.Schull, J.Naciri, M.H.Moore, R.Shashidhar, *Journal of the American Chemical Society*, 124, **2002**, 10654.
- <sup>50</sup> D. Vuillaume, S. Lenfant, *Microelectronic Engineering*, 70, **2003**, 539.
- <sup>51</sup> D. Cahen, G. Hodes, *Advanced Materials*, 14, **2002**, 789.
- <sup>52</sup> S.A. Contera, H. Iwasaki, *Ultramicroscopy*, 91, **2002**, 231.
- <sup>53</sup> M. Schweizer, H. Hagenstrom, D.M. Kolb, *Surface Science*, 490, **2001**, L627.
- <sup>54</sup> M. Hibino, A. Sumi, I. Hatta, *Thin Solid Films*, 273, **1996**, 272.
- <sup>55</sup> M. Saito, M. Sugi, T. Fukui, S. Iizima, *Thin Solid Films*, 100, **1983**, 117.
- <sup>56</sup> M. Sugi, K.Sakai, M. Saito, Y. Kawabata, S. Iizima, *Thin Solid Films*, 132, **1985**, 69.
- <sup>57</sup> A. Aviram, C. Joachim, M.Pomerantz, *Chemical Physical letters*, 146, **1988**, 490.
- <sup>58</sup> A. Aviram, *Chemical Physical letters*, 162, **1989**, 416.
- <sup>59</sup> N.J. Geddes, J.R. Sambles, D.J. Jarvis, W.G. Parker, D.J. Sandman, *Applied Physical Letters* 56, **1990**, 1916.
- <sup>60</sup> N. Okazaki, .R. Sambles, M.J. Jory, G.J. Ashwell, *Applied Physical Letters*, 81, **2002**, 2300.
- <sup>61</sup> D. Vuillaume, B. Chen, R. M. Metzger, *Langmuir*, 15, **1999**, 4011.
- <sup>62</sup> A.C. Brady, B. Hodder, A.S. Martin, J.R. Sambles, C.P. Ewels, R. Jones, P.R. Briddon, A.M. Musa, C.A. Panetta, D.L. Mattern, *Journal of Materials Chemistry*, 9, **1999**, 2271

- 
- <sup>63</sup> R.M. Metzger, T. Xu, I.R. Peterson, *Journal of Physical Chemistry B*, 105, **2001**, 7280.
- <sup>64</sup> G. Ho, J.R. Heath, M. Kondratenko, D. Perepichka, K. Arseneault, M. Pezolet, M. Bryce, *Chemistry European Journal*, 11, **2005**, 2914.
- <sup>65</sup> A.S. Martin, J.R. Sambles, *Physica Scripta*, 49, **1993**, 718.
- <sup>66</sup> G.J. Ashwell, D. Gandolfo, *Journal of Materials Chemistry*, 11, **2001**, 246.
- <sup>67</sup> G.J. Ashwell, A. Mohib, *Journal of the American Chemical Society*, 127, **2005**, 16238.
- <sup>68</sup> G.J. Ashwell, K. Moczko, M. Sujka, A. Chwialkowska, L.R.H. High, D.J. Sandman, *Physical Chemistry Chemical Physics*, 8, **2007**, 996.
- <sup>69</sup> J.W. Baldwin, R.R. Amaresh, I.R. Peterson, W.J. Shumate, M.P. Cava, M.A. Amiri, R. Hamilton, G.J. Ashwell, R.M. Metzger, *Journal of Physical Chemistry B*, 106, **2002**, 12158.
- <sup>70</sup> A.S. Martin, J.R. Sambles, G.J. Ashwell, *Physical Review Letters*, 70, **1993**, 218.
- <sup>71</sup> G.J. Ashwell, A. Chwialkowska, L.R.H. High, *Journal of Materials Chemistry*, 14, **2004**, 2389.
- <sup>72</sup> T. Xu, I.R. Peterson, M.V. Lakshmikantham, R.M. Metzger, *Angewandte Chemie International Edition* 40, **2001**, 1749.
- <sup>73</sup> D.H. Waldeck, D.N. Beratan, *Science*, 261, **1993**, 576.
- <sup>74</sup> A.S. Martin, J.R. Sambles, G.J. Ashwell, *Thin Solid Films*, 210/211, **1992**, 313.
- <sup>75</sup> M. Pomerantz, A. Aviram, R.A. McCorkle, L. Li, A.G. Schrott, *Science*, 255, **1992**, 1115.
- <sup>76</sup> M. Giesen-Scibert, R. Jentjens, M. Poensgen, H. Ibach, *Physical Review Letters*, 71, **1993**, 3521.
- <sup>77</sup> T. Xu, T.A. Morris, G.J. Szulczewski, R.M. Metzger, M. Szablewski, *Journal of Materials Chemistry*, 12, **2002**, 3167.
- <sup>78</sup> M. Metzger, *Materials Science and Engineering*, C3, **1995**, 277.
- <sup>79</sup> G.J. Ashwell, D. Gandolfo, R. Hamilton, *Journal of Materials Chemistry*, 12, **2002**, 416.
- <sup>80</sup> G.J. Ashwell, D. Gandolfo, *Journal of Materials Chemistry*, 12, **2002**, 411.
- <sup>81</sup> G.J. Ashwell, W.D. Tyrrell, B.J. Robinson, *Molecular diodes: an altered polarity for rectification in ultra-thin film when the orientation of the dipole is reverse*, 12<sup>th</sup> International symposium on Electrets, 11-14 Sept. 2005.
- <sup>82</sup> G.J. Ashwell, B.J. Robinson, M.A. Amiri, D. Locatelli, S. Quici, D. Roberto, *Journal of Materials Chemistry*, 15, **2005**, 4203.



- 
- <sup>83</sup> C. Krzeminski, C. Delerue, G. Allan, D. Villaume, R.M. Metzger, *Physical Review B*, 64, 2001, 085405.
- <sup>84</sup> P.E. Kornilovitch, A.M. Bratkovsky, R.S. Williams, *Physical Review B*, 66, **2002**, 165436.
- <sup>85</sup> G.J. Ashwell, R.J. Stokes, *Journal of Materials Chemistry Communications* 14, **2004**, 1228.
- <sup>86</sup> G.J. Ashwell, W.D. Tyrrell, A.J. Whittam, *Journal of Materials Chemistry*, 13, **2003**, 2855.
- <sup>87</sup> G.J. Ashwell, A. Mohib, J.R. Miller, *Journal of Materials Chemistry*, 15, **2005**, 1160.
- <sup>88</sup> J.C. Ellenbogen, J.C. Love, *Architectures for Molecular Electronic Computers: 1 Logic Structures and an Adder Built from Molecular Electronic Diodes*, MITRE Research Article, available at [http://www.mirte.org/tech/nanotech/Arch\\_for\\_MolecElec\\_Comp\\_1.html](http://www.mirte.org/tech/nanotech/Arch_for_MolecElec_Comp_1.html)
- <sup>89</sup> S. Zhou, Y. Liu, Y. Xu, W. Hu, D. Zhu, X. Qiu, C. Wang, C. Bai, *Chemical Physics Letters*, 297, **1998**, 77.
- <sup>90</sup> S. Zhou, Y. Liu, X. Qiu, Y. Xu, X. Huang, Y. Li, L. Jiang, D. Zhu, *Advanced Functional Materials*, 12, **2002**, 65.
- <sup>91</sup> R.M. Metzger, J. W. Baldwin, W.J. Shumate, I.R. Peterson, P. Mani, G. J. Mankey, T. Morris, G. Szulczewski, S. Bosi, M. Prato, A. Comito, Y. Robin, *Journal of Physical Chemistry B*, 107, **2003**, 1021.
- <sup>92</sup> G.J. Ashwell, M.A. Amiri, *Journal of Materials Chemistry*, 12, **2002**, 2181.
- <sup>93</sup> J.R. Miller, *Analysis of Rectifying Molecular Thin Films*, PhD Thesis, Cranfield, 2005.
- <sup>94</sup> A. Honciuc, A. Jaiswal, A. Gong, K. Ashworth, C.W. Spangler, I.R. Peterson, L.R. Dalton, R.M. Metzger, *Journal of Physical Chemistry B*, 109, **2005**, 857.
- <sup>95</sup> M.A. Rampi, G.M. Whitesides; *Chemical Physics*, 281, **2002**, 373.
- <sup>96</sup> R. McGeary, J. Dieringer, A. Osman Solak, B. Snyder, A.M. Nowak, W.R. McGovern, S. DuVall, *Journal of the American Chemical Society*, 125, **2003**, 10748.
- <sup>97</sup> McGeary, J. Dieringer, A. Osman Solak, B. Snyder, A.M. Nowak, W.R. McGovern, S. DuVall, *Journal of the American Chemical Society*, 126, **2004**, 6200.
- <sup>98</sup> J.J. Langer, M. Martynski, *Synthetic Metals*, 107, **1999**, 1.
- <sup>99</sup> C.M. Fisher, M. Burghard, S. Roth, *Synthetic Metals*, 71, **1995**, 1975.
- <sup>100</sup> N.I. Kovtyukhova, B.R. Martin, J.K.N. Mbindyo, T.E. Mallouk, M. Cabassi, T.S. Mayer, *Materials Science and Engineering C*, 19, **2002**, 255.
- <sup>101</sup> R. Yamada, H. Wano, K. Uosaki, *Langmuir*, 16, **2000**, 5523.
- <sup>102</sup> B. Mukherjee, A.J. Pal, *Chemical Physics Letters*, 416, **2005**, 289.

- 
- <sup>103</sup> G.J. Ashwell, M. Berry, *Journal of Materials Chemistry Communications* 15, **2005**, 108.
- <sup>104</sup> G.J. Ashwell, J. Ewington, B.J. Robinson, *Chemical Communications*, 6, **2006**, 618.
- <sup>105</sup> G.J. Ashwell, W.D. Tyrrell, B. Urasinska, C. Wang, M.R. Bryce, *Chemical Communications*, 15, **2006**, 1640.
- <sup>106</sup> J. Noh, M. Hara, *Langmuir*, 18, **2002**, 1953.
- <sup>107</sup> G.J. Ashwell, B. Urasinska, W.D. Tyrrell, *Physical Chemistry Chemical Physics*, 28, **2006**, 3314.
- <sup>108</sup> G.J. Ashwell, (1992), *Molecular electronics*, John Wiley & Sons, New York;
- <sup>109</sup> M. Fujihira, K. Nishiyama, H. Yamada, *Thin Solid Films*, 132, **1985**, 77.
- <sup>110</sup> C.D. Muller, A. Falcou, N. Reckefuss, M. Rojahn, V. Wiederhirn, P. Rudati, H. Frohne, O. Nuyken, H. Becker, K. Meerholz, *Nature*, 421, **2003**, 829.
- <sup>111</sup> N.V. Lavrik, P.G. Datskos, *Applied Physics Letters*, 82, **2003**, 2697.
- <sup>112</sup> Y. Huang, X. Duan, Y. Cui, L. Lauhon, K. Kim, C.M. Lieber, *Science*, 294, **2001**, 1313.
- <sup>113</sup> M. Cavallini, F. Biscarini, S. Leon, F. Zerbetto, G. Bottari, D.A. Leigh, *Science*, 299, **2003**, 531.
- <sup>114</sup> K. Ziemelis, *Nature*, 292, **1998**, 619.
- <sup>115</sup> G. Horowitz, *Advanced Materials*, 2, **1990**, 287.
- <sup>116</sup> J.H. Burroughes, C.A. Jones, R.H. Friend, *Nature*, 335, **1988**, 137.
- <sup>117</sup> H.W.C. Postma, T. Teepen, Z. Yao, M. Grifoni, C. Dekker, *Science*, 293, **2001**, 76.
- <sup>118</sup> B. Franklin, *Of the stilling of wave by means of oil*, *Philosophical Transactions of the Royal Society of London*, 64, 1774, 445.
- <sup>119</sup> Lord Rayleigh, *Philosophical Magazine*, 48, **1899**, 321.
- <sup>120</sup> A. Pockels, *Surface tension*, *Nature*, 43, **1891**, 437.
- <sup>121</sup> M.C. Petty, *Thin Solid Films*, 210/211, **1992**, 417.
- <sup>122</sup> A. Chyla, (2004) *Warstwy Langmuira–Blodgett I ich wykorzystanie w elektronice molekularnej*, Oficyna Wydawnicza Politechniki Wrocławskiej, Wrocław.
- <sup>123</sup> M.C. Petty, (1996) *Langmuir–Blodgett films An introduction*, Cambridge University press, Cambridge.

- 
- <sup>124</sup> G. Roberts (Ed.), (1990) *Langmuir–Blodgett films*, Plenum press, London.
- <sup>125</sup> F.H.C. Stewart, *Australian Journal of Chemistry*, 14, **1961**, 57.
- <sup>126</sup> Elbert, Folda, Ringsdorf, *Journal of American Chemical Society*, 106, **1984**, 7687.
- <sup>127</sup> R.M. Metzger, R.R. Schumaker, M.P. Cava, R.K. Laidlaw, C.A. Panetta, E. Torres, *Langmuir*, 4, **1988**, 298.
- <sup>128</sup> S.Y. Luk, J.O. Williams, *Journal of Chemical Society Chemical Communications*, **1989**, 159.
- <sup>129</sup> M.J. Cook, J.McMurdo, D.A. Miles, R.H. Poynter, J.M. Simmons, S.D. Haslam, R.M. Richardson, K. Welford, *Journal of Materials Chemistry*, 4(8), **1999**, 1205.
- <sup>130</sup> S. Baker, M.C. Petty, G.G. Roberts, M.V. Twigg, *Thin Solid Films*, 99, **1983**, 53.
- <sup>131</sup> G.J. Ashwell, M.P.S. Roberts, N.D. Rees, G.S. Bahra, C.R. Brown, *Langmuir*, 14, **1998**, 5279.
- <sup>132</sup> G.J. Ashwell, A.N. Dyer, A. Green, N. Sato, T. Sakuma, *Journal of Materials Chemistry*, 10, **2000**, 2473.
- <sup>133</sup> C. Ewins, B. Stewart, *Journal of Chemical Society and Faraday Transactions*, 90(7), **1994**, 969.
- <sup>134</sup> G. Williams, C. Pearson, M.R. Bryce, M.C. Petty, *Thin Solid Films*, 209, **1992**, 150.
- <sup>135</sup> T. Nakamura, H. Tachibana, M. Yumura, M. Matsumoto, R. Azumi, M. Tanaka, Y. Kawabata, *Langmuir*, 8, **1992**, 4.
- <sup>136</sup> E.W. Wong, C.P. Collier, M. Behloradsky, F. M. Raimo, J.F. Stoddart, J.R. Heath, *Journal of the American Chemical Society*, 122, **2000**, 5831.
- <sup>137</sup> Y. Tang, Y. Wang, X. Wang, S. Xun, C. Mei, L. Wang, D. Yan, *Journal of Physical Chemistry B*, 109, **2005**, 8813.
- <sup>138</sup> H.N. Shreenivasa Murthy, M. Bodyagin, S. Diele, U. Baumeister, G. Pelzl, W. Weissflog, *Journal of Materials Chemistry*, 16, **2006**, 1634.
- <sup>139</sup> M. Blanca Ros, J. Serrano, M. Rsario de la Fuente, C.L. Folcia, *Journal of Materials Chemistry*, 15, **2005**, 5093.
- <sup>140</sup> L.Zou, J. Wang, V.J. Beleva, E.E. Koojman, S.V. Primak, J.Risse, W. Weissflog, A. Jakli, E.K. Mann, *Langmuir*, 20, **2004**, 2772.
- <sup>141</sup> N. Duff, J. Wang, E.K. Mann, D.J. Lacks, *Langmuir*, 22, **2006**, 9082.
- <sup>142</sup> T. Yamamoto, S. Oguchi, T. Manaka, M. Iwamoto, *Thin Solid Films*, 499, **2006**, 242.

- 
- <sup>143</sup> T. Yamamoto, T. Manaka, M. Iwamoto, *Colloids and Surfaces A: Physicochemical and Engineering Aspects*, 284-285, **2006**, 154.
- <sup>144</sup> J. Gong, L. Wan, *Journal of Physical Chemistry B*, 109, **2005**, 16733.
- <sup>145</sup> F. Grunfeld (Ed.) Langmuir-Blodgett troughs operating manual, 6<sup>th</sup> edition (2001), supplied by Nima technology Ltd. also available at: <http://www.nima.co.uk/help/manuals.html> (accessed 60)
- <sup>146</sup> A.H. Ellison, *Journal of Physical Chemistry*, 66, **1962**, 1867.
- <sup>147</sup> Nima technology Ltd. Website: [www.nima.co.uk](http://www.nima.co.uk)
- <sup>148</sup> J. Ch. Love, L. A. Estroff, J. K. Kriebel, R. G. Nuzzo, G. M. Whitesides, *Chemical Reviews*, 105, **2005**, 1103.
- <sup>149</sup> T. Nakamura, T. Matsumoto, H. Tada, K. I. Sugiura (Eds), (2003) *Chemistry of nanomolecular systems*, Springer, New York.
- <sup>150</sup> Th. Wink, S.J. van Zuilen, A. Bult, W.P. van Bennekom, *The Analyst*, 122, **1997**, 43R.
- <sup>151</sup> W.C. Bigelow, D.L. Pickett, W.A. Zisman, *Journal of Colloids Science*, 1, **1946**, 513.
- <sup>152</sup> G. E. Poirier, *Chemical Reviews*, 97, **1997**, 1117.
- <sup>153</sup> C. D. Bain, E. B. Troughton, Y. Tai Tao, J. Evall, G.M. Whitesides, R.G. Nuzzo, *Journal of the American Chemical Society*, 111(1), **1989**, 321.
- <sup>154</sup> R. G. Nuzzo, F. Fusco, D.L. Allara, *Journal of the American Chemical Society*, 109, **1987**, 2358.
- <sup>155</sup> Self-assembled monolayer formation picture available at: <http://www.mtl.kyoto-u.ac.jp/english/laboratory/nanosopic/nanosopic.htm>
- <sup>156</sup> C. D. Bain, G. M. Whitesides, *Journal of the American Chemical Society*, 111(18), **1989**, 7164.
- <sup>157</sup> C. D. Bain, J. Evall, G. M. Whitesides, *Journal of the American Chemical Society*, 111(18), **1989**, 7155.
- <sup>158</sup> H.A. Biebuyck, C.D. Bain, George M. Whitesides, *Langmuir*, 9, **1993**, 1766.
- <sup>159</sup> J.M. Tour, L. Jones II, D.L. Pearson, J.J.S. Lamba, T.P. Burgin, G. M. Whitesides, D.L. Allara, A.N. Parikh, S.V. Atre, *Journal of the American Chemical Society*, 117, **1995**, 9529.
- <sup>160</sup> H. Takiguchi, K. Sato, T. Ishida, K. Abe, K. Yase, K. Tamada, *Langmuir*, 16, **2000**, 1703.
- <sup>161</sup> R.G. Nuzzo, D.L. Allara, *Journal of the American Chemical Society*, 105, **1983**, 4481.

- 
- <sup>162</sup> H.A. Biebuyck, C. D. Bain, G. M. Whitesides, *Langmuir*, 10, **1994**, 1825.
- <sup>163</sup> J. B. Schlenoff, M. Li, H. Ly, *Journal of the American Chemical Society*, 117, **1995**, 12528.
- <sup>164</sup> G. Yang, G. Liu, *Journal of Physical Chemistry B*, 107, **2003**, 8746.
- <sup>165</sup> K Walzer, E Marx, NC Greenham, RJ Less, PR Raithby, K Stokbro, *Journal of the American Chemical Society*, 126, **2004**, 1229.
- <sup>166</sup> M. D. Porter, T. B. Bright, D. L. Allara, C. E.D. Chidsey, *Journal of the American Chemical Society*, 109, **1987**, 3559.
- <sup>167</sup> S.E. Creager, L.A. Hockett, G.F. Rowe, *Langmuir*, 8, **1992**, 854.
- <sup>168</sup> D.M. Cyr, B. Venkataraman, G.Flynn, *Chemical Materials*, 8, **1996**, 1600.
- <sup>169</sup> Formation of SAMs from solution, available at: [http://www.ias.tuwien.ac.at/research/fghh/images/selfAssembly\\_small.jpg](http://www.ias.tuwien.ac.at/research/fghh/images/selfAssembly_small.jpg)
- <sup>170</sup> C.K.Hanley, J.A. Quinn, T.K. Vanderlick, *Langmuir*, 10, **1994**, 1527.
- <sup>171</sup> A.Baba, F.Kaneko, R.C.Advincula, Submitted to ACS Polymer Preprints Spring 1999 Meeting
- <sup>172</sup> C.K. O'Sullivan, G.G. Guilbault, *Biosensors and Bioelectronics*, 14, **1999**, 663.
- <sup>173</sup> M.R.Deakin, D.A.Buttry, *Analytical Chemistry*, 61, **1989**, 1147.
- <sup>174</sup> L.E. Bailey, D. Kambhampati, K.K. Kanazawa, W. Knoll, C.W. Frank, *Langmuir*, 18, **2002**, 479.
- <sup>175</sup> Quartz crystal microbalance structure, available at: <http://www2.nose-network.org/webtutorial/transducers/qmb.htm>
- <sup>176</sup> A.Wajid, *Sensors and Actuators A*, 63, **1997**, 41.
- <sup>177</sup> G. Sauerbrey, *Z. Physik*, 155, **1959**, 206.
- <sup>178</sup> F. Kaneko, W. Saito, T. Sato, H. Hatakeyama, K. Shinbo, K. Kato, T. Wakamatsu, *Thin Solid films*, 438-439, **2003**, 108.
- <sup>179</sup> J.W. Sadowski, I.K.J. Korhonen, J.P.K. Peltonen, *Optical engineering*, 34, **1995**, 2581.
- <sup>180</sup> H.E. de Bruijn, R.P.H. Kooyman, J. Greve, *Applies optics*, 29, **1990**, 1974.
- <sup>181</sup> N.M.Mulchan, M.Rodriguez, K. O'Shea, Y.Darici, *Sensors and Actuators B*, 88, **2003**, 132.
- <sup>182</sup> C. Koslinger, E. Uttenthaler, S. Drost, F. Aberl, H. Wolf, G. Brink, A. Stanglmaier, E. Sackmann, *Sensors and Actuators B*, 24-25, **1995**, 107.

- 
- <sup>183</sup> W.L. Barnes, J.R. Sambles, *Journal of Physics D.: Applied Physics*, 20, **1987**, 1125
- <sup>184</sup> Picture of Kretschmann configuration available at <http://www.uweb.engr.washington.edu/research/tutorials/plasmon.html>
- <sup>185</sup> E. Kretschmann, *Z. Physik*, 241, **1971**, 313.
- <sup>186</sup> H. Rohrer, *Surface Science*, 299-300, **1994**, 956.
- <sup>187</sup> P.K.Hansma, J.Tersoff, *Journal of Applied Physics*, 61, **1987**, R1.
- <sup>188</sup> L.J. Whitman, *Tunnelling Microscopy and Spectroscopy*, To appear in Encyclopedia of Applied Physics, available at: <http://stm2.nrl.navy.mil/~lwhitman/pdfs/eapchap.pdf>, (accessed 40).
- <sup>189</sup> Picture of STM apparatus available at: [http://www.iap.tuwien.ac.at/www/surface/STM\\_Gallery/stm\\_schematic.html](http://www.iap.tuwien.ac.at/www/surface/STM_Gallery/stm_schematic.html)
- <sup>190</sup> Günter, (1990) *Nonlinear optical effects and materials*, Springer, Berlin
- <sup>191</sup> R.W. Boyd, (1992), *Nonlinear optics*, Academic Press, London
- <sup>192</sup> T.Verbiest, S.Houbrechts, M.Kauranen, KClays, A.Persoons, *Journal Materials Chemistry*, 7, **1997**, 2175.
- <sup>193</sup> M. Amiri, *Optically nonlinear Langmuir–Blodgett films*, *PhD Thesis*, Cranfield University, 2003.
- <sup>194</sup> G.J. Ashwell, *Journal Materials Chemistry*, 9, **1999**, 1991.
- <sup>195</sup> T. Bjornholm, T. Gaisler, J. Larsen, M. Jorgensen, *Journal of Chemistry Chemical Communications*, 1992, 825
- <sup>196</sup> W.D. Tyrrell, *Self-assembled films for molecular rectification*, *PhD Thesis*, Cranfield University, 2004.
- <sup>197</sup> R. Hamilton, *Materials for molecular electronics*, *PhD Thesis*, Cranfield University, 2003
- <sup>198</sup> J. Freud, J. Halbritter, J.K.H. Horber, *Microscopy Research and technique*, 44, **1999**, 327.
- <sup>199</sup> N.A. Bell, C.S. Bradley, R.A. Broughton, S.J.Coles, D.E. Hibbs, M.B. Hursthouse, A.K.Ray, D.J. Simmonds, S.C. Thorpe, *Journal Materials Chemistry*, 15, **2005**, 1437.
- <sup>200</sup> K. Han, X. Lu, J.Xu, G.Zhou, S. Sa, W.Wang, Z.Cai, J.Zhou, *Journal of Physics D: Applied Physics*, 30, **1997**, 2923.